Supporting Information to the paper

# Green and highly efficient synthesis of perylene and naphthalene bisimides in nothing but water

By

Bettina Baumgartner,[a] Anastasiya Svirkova,[b] Johannes Bintinger,[c] Christian Hametner,[c] Martina Marchetti-Deschmann,[b] and Miriam M. Unterlass[a*]

[a] Technische Universität Wien, Institute of Materials Chemistry, Getreidemarkt 9/BC/2, 1060 Vienna, Austria
[b] Technische Universität Wien, Institute of Chemical Technologies and Analytics, Getreidemarkt 9/164-IAC, 1060 Vienna, Austria
[c] Technische Universität Wien, Institute of Applied Synthetic Chemistry, Getreidemarkt 9/163, 1060 Vienna, Austria
*corresponding author: *miriam.unterlass@tuwien.ac.at*

# 1. Methods

FT-IR-ATR spectra were recorded on a Bruker Tensor 27 working in ATR MicroFocusing MVP-QL with a diamond crystal, using OPUS (version 4.0) software for data analysis. Resolution was set to 2-4 $cm^{-1}$, and spectra were recorded from 4000 to 600 $cm^{-1}$.

$^{1}H$ solution NMR spectra were recorded on a Bruker Avance DRX-400 (400 MHz for $^{1}H$ and 100 MHz for $^{13}C$) or Avance III HD 600 (600 MHz and 151 MHz, resp.).

Powder X-ray diffraction data was collected with a PANalytical X'Pert Pro multi-purpose diffractometer (MPD) in Bragg Brentano geometry operating with a Cu anode at 40 kV, 40 mA, and an X-Celerator multichannel detector was used. Samples were ground and mounted as loose powders on silicon single crystal sample holders. The diffraction patterns were recorded between 5 and 60° (2θ) with 69.215 s/step and a step size of 0.0050134°, sample holders where rotated during the measurement with 4 s/turn.

Scannning electron microscopy was carried out with a *Quanta 200F FEI* microscope. Typically the samples were measured at 5 kV or 10 kV, with a working distance of 9-10 mm and spot size 2.0 or 2.5. Prior to imaging, samples were loaded on carbon-coated stubs and coated by sputtering with a 17 nm thick layer of Au/Pd 60/40 alloy with a *Quarum Q105T S* sample preparation system.

UV/VIS absorption and fluorescence emission spectra were recorded in $CH_2Cl_2$ or $CHCl_3$ solutions (0.1 - 1 nM) with a Perkin Elmer Lambda 750 spectrometer and an Edinburgh FLS920, respectively.

MALDI MS and LDI MS experiments were carried out on a Synapt G2 HDMS (Waters, UK). Samples were prepared at 5 mg/mL in chloroform. In positive mode α-Cyano-4-hydroxycinnamic acid (CHCA, 3 mg/ml in methanol:chloroform (1:1)) was used as matrix for MALDI measurements; in negative mode - only LDI MS analyzes were performed. 1 $\mu$L of the sample solution or suspension was deposited with and without matrix on a stainless steel target and dried at room temperature. Mass range 80 – 1000 Da. Accurate m/z determination was achieved by using LockMass calibration with NaI clusters for negative mode and CHCA and Bradykinin 1-7 for positive mode.

HT experiments were performed in Teflon-lined Parr 4744 45 mL General Purpose Vessels.

# 2. Chemicals

Perylene-3,4,9,10-tetracarboxylic dianhydride (PBA, 97 %, Sigma Aldrich), 1,4,5,8-Naphthalenetetracarboxylic dianhydride (NBA, 98 %, Sigma Aldrich), Amylamin (*n*-$C_5$, 95 %, Sigma Aldrich), Hexylamin (*n*-$C_6$, 99 %, Sigma Aldrich), Heptylamin (*n*-$C_7$, 99 %, Sigma Aldrich), Octylamin (*n*-$C_8$, 99 %, Sigma Aldrich), Nonylamine (*n*-$C_9$, 98 %, ABCR), Decylamin (*n*-$C_{10}$, 95 %, Sigma Aldrich), Undecylamine (*n*-$C_{11}$, 98 %, ABCR), Dodecylamine (*n*-$C_{12}$, 98 %, Sigma Aldrich), Tetradecylamine (*n*-$C_{14}$, 95 %, Sigma Aldrich), Pentadecylamine (*n*-$C_{15}$, 96 %, Sigma Aldrich), Hexadecylamine (*n*-$C_{16}$, 98 %, Sigma Aldrich), Octadecylamine (*n*-$C_{18}$, 97 %, Sigma Aldrich), N,N-diisopropylethylamine (Hünig's Base, HB, 98 %, Fluka) were used as received. Cyclohexylamine (*c*-$C_6$) and Aniline (An) were freshly distilled.

# 3. Experimental Details

## 3.1. Synthesis of NBIs and PBIs

1 equivalent of perylene-3,4,9,10-tetracarboxylic dianhydride (0.4 mmol) or 1,4,5,8-naphthalenetetracarboxylic dianhydride (0.4 mmol), respectively, 2 equivalents of the respective amine (0.8 mmol) and 15 mL distilled water were stirred at room temperature for 20 min. Selected HT experiments were carried out with Hünig's base (HB, N,N-

Diisopropylethylamine) as catalyst (see **TableS1**). Therefore, 1-2 droplets of HB were added to the reaction mixture. The mass of these droplets was determined and used to calculate the mole fraction of catalyst with respect to the corresponding amine.
The reaction mixture was transferred into a Teflon-lined autoclave with glass inlet and placed in a preheated oven for the reaction $t_R$. After $t_R$, the autoclave was allowed to cool down (see **TableS1** for details). The crude product was isolated *via* filtration and dried at 40 °C *in vacuo*.

**TableS1**: Overview of HT experiments. HB = Hünig's base

| Dianhydride | Amine | $t_R$ (h) | $T_R$ (°C) | Catalyst |
|---|---|---|---|---|
| PBA | *n*-$C_5$ | 24 | 200 | -- |
| | *n*-$C_6$ | 24 | 200 | -- |
| | *n*-$C_7$ | 24 | 200 | -- |
| | *n*-$C_8$ | 24 | 200 | -- |
| | *n*-$C_8$ | 4 | 200 | 10 mol% HB |
| | *n*-$C_8$ | 4 | 200 | 17 mol% HB |
| | *n*-$C_9$ | 24 | 200 | -- |
| | *n*-$C_{10}$ | 24 | 200 | -- |
| | *n*-$C_{11}$ | 24 | 200 | -- |
| | *n*-$C_{12}$ | 24 | 200 | -- |
| | *n*-$C_{14}$ | 24 | 200 | -- |
| | *n*-$C_{14}$ | 4 | 200 | 30 mol% HB |
| | *n*-$C_{14}$ | 8 | 200 | 20 mol% HB |
| | *n*-$C_{15}$ | 24 | 200 | -- |
| | *n*-$C_{16}$ | 24 | 200 | -- |
| | *n*-$C_{18}$ | 24 | 200 | -- |
| | *n*-$C_{18}$ | 4 | 200 | 10 mol% HB |
| | *n*-$C_{18}$ | 4 | 200 | 25 mol% HB |
| | *n*-$C_{18}$ | 17 | 200 | 10 mol% HB |
| | *c*-$C_6$ | 17 | 200 | -- |
| | *c*-$C_6$ | 4 | 200 | 20 mol% HB |
| | *c*-$C_6$ | 17 | 200 | 10 mol% HB |
| | An | 17 | 200 | 10 mol% HB |
| | An | 4 | 200 | 20 mol% HB |
| | | | | |
| NBA | *n*-$C_8$ | 16 | 200 | -- |
| | *n*-$C_8$ | 4 | 200 | 10 mol% HB |
| | *n*-$C_{18}$ | 16 | 200 | -- |
| | *n*-$C_{18}$ | 4 | 200 | 10 mol% HB |
| | *c*-$C_6$ | 17 | 200 | -- |
| | *c*-$C_6$ | 4 | 200 | 10 mol% HB |
| | An | 17 | 200 | -- |

**N,N'-Bis(pentyl)-3,4:9,10-perylenebis(dicarboximide) (*n*-$C_5$-PBI)**
UV/Vis λmax($CH_2Cl_2$)/nm 457, 487 and 524.
Fluorescence λmax($CH_2Cl_2$)/nm 530, 572 and 620.
$^1$H NMR: δH(600 MHz; $CDCl_3$/d-TFA; $Me_4Si$) 0.74 - 0.97 (6 H, m, -$CH_3$) 1.26 - 1.54 (8 H, m, -$CH_2$-) 1.68 - 1.89 (6 H, m, -$CH_2$-) 4.25 (4 H, quin., *J*=7.78 Hz, -N-$CH_2$-) 8.61 - 8.89 (8 H, m, Ph)

$^{13}C$ NMR δC(151 MHz; $CDCl_3$/d-TFA; $Me_4Si$) 13.8, 22.7, 26.9, 28.1, 31.6, 42.1, 122.6, 124.5, 126.6, 129.5, 133.3, 135.9, 160.9 - 163.7
IR $v_{max}/cm^{-1}$ 2954, 2928 and 2853 (CH), 1693 and 1655 (C=O, imide), 1591 and 1508 (conj. C-C), 1342 (C-N)
HRMS (MALDI): [M+H]+ m/z calcd for $C_{34}H_{30}N_2O_4$, 530.2206, found 531.2318

**N,N'-Bis(hexyl)-3,4:9,10-perylenebis(dicarboximide) (*n*-$C_6$-PBI)**
UV/Vis λmax($CH_2Cl_2$)/nm 457, 487 and 524.
Fluorescence λmax($CH_2Cl_2$)/nm 530, 572 and 620.
$^1H$ NMR: δH(600 MHz; $CDCl_3$/d-TFA; $Me_4Si$) 0.91 (6 H, t, *J*=7.04, 1.76 Hz, -$CH_3$) 1.10 - 1.58 (12 H, m, -$CH_2$-) 1.67 - 1.89 (4 H, m, -$CH_2$-) 4.24 (4 H, quin, *J*=7.85 Hz, -N-$CH_2$-) 8.72 (4 H, d, *J*=8.05 Hz, Ph) 8.78 (4 H, d, *J*=8.05 Hz, Ph)
$^{13}C$ NMR δC(151 MHz; $CDCl_3$/d-TFA; $Me_4Si$) 13.9, 22.7, 26.9, 28.1, 31.6, 42.1, 122.6, 124.5, 126.6, 129.5, 133.3, 135.9, 160.3 - 164.2
IR $v_{max}/cm^{-1}$ 2957, 2926 and 2857 (CH), 1693 and 1652 (C=O, imide), 1594 and 1508 (conj. C-C), 1337 (C-N)

**N,N'-Bis(heptyl)-3,4:9,10-perylenebis(dicarboximide) (*n*-$C_7$-PBI)**
UV/Vis λmax($CH_2Cl_2$)/nm 457, 487 and 524.
Fluorescence λmax($CH_2Cl_2$)/nm 530, 572 and 620.
$^1H$ NMR: δH(400 MHz; $CDCl_3$/d-TFA; $Me_4Si$) 0.89 (6 H, t, *J*=6.90 Hz, -$CH_3$) 1.21 - 1.55 (16 H, m, -$CH_2$-) 1.77 (4 H, quin, *J*=7.70 Hz, -$CH_2$-) 4.25 (4 H, quin, *J*=7.70 Hz, -$CH_2$-) 8.75 (4 H, d, *J*=8.05 Hz, Ph) 8.78 (4 H, d, *J*=8.05 Hz, Ph)
$^{13}C$ NMR δC(151 MHz; $CDCl_3$/d-TFA; $Me_4Si$) 13.9, 22.7, 27.2, 28.1, 29.1, 31.9, 42.1, 122.6, 124.5, 126.6, 129.5, 133.3, 135.9, 159.8 - 164.1
IR $v_{max}/cm^{-1}$ 2955, 2926 and 2854 (CH), 1691 and 1651 (C=O, imide), 1591 and 1508 (conj. C-C), 1342 (C-N)

**N,N'-Bis(octyl)-3,4:9,10-perylenebis(dicarboximide) (*n*-$C_8$-PBI)**
UV/Vis λmax($CH_2Cl_2$)/nm 457, 487 and 524.
Fluorescence λmax($CH_2Cl_2$)/nm 530, 572 and 620.
$^1H$ NMR: δH(600 MHz; $CDCl_3$/d-TFA; $Me_4Si$) 0.88 (6 H , t, *J*=7.00 Hz , -$CH_3$) 1.13 - 1.49 (20 H, m, -$CH_2$-) 1.76 (4 H , quin., *J*=6.70 Hz, -$CH_2$-) 4.24 (4 H, t, J = 7.98 Hz, N-$CH_2$-) 8.72 (4 H, d, *J*=8.05 Hz, Ph) 8.77 (4 H, d, *J*=8.05 Hz, Ph)
$^{13}C$ NMR δC(151 MHz; $CDCl_3$/d-TFA; $Me_4Si$) 14.0, 22.8, 27.2, 28.1, 29.4, 32.0, 42.0, 122.6, 124.4, 126.5, 129.4, 133.1, 135.7, 159.9 - 163.6
IR $v_{max}/cm^{-1}$ 2955, 2926 and 2854 (CH), 1693 and 1653 (C=O, imide), 1591 and 1506 (conj. C-C), 1344 (C-N)
HRMS (MALDI): $[M+H]^+$ m/z calcd for $C_{40}H_{42}N_2O_4$, 614.3145, found 615.3311

**N,N'-Bis(nonyl)-3,4:9,10-perylenebis(dicarboximide) (*n*-$C_9$-PBI)**
UV/Vis λmax($CH_2Cl_2$)/nm 457, 487 and 524.
Fluorescence λmax($CH_2Cl_2$)/nm 530, 572 and 620.
$^1H$ NMR: δH(600 MHz; $CDCl_3$/d-TFA; $Me_4Si$) 0.88 (6 H , t, J = 7.29 Hz , -$CH_3$) 1.13 - 1.33 (24 H, m, -$CH_2$-) 1.45 (4 H, q, J = 7.03 Hz, -$CH_2$-) 1.76 (4 H , quin., *J*=7.81 Hz, -$CH_2$-) 4.23 (4 H, t, J = 7.95 Hz, N-$CH_2$-) 8.68 (4 H, d, *J*=7.95 Hz, Ph) 8.74 (4 H, d, *J*=7.95 Hz, Ph)
$^{13}C$ NMR δC(151 MHz; $CDCl_3$/d-TFA; $Me_4Si$) 14.1, 22.8, 27.2, 28.1, 29.0 - 30.5, 32.0, 42.0, 122.6, 124.3, 126.4, 129.4, 133.1, 135.6, 159.7 - 163.4
IR $v_{max}/cm^{-1}$ 2951, 2928 and 2852 (CH), 1693 and 1653 (C=O, imide), 1591 and 1508 (conj. C-C), 1342 (C-N)

HRMS (MALDI): $[M+H]^+$ m/z calcd for $C_{42}H_{46}N_2O_4$, 642.3458, found 643.3658

**N,N'-Bis(decyl)-3,4:9,10-perylenebis(dicarboximide) (*n*-$C_{10}$-PBI)**
UV/Vis λmax($CHCl_3$)/nm 459, 489 and 536.
Fluorescence λmax($CHCl_3$)/nm 532, 574 and 623.
$^1$H NMR: δH(600 MHz; $CDCl_3$/d-TFA; $Me_4Si$) 0.82 - 0.95 (6 H, m, -$CH_3$ ) 1.15 - 1.51 (28 H, m, -$CH_2$-) 1.76 (4 H, quin, *J*=7.63 Hz, -$CH_2$-) 4.23 (4 H, t, J = 7.95 Hz, -N-$CH_2$-) 8.64 (4 H, d, *J*=8.22 Hz, Ph) 8.72 (4 H, d, *J*=8.22 Hz, Ph)
$^{13}$C NMR δC(151 MHz; $CDCl_3$/d-TFA; $Me_4Si$)14.2, 22.8, 26.5 - 28.5, 29.1 - 30.3, 32.0, 41.8, 122.6, 124.1, 126.3, 129.3, 132.8, 135.4, 160.1 - 162.5
IR $v_{max}$/cm$^{-1}$ 2957, 2926 and 2851 (CH), 1695 and 1650 (C=O, imide), 1591 and 1508 (conj. C-C), 1344 (C-N)

**N,N'-Bis(undecyl)-3,4:9,10-perylenebis(dicarboximide) (*n*-$C_{11}$-PBI)**
UV/Vis λmax($CHCl_3$)/nm 459, 489 and 536.
Fluorescence λmax($CHCl_3$)/nm 532, 574 and 623.
$^1$H NMR: δH(600 MHz; $CDCl_3$/d-TFA; $Me_4Si$) 0.81 - 0.94 (6 H, m , -$CH_3$) 1.20 - 1.52 (24 H, m, -$CH_2$-) 1.75 (4 H , quin., *J*=7. 63 Hz, -$CH_2$-) 4.24 (4 H, t, J = 7.98 Hz, N-$CH_2$-) 8.66 (4 H, d, *J*=7.92 Hz, Ph) 8.73 (4 H, d, *J*=7.92 Hz, Ph)
$^{13}$C NMR δC(151 MHz; $CDCl_3$/d-TFA; $Me_4Si$) 14.2, 22.9, 26.5 - 28.6, 28.9 - 30.6, 32.1, 41.9, 122.6, 124.2, 126.4, 129.3, 132.9, 135.5, 160.1 - 162.6
IR $v_{max}$/cm$^{-1}$ 2953, 2924 and 2849 (CH), 1695 and 1653 (C=O, imide), 1591 and 1508 (conj. C-C), 1342 (C-N)

**N,N'-Bis(dodecyl)-3,4:9,10-perylenebis(dicarboximide) (*n*-$C_{12}$-PBI)**
UV/Vis λmax($CHCl_3$)/nm 459, 489 and 536.
Fluorescence λmax($CHCl_3$)/nm 532, 574 and 623.
$^1$H NMR: δH(600 MHz; $CDCl_3$/d-TFA; $Me_4Si$) 0.87 (6 H, t, *J*=7.04 Hz, , -$CH_3$) 1.03 - 1.53 (36 H, m, -$CH_2$-) 1.75 (4 H, quin, *J*=7.63 Hz, -$CH_2$-) 4.24 (4 H, t, *J* = 7.93 Hz, N-$CH_2$-) 8.67 (4 H, d, *J*=7.92 Hz, Ph) 8.74 (4 H, d, *J*=7.92 Hz, Ph)
$^{13}$C NMR δC(151 MHz; $CDCl_3$/d-TFA; $Me_4Si$) 14.2, 22.9, 27.2, 28.1, 28.8 - 30.9, 32.1, 41.9, 122.6, 124.2, 126.4, 129.4, 132.9, 135.5, 160.4 - 162.9
IR $v_{max}$/cm$^{-1}$ 2957, 2920 and 2849 (CH), 1693 and 1652 (C=O, imide), 1591 and 1508 (conj. C-C), 1344 (C-N)

**N,N'-Bis(tetradecyl)-3,4:9,10-perylenebis(dicarboximide) (*n*-$C_{14}$-PBI)**
UV/Vis λmax($CHCl_3$)/nm 459, 489 and 536.
Fluorescence λmax($CHCl_3$)/nm 532, 574 and 623.
$^1$H NMR: δH(600 MHz; $CDCl_3$/d-TFA; $Me_4Si$) 0.87 (6 H , t, *J*=7.04 Hz , -$CH_3$) 1.13 - 1.51 (44 H, m, -$CH_2$-) 1.76 (4 H , quin., *J*=7.49 Hz, -$CH_2$-) 4.24 (4 H, t, *J* = 7.95 Hz, N-$CH_2$-) 8.71 (4 H, d, *J*=7.95 Hz, Ph) 8.76 (4 H, d, *J*=7.95 Hz, Ph)
$^{13}$C NMR δC(151 MHz; $CDCl_3$/d-TFA; $Me_4Si$) 14.1, 22.9, 27.2, 28.1, 28.9 - 31.3, 32.2, 42.0, 122.6, 124.4; 126.5, 129.4, 133.1, 135.7, 160.6 - 163.0
IR $v_{max}$/cm$^{-1}$ 2955, 2921 and 2849 (CH), 1695 and 1653 (C=O, imide), 1591 and 1508 (conj. C-C), 1344 (C-N)
HRMS (MALDI): $[M+H]^+$ m/z calcd for $C_{52}H_{66}N_2O_4$, 782.5023, found 783.5079

**N,N'- Bis(pentadecyl)-3,4:9,10-perylenebis(dicarboximide) (*n*-$C_{15}$-PBI)**
UV/Vis λmax($CHCl_3$)/nm 459, 489 and 536.
Fluorescence λmax($CHCl_3$)/nm 532, 574 and 623.

$^1$H NMR: δH(600 MHz; $CDCl_3$/d-TFA; $Me_4Si$) 0.87 (6 H , t, *J* = 7.81 Hz , -$CH_3$) 1.15 - 1.57 (48 H, m, -$CH_2$-) 1.78 (4 H , quin., *J*=7.63 Hz, -$CH_2$-) 4.25 (4 H, t, *J* = 7.81 Hz, N-$CH_2$-) 8.73 (4 H, d, *J*=7.92 Hz, Ph) 8.74 (4 H, d, *J*=7.92 Hz, Ph)
$^{13}$C NMR δC(151 MHz; $CDCl_3$/d-TFA; $Me_4Si$) 14.1, 22.9, 27.3, 28.2, 29.1 - 31.2, 32.2, 42.2, 122.6, 124.5, 126.6, 129.5, 133.3, 135.9, 160.5 - 163.3
IR $v_{max}$/cm$^{-1}$ 2953, 2922 and 2849 (CH), 1695 and 1653 (C=O, imide), 1591 and 1508 (conj. C-C), 1344 (C-N)
HRMS (MALDI): $[M+H]^+$ m/z calcd for $C_{54}H_{70}N_2O_4$, 810.5336, found 811.5757

**N,N'-Bis(hexadecyl)-3,4:9,10-perylenebis(dicarboximide) (*n*-$C_{16}$-PBI)**
$^1$H NMR: δH(600 MHz; $CDCl_3$/d-TFA; $Me_4Si$) 0.81 - 0.95 (6 H , m, -$CH_3$) 1.16 - 1.52 (52 H, m, -$CH_2$-) 1.78 (4 H , quin., *J*=7.48 Hz, -$CH_2$-) 4.26 (4 H, t, *J*=7.78 Hz, N-$CH_2$-) 8.79 (4 H, d, *J*=7.82 Hz, Ph) 8.82 (4 H, d, *J*=7.82 Hz, Ph)
$^{13}$C NMR δC(151 MHz; $CDCl_3$/d-TFA; $Me_4Si$) 13.7, 22.6, 26.9, 27.8; 28.3 - 30.2, 31.9, 41.1 - 42.5, 122.3, 124.2, 125.8 - 126.7, 128.5 - 129.8, 133.0, 135.7, 160.3 - 163.1
IR $v_{max}$/cm$^{-1}$ 2955, 2920 and 2849 (CH), 1695 and 1653 (C=O, imide), 1591 and 1506 (conj. C-C), 1344 (C-N)

**N,N'-Bis(octadecyl)-3,4:9,10-perylenebis(dicarboximide) (*n*-$C_{18}$-PBI)**
$^1$H NMR: δH(400 MHz; $CDCl_3$/d-TFA; $Me_4Si$) 0.87 (6 H , t, J = 7.09 Hz , -$CH_3$) 1.13 - 1.52 (60 H, m, -$CH_2$-) 1.77 (4 H, m, -$CH_2$-) 4.25 (4 H, t, J = 7.82 Hz, N-$CH_2$-) 8.77 (4 H, d, *J*=8.20 Hz, Ph) 8.80 (4 H, d, *J*=8.20 Hz, Ph)
$^{13}$C NMR δC(151 MHz; $CDCl_3$/d-TFA; $Me_4Si$) 14.1, 22.9, 27.2, 28.2, 29.2 - 31.0, 32.2, 42.1, 122.6, 124.5, 126.6, 129.6, 133.3, 136.0, 160.7 - 163.4
IR $v_{max}$/cm$^{-1}$ 2955, 2918 and 2850 (CH), 1695 and 1655 (C=O, imide), 1591 and 1508 (conj. C-C), 1344 (C-N)
HRMS (MALDI): $[M]^-$ m/z calcd for $C_{60}H_{82}N_2O_4$, 894.6275, found 894.6451

**N,N'-Bis(octyl)-1,4,5,8-naphthalenebis(dicarboximide) (*n*-$C_8$-NBI)**
$^1$H NMR: δH(600 MHz; $CDCl_3$; $Me_4Si$) 0.87 (6 H, t, *J*=6.60 Hz, -$CH_3$) 1.21 - 1.51 (20 H, m, -$CH_2$-) 1.74 (4 H, t, *J*=7.56 Hz, -$CH_2$-) 4.21 (4 H, t, *J*=7.63 Hz, N-$CH_2$-) 8.84 (4 H, s, Ph)
$^{13}$C NMR δC(151 MHz; $CDCl_3$; $Me_4Si$) 14.2, 22.8, 27.2, 28.2, 29.4, 31.9, 41.1, 126.3 - 127.4, 131.1, 163.0
IR $v_{max}$/cm$^{-1}$ 2918 and 2853 (CH), 1701 and 1654 (C=O, imide), 1581 (conj. C-C), 1332 (C-N)
HRMS (MALDI): $[M+H]^+$ m/z calcd for $C_{30}H_{38}N_2O_4$, 490.2832, found 491.2935

**N,N'-Bis(octadecyl)- 1,4,5,8-naphthalenebis(dicarboximide) (*n*-$C_{18}$-NBI)**
$^1$H NMR: δH(600 MHz; $CDCl_3$/d-TFA; $Me_4Si$) 0.87 (6 H, t, *J*=7.04 Hz, -$CH_3$) 1.11 - 1.50 (60 H, m, -$CH_2$-) 1.73 (4 H, t, *J*=7.34 Hz, -$CH_2$-) 4.21 (4 H, quin, *J*=7.60 Hz N-$CH_2$-) 8.84 (4 H, s, Ph)
$^{13}$C NMR δC(151 MHz; $CDCl_3$/d-TFA; $Me_4Si$) 14.2, 22.9, 27.2, 28.1, 28.7 - 30.8, 32.1, 41.9, 125.2 - 127.9, 132.1, 160.7 - 162.5
IR $v_{max}$/cm$^{-1}$ 2916 and 2848 (CH), 1701 and 1654 (C=O, imide), 1581 (conj. C-C), 1348 (C-N)
HRMS (MALDI): $[M]^-$ m/z calcd for $C_{50}H_{78}N_2O_4$, 770.5962, found 770.6016

**N,N'-Bis(cyclohexyl)- 1,4,5,8-naphthalenebis(dicarboximide) (*c*-$C_6$-NBI)**
$^1$H NMR: δH(600 MHz; $CDCl_3$/d-TFA; $Me_4Si$) 1.23 - 1.38 (2 H, m, -$CH_2$-) 1.40 - 1.53 (4 H, m, -$CH_2$-) 1.72 - 1.84 (4 H, m, -$CH_2$-) 1.94 (4 H, d, *J*=13.50 Hz, -$CH_2$-) 2.48 (4 H, quin, *J*=3.67 Hz, -$CH_2$-) 4.93 - 5.08 (2 H, m, N-$CH_2$-) 8.77 (4 H, s)

$^{13}C$ NMR δC(151 MHz; $CDCl_3$/d-TFA; $Me_4Si$) 25.3, 26.5, 29.2, 55.8, 125.8 - 127.7, 132.0, 160.3 - 163.2, 163.5 - 164.9, 164.5
IR $v_{max}/cm^{-1}$ 2938 and 2853 (CH), 1711 and 1649 (C=O, imide), 1579 (conj. C-C), 1328 (C-N)
HRMS (MALDI): $[M+H]^+$ m/z calcd for $C_{26}H_{26}N_2O_4$, 430.1893, found 431.2000

**N,N'-Bis(phenyl)- 1,4,5,8-naphthalenebis(dicarboximide) (An-NBI)**
$^1H$ NMR: δH(600 MHz; $CDCl_3$/d-TFA; $Me_4Si$) 7.35 (4 H, d, *J*=5.58 Hz, Ph) 7.60 (6 H, m, Ph) 8.96 (4 H, s, Ph)
$^{13}C$ NMR δC(151 MHz; $CDCl_3$/d-TFA; $Me_4Si$) 127.1, 127.5, 128.4, 130.3 - 130.9, 133.0, 133.4, 161.1 - 163.0, 164.8
IR $v_{max}/cm^{-1}$ 3070 (CH), 1711 and 1662 (C=O, imide), 1581 (conj. C-C), 1350 (C-N)
HRMS (MALDI): $[M+H]^+$ m/z calcd for $C_{26}H_{14}N_2O_4$, 418.0954, found 419.1004

### 3.2. Reflux Experiments

1 eq. of PBA and 2 eq. of respective amine (*n*-$C_5$-$NH_2$, *n*-$C_{11}$-$NH_2$, *n*-$C_{14}$-$NH_2$, *n*-$C_{18}$-$NH_2$) were stirred in 100 mL water at reflux temperature for 72 h. After 2 h, 4 h, 6 h and 24 h samples were taken and dried at 40 °C *in vacuo*. The reaction mixture was filtrated and dried at 40 °C *in vacuo*.

### 3.3. Aspect

The aspect of crude PBIs obtained after 24 h at 200 °C are depicted in FigureS1 and FigureS2.

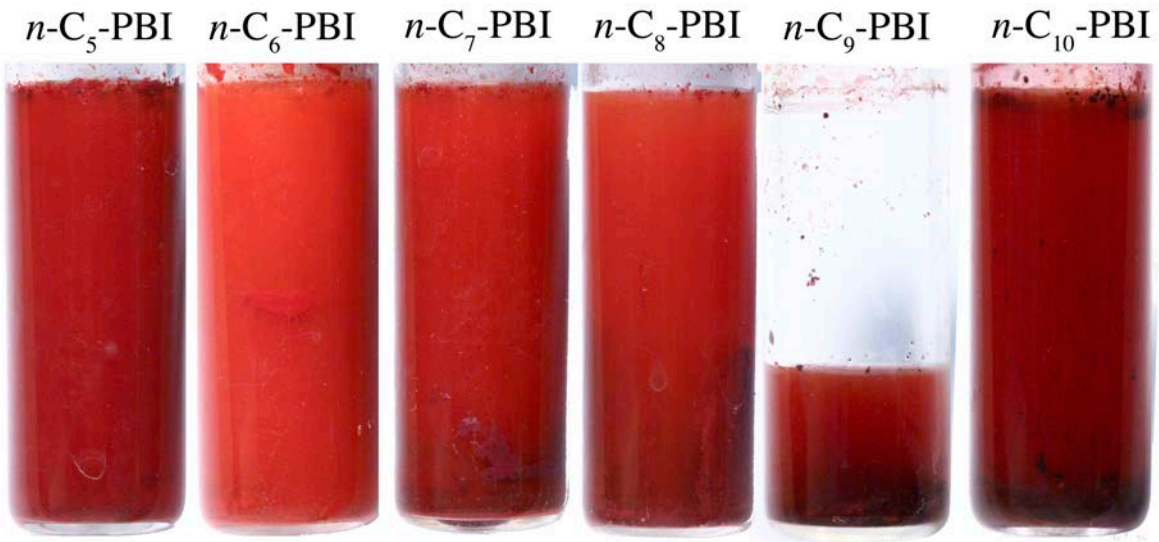


**FigureS1:** *Aspect of crude PBIs (n-$C_5$-PBI to n-$C_{10}$-PBI) after HT synthesis at 200 °C for 24 h.*

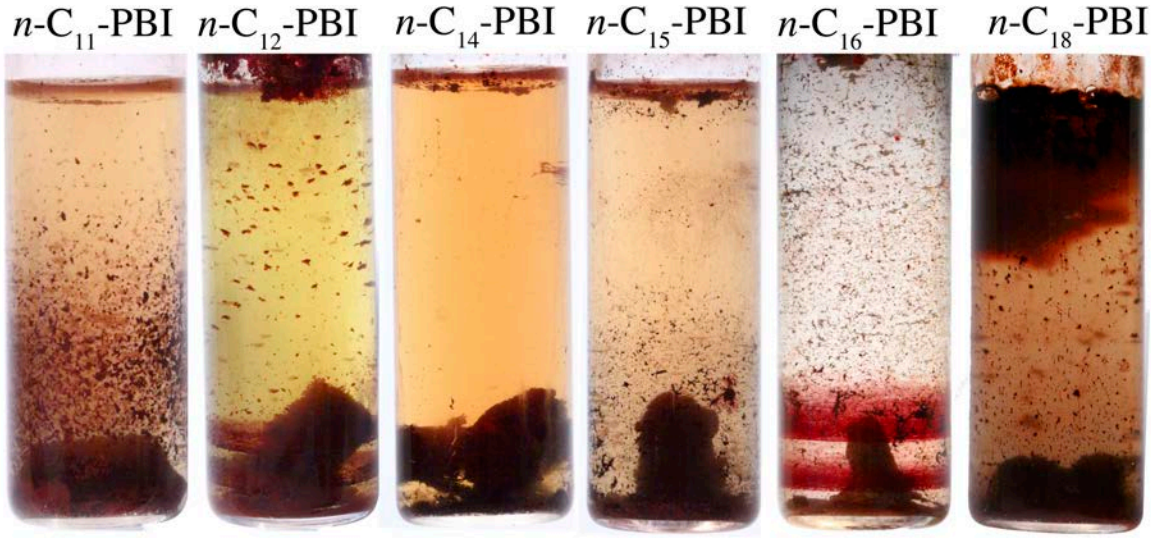


**FigureS2:** *Aspect of crude PBIs (n-$C_{11}$-PBI, n-$C_{12}$-PBI, n-$C_{14}$-PBI, n-$C_{15}$-PBI, n-$C_{16}$-PBI, n-$C_{18}$-PBI,) after HT synthesis at 200 °C for 24 h.*

### 3.4. Solubility Tests

The solubility of PBIs was tested in various solvents according to the following procedure: 100 mL of the respective solvent was added to 5-10 mg of the respective solid. The resulting dispersion was heated up to the boiling temperature of the respective solvent. The dispersion was kept at reflux for several hours. **TableS2** shows the used solvents and the outcome of the solubility tests.

**TableS2**: *Solubility experiments of PBIs*. Used solvents and boiling points: acetone (bp = 56 °C), MeOH = methanol (bp = 65 °C), EtOH = ethanol (bp = 78 °C), THF = tetrahydrofuran (bp = 66 °C), NMP = *N*-methyl-2-pyrrolidone (bp = 202 °C), DMSO = dimethylsulfoxide (bp = 189 °C), DMF = dimethylformamide (bp = 152 °C), diethylether (bp = 35 °C), $CH_2Cl_2$ = dichloromethane (bp = 40 °C), $CHCl_3$ = chloroform (bp = 61 °C).

| | ***nC8-PBI*** | ***nC18-PBI*** | ***cC6-PBI*** | ***An-PBI*** |
|---|---|---|---|---|
| **acetone** | No | No | No | No |
| **MeOH** | No | No | No | No |
| **$CH_2Cl_2$** | Yes | Yes | Yes | Yes |
| **$CHCl_3$** | Yes | Yes | Yes | Yes |
| **EtOH** | No | No | No | |
| **THF** | Yes | Yes | Yes | Yes |
| **diethylether** | No | No | No | No |
| **ACN** | No | No | No | No |
| **DMSO** | Yes | Yes | Yes | Yes |
| **DMF** | Yes | Yes | Yes | Yes |
| **Benzene** | Yes | Yes | Yes | Yes |

The solubility is further illustrated in FigureS3 and FigureS4: The solubility of *n*-alkyl PBIs depending on chain length and solvent (TFA = trifluoroacetic acid, THF = tetrahydrofuran, DMSO = dimethylsulfoxide, DMF = dimethylformamide, $CH_2Cl_2$ = dichloromethane, $CHCl_3$ = chloroform) in daylight and UV light.

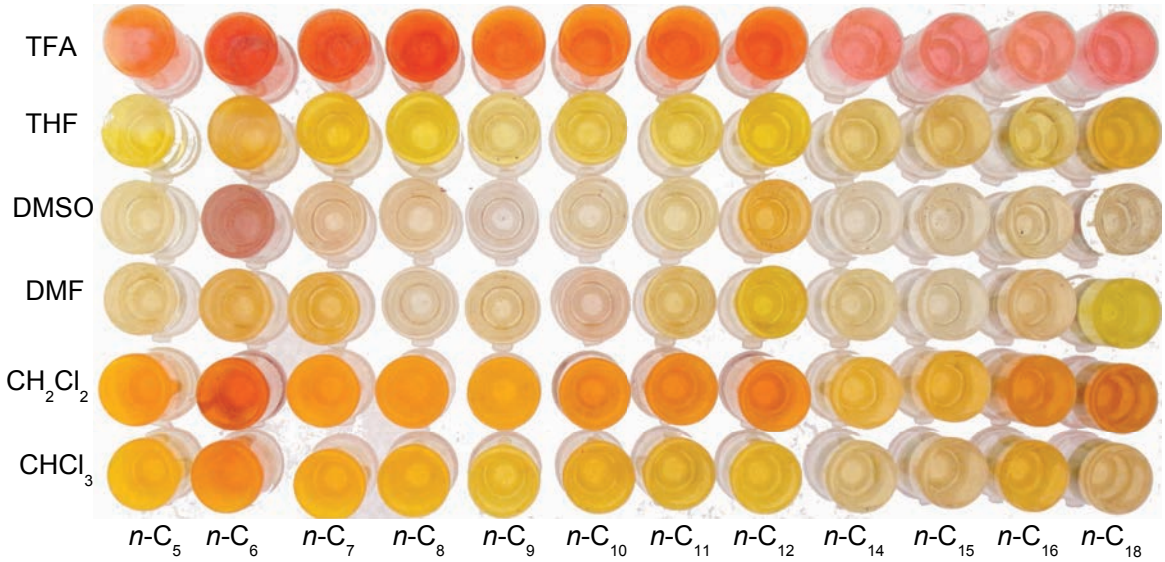


**FigureS3:** *Solubility tests for n-alkyl PBIs in various solvents (TFA = trifluoroacetic acid, THF = tetrahydrofuran, DMSO = dimethylsulfoxide, DMF = dimethylformamide, $CH_2Cl_2$ = dichloromethane, $CHCl_3$ = chloroform) at daylight.*

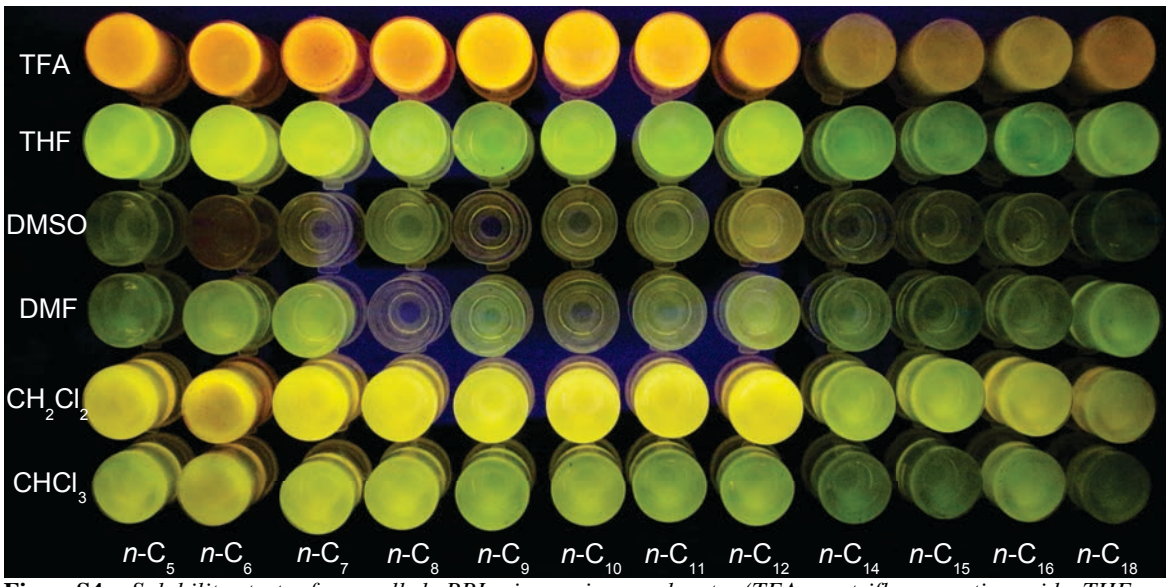


**FigureS4:** *Solubility tests for n-alkyl PBIs in various solvents (TFA = trifluoroacetic acid, THF = tetrahydrofuran, DMSO = dimethylsulfoxide, DMF = dimethylformamide, $CH_2Cl_2$ = dichloromethane, $CHCl_3$ = chloroform) at UV light.*

**TableS3:** ***Solubility n-alkylamines.*** *Used solvents and boiling points: water (bp = 100 °C), acetone (bp = 56 °C), MeOH = methanol (bp = 65 °C), Hexane (bp = 68 °C), EtOH = ethanol (bp = 78 °C)*

| | ***n-heptylamine*** | ***n-dodecylamine*** | ***n-pentadecylamine*** | ***n-octadecylamine*** |
|---|---|---|---|---|
| **$H_2O$** | Yes | No | No | No |
| **MeOH** | Yes | Yes | Yes | Yes |
| **EtOH** | Yes | Yes | Yes | No |
| **Hexane** | Yes | No | No | Yes |
| **Acetone** | Yes | Yes | Yes | No |

### 3.5. FT-IR-ATR Analysis

ATR-FTIR spectra of crude *n*-$C_x$-PBI (x = 5-12, 14, 15, 16, 18) synthesized at 200 °C for 24 h are depicted in FigureS5, FigureS6 and FigureS7. All spectra show typical imide modes at 1693 and 1654 $cm^{-1}$. Peaks that correspond to unreacted PBA (1772 $cm^{-1}$) are found in the spectra of *n*-$C_6$-PBI, *n*-$C_7$-PBI, *n*-$C_{11}$-PBI, *n*-$C_{12}$-PBI, *n*-$C_{16}$-PBI and *n*-$C_{18}$-PBI.

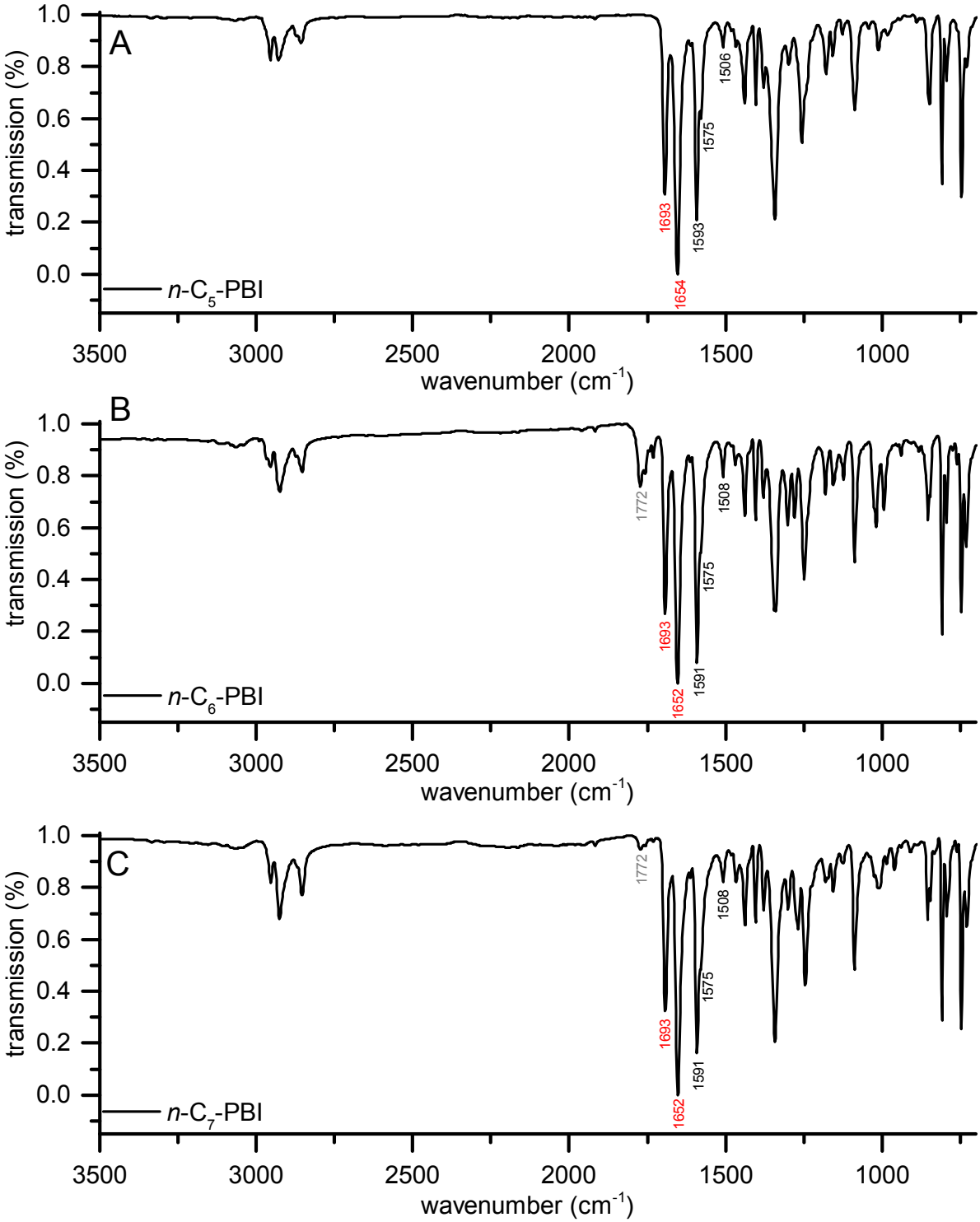


**FigureS5:** *ATR-FTIR spectra of n-$C_5$-PBI – n-$C_7$-PBI synthesized at 200 °C for 24 h. Characteristic bonds are assigned: imide bonds (C=O) in red, perylene body (C-C) in black and residual PBA in gray.*

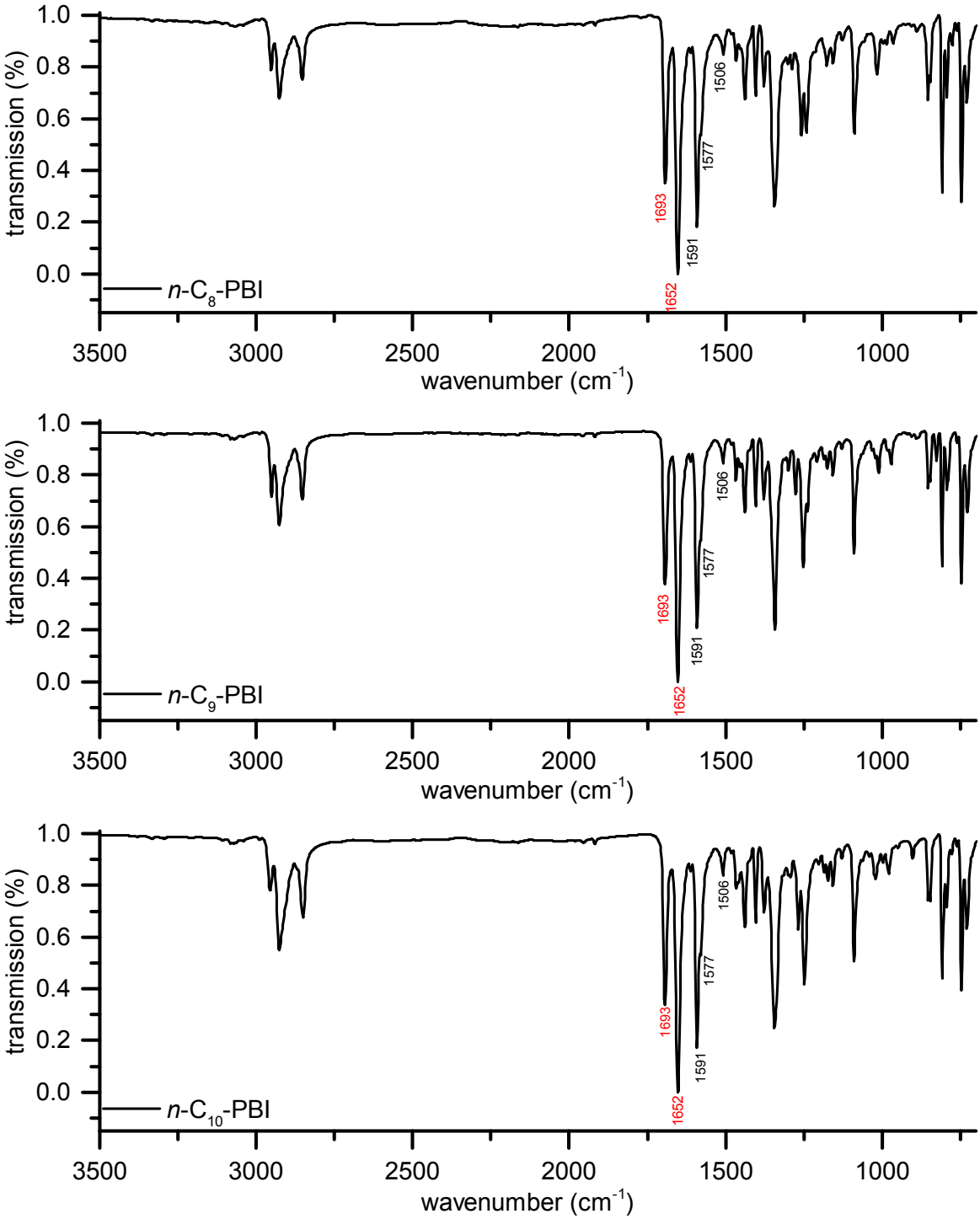


**FigureS6:** *ATR-FTIR spectra of n-$C_8$-PBI – n-$C_{10}$-PBI synthesized at 200 °C for 24 h. Characteristic bonds are assigned: imide bonds (C=O) in red, perylene body (C-C) in black.*

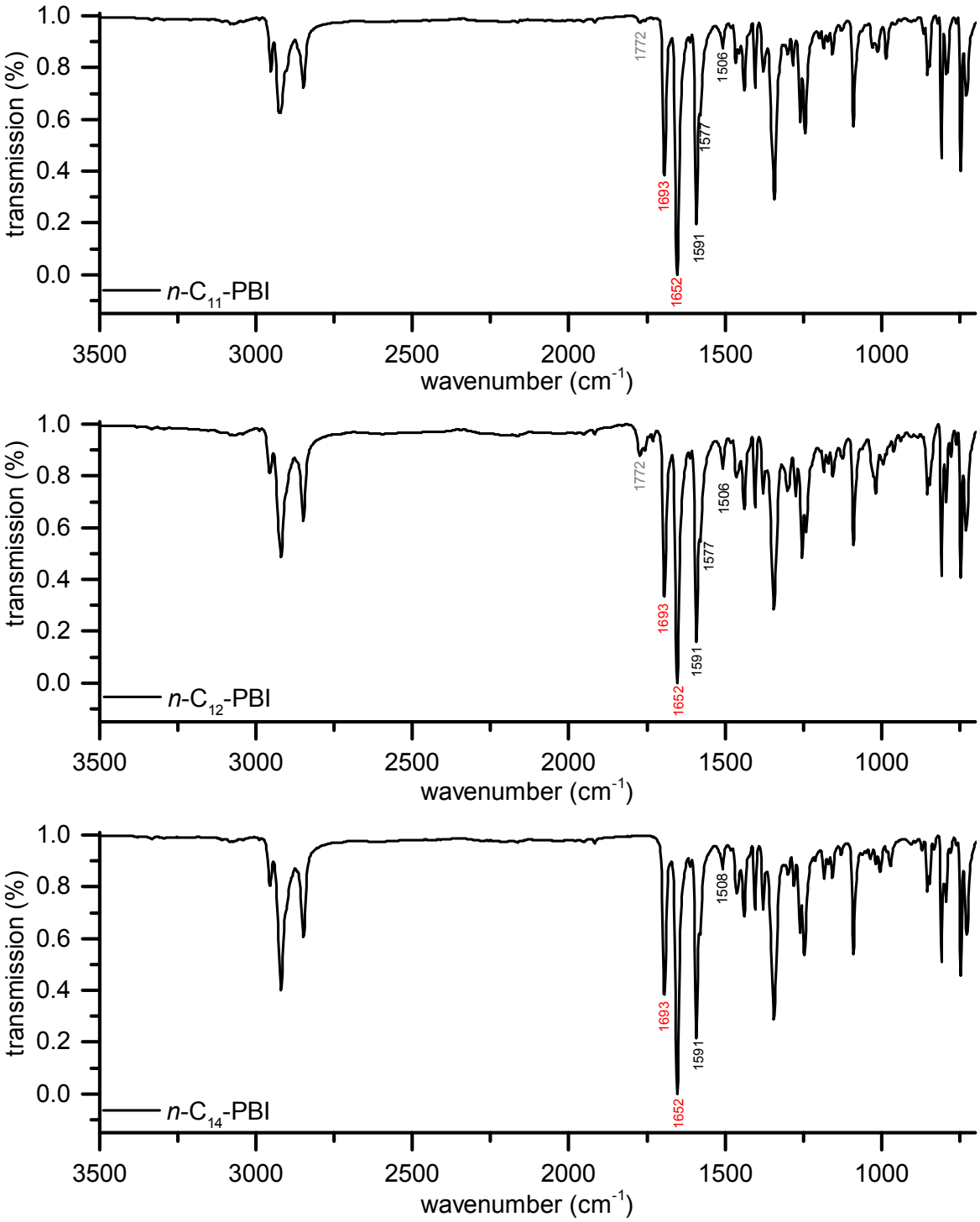


**FigureS7:** *ATR-FTIR spectra of n-$C_{11}$-PBI, n-$C_{12}$-PBI and n-$C_{14}$-PBI synthesized at 200 °C for 24 h. Characteristic bonds are assigned: imide bonds (C=O) in red, perylene body (C-C) in black and residual PBA in gray.*

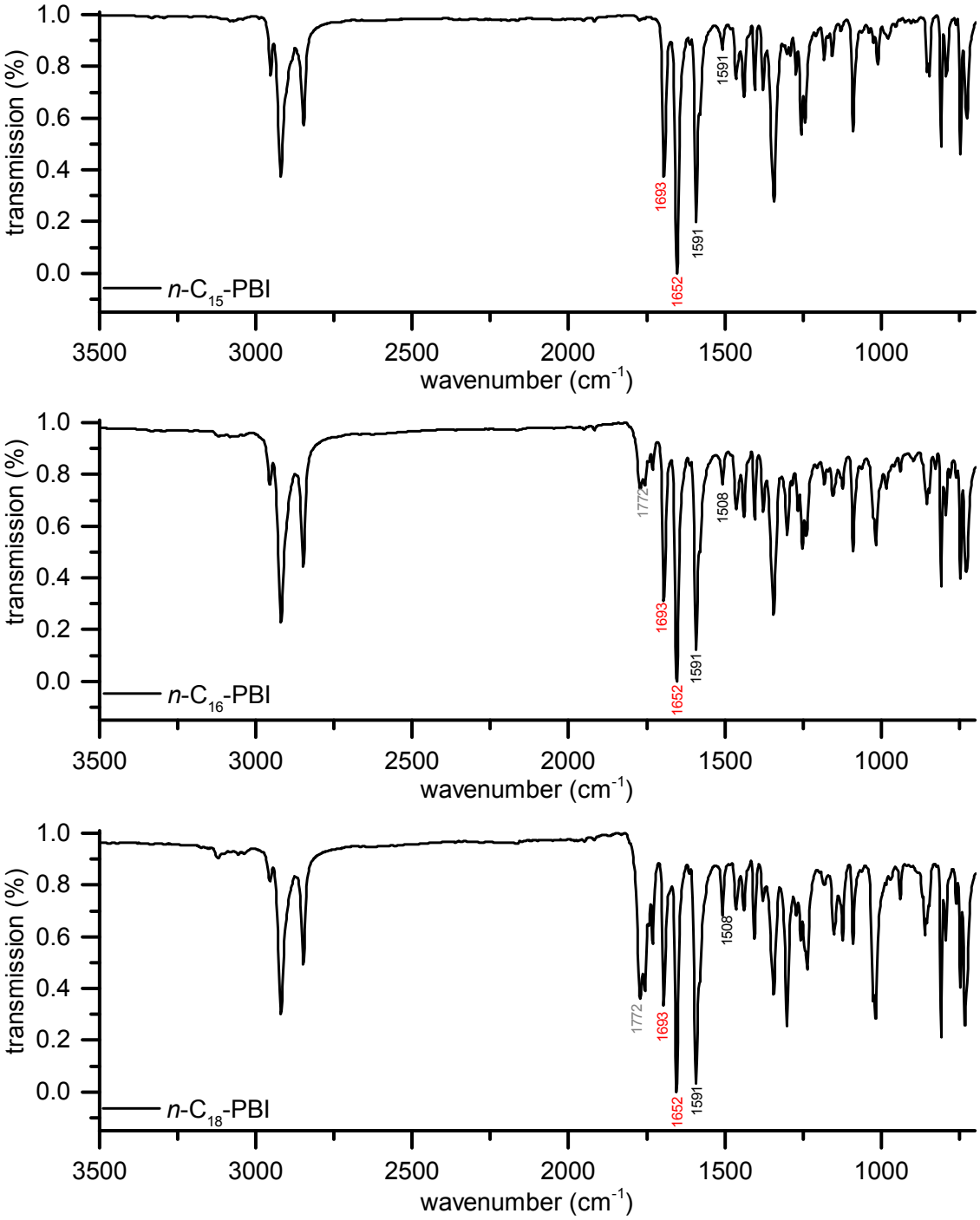


**FigureS8:** *ATR-FTIR spectra of n-$C_{15}$-PBI, n-$C_{16}$-PBI and n-$C_{18}$-PBI synthesized at 200 °C for 24 h. Characteristic bonds are assigned: imide bonds (C=O) in red, perylene body (C-C) in black and residual PBA in gray.*

FigureS9 depicts ATR-FTIR spectra of *n*-$C_5$-PBI, *n*-$C_{11}$-PBI, *n*-$C_{14}$-PBI and *n*-$C_{18}$-PBI obtained from reflux experiments ($t_R$ = 2 h, 4 h, 6 h, 24 h, 72 h). All spectra show characteristic imide modes (1693 and 1654 $cm^{-1}$) and anhydride modes from unreacted PBA (1772 $cm^{-1}$).

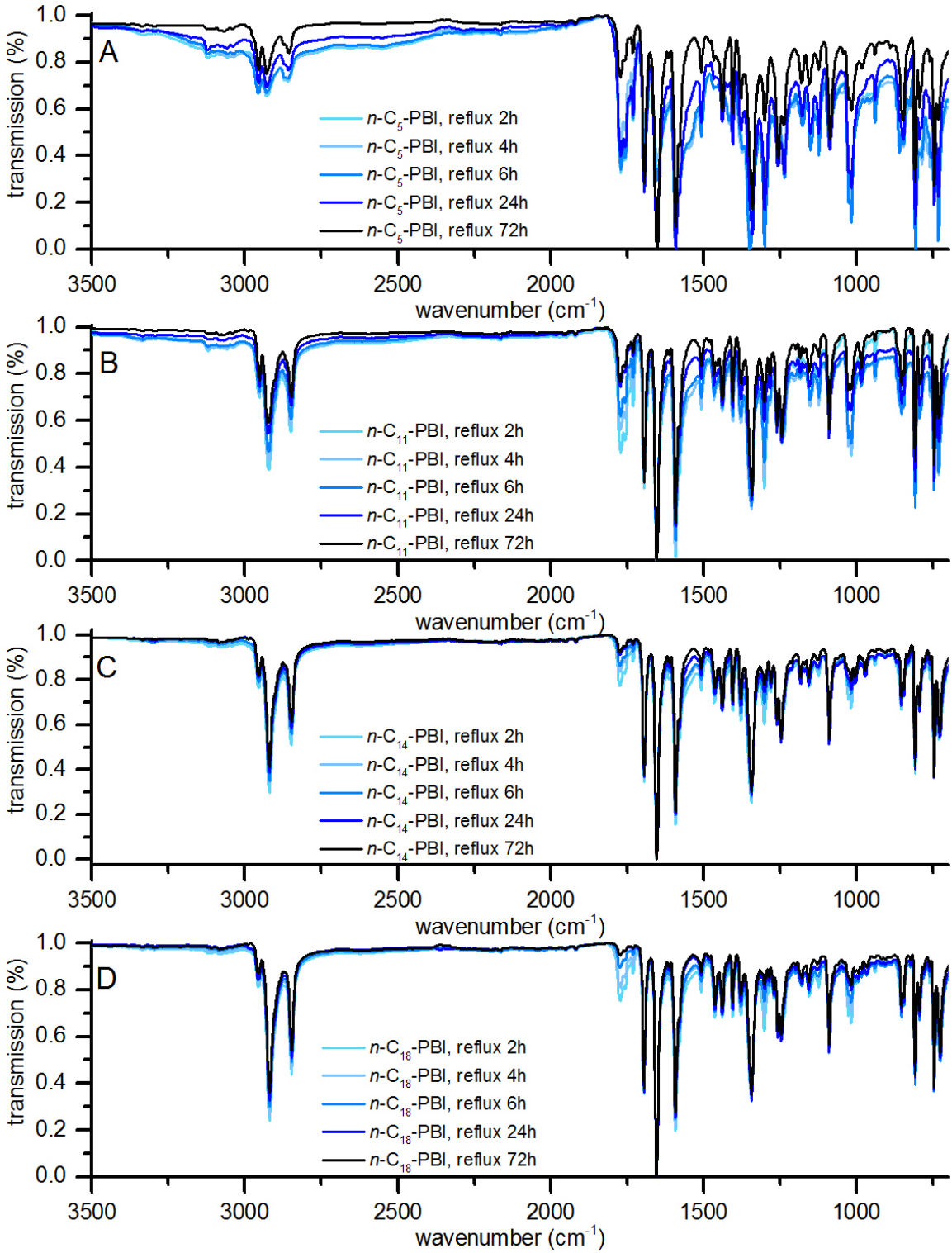


**FigureS9:** *ATR-FTIR spectra of n-$C_5$-PBI, n-$C_{11}$-PBI, n-$C_{14}$-PBI and n-$C_{18}$-PBI synthesized at reflux temperature.*

FigureS10 and FigureS11 show ATR-FTIR spectra of *n*-$C_8$-PBI, *n*-$C_{14}$-PBI, *n*-$C_{18}$-PBI, *c*-$C_6$-PBI and *An*-PBI synthesized at 200 °C for less than 24 h with *Hünig's* base as catalyst.

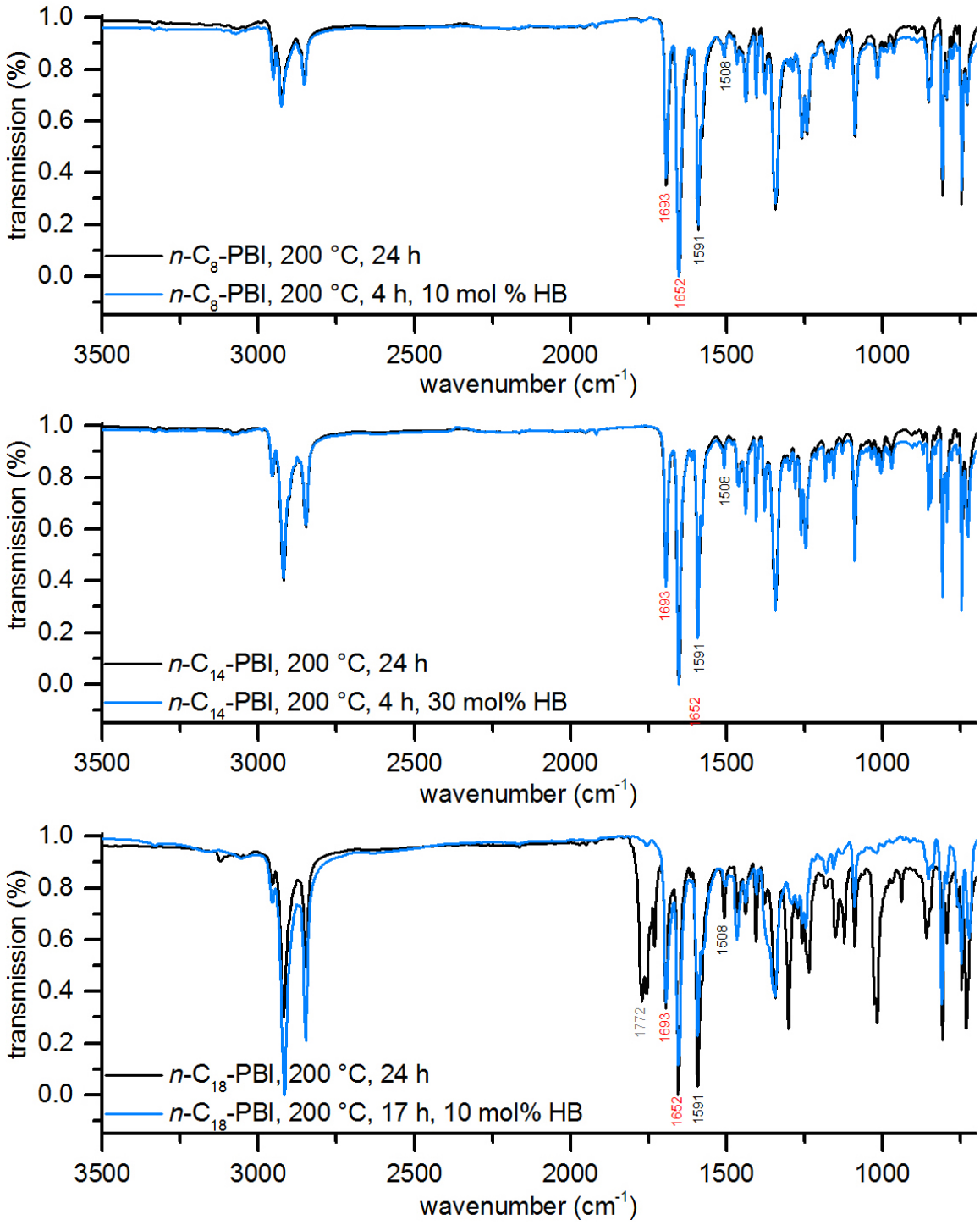


**FigureS10:** *ATR-FTIR spectra of n-$C_8$-PBI, n-$C_{14}$-PBI and n-$C_{18}$-PBI synthesized with Hünig's base at 200 °C for various reaction times.*

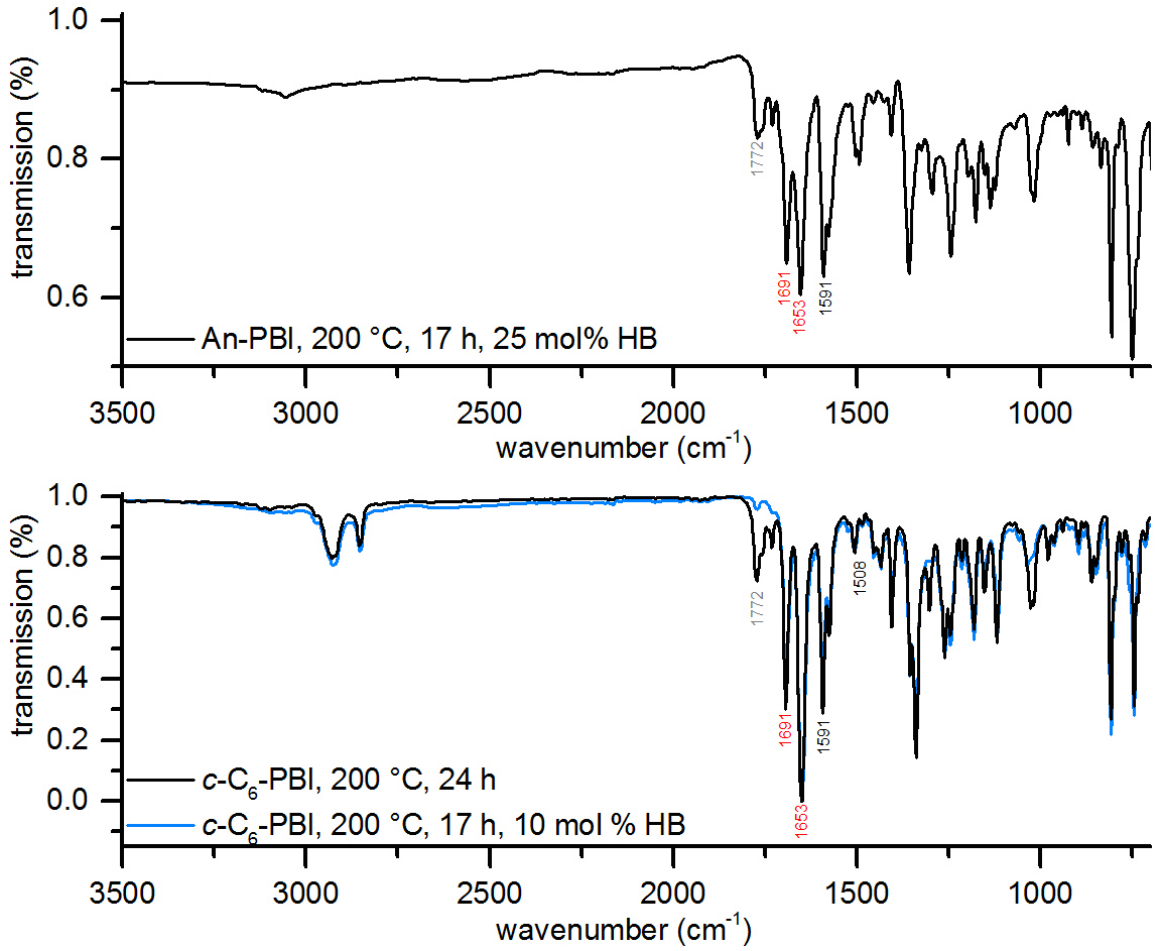


**FigureS11:** *ATR-FTIR spectra of c-$C_6$-PBI and An-PBI synthesized with Hünig's base at 200 °C for various reaction times.*

ATR-FTIR spectra of crude NBIs synthesized at 200 °C with and without *Hünig's* base catalyst are depicted in **FigureS9** and **FigureS10**. All spectra show typical imide modes at 1701 and 1654 $cm^{-1}$. Peaks that correspond to unreacted NBA (1766 $cm^{-1}$) are found in the spectra of *n*-$C_8$-NBI, *n*-$C_{18}$-NBI and *c*-$C_6$-NBI.

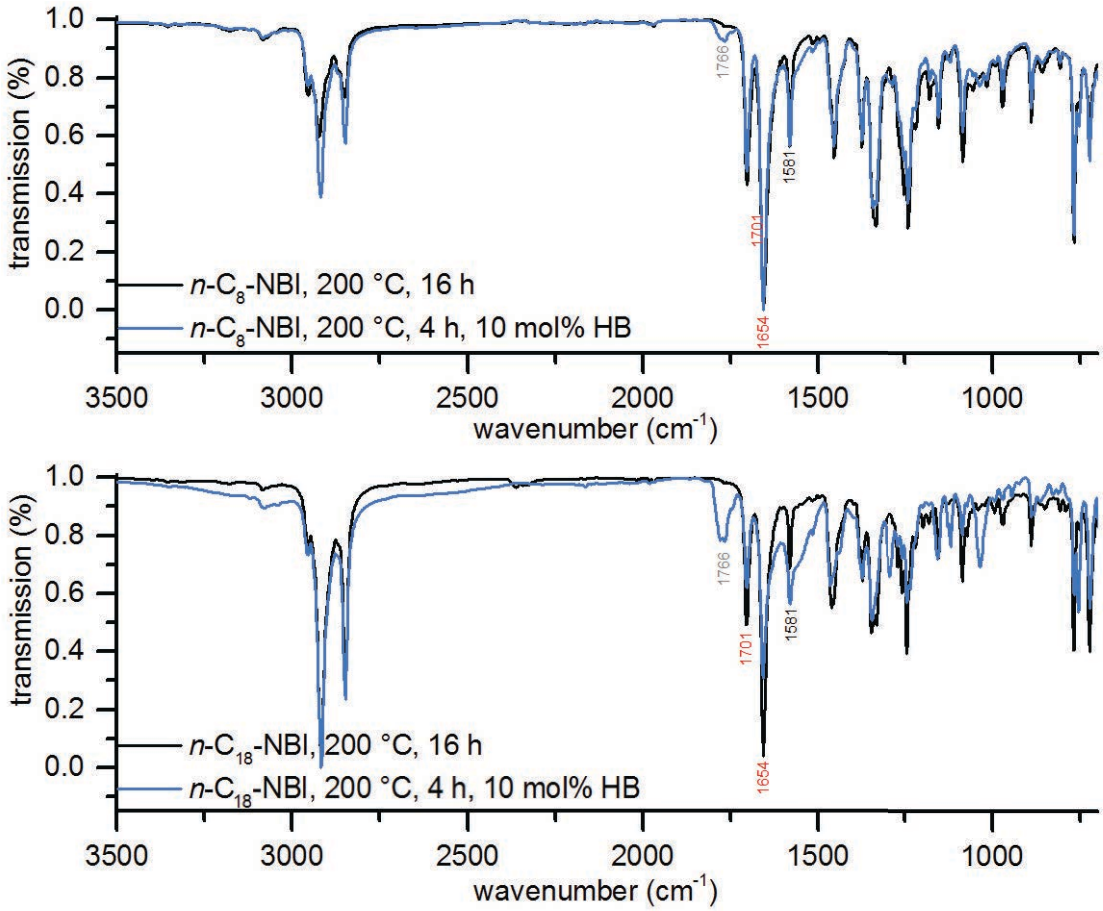


**FigureS12:** *ATR-FTIR spectra of n-$C_8$-NBI and n-$C_{18}$-NBI.*

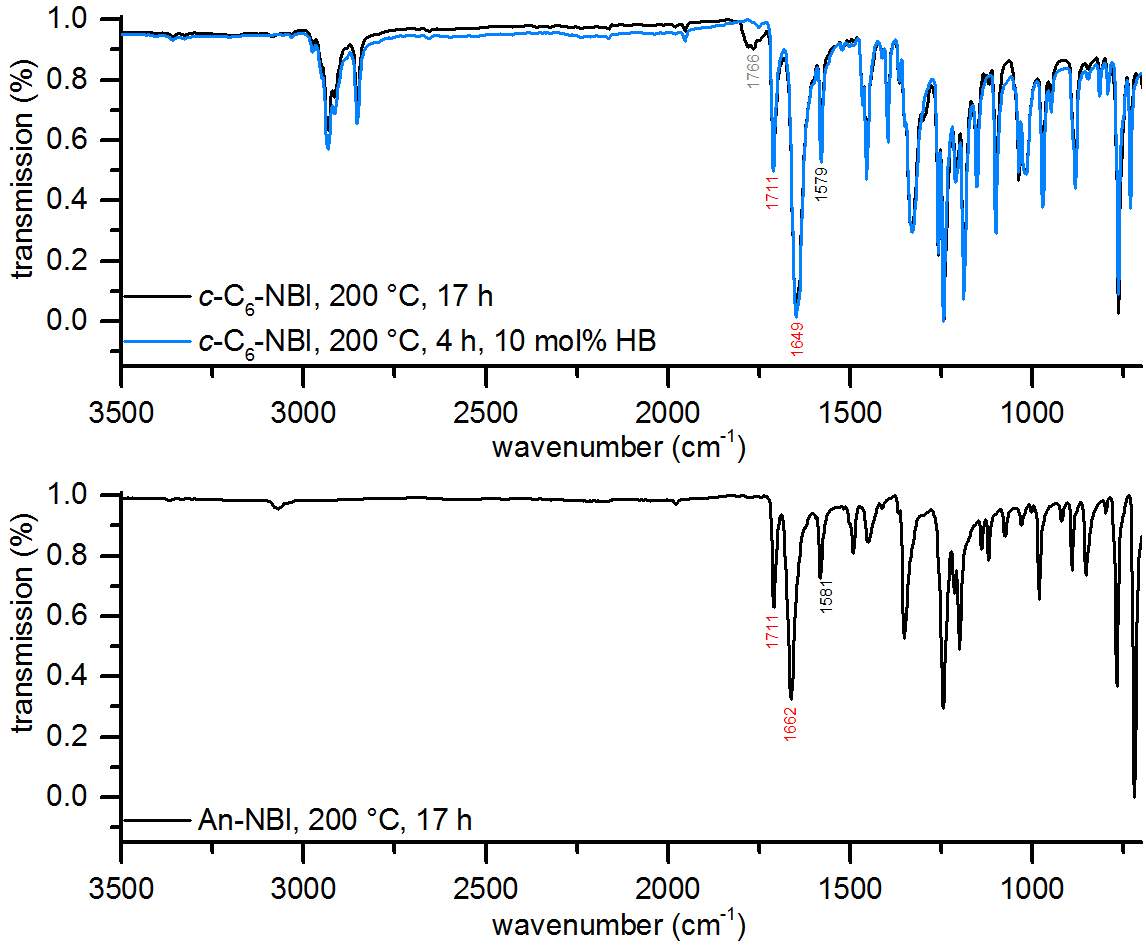


**FigureS13:** *ATR-FTIR spectra of c-$C_6$-NBI synthesized for $t_R$ = 4 h with Hünig's Base as catalyst and $t_R$ = 17, and An-NBI synthesized for $t_R$ = 17 h at 200 °C.*

### 3.6. NMR Analysis

Due to the low solubility of PBIs in organic solvents, $^1$H and $^{13}$C NMR spectra where recorded in $CDCl_3$ with d-TFA (v:v = 5:1).

For all substances we find characteristic NBI and PBI signals (see **section 3.1** for NMR codes).

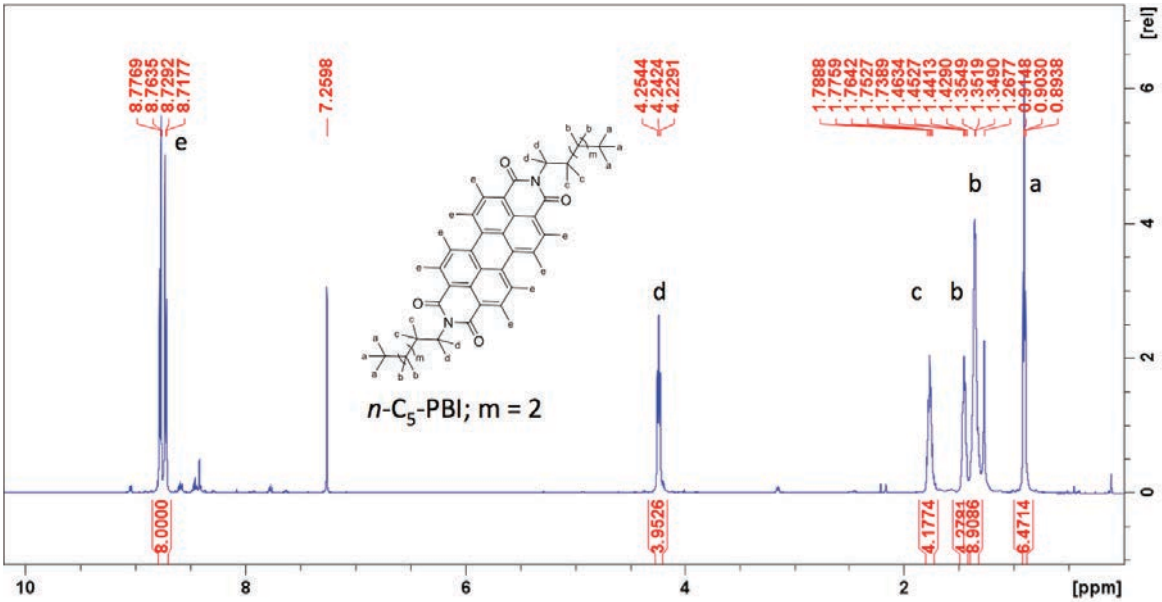


**FigureS14:** *[1]H NMR spectra of n-C$_5$-PBI, synthesized at 200 °C for 24 h.*

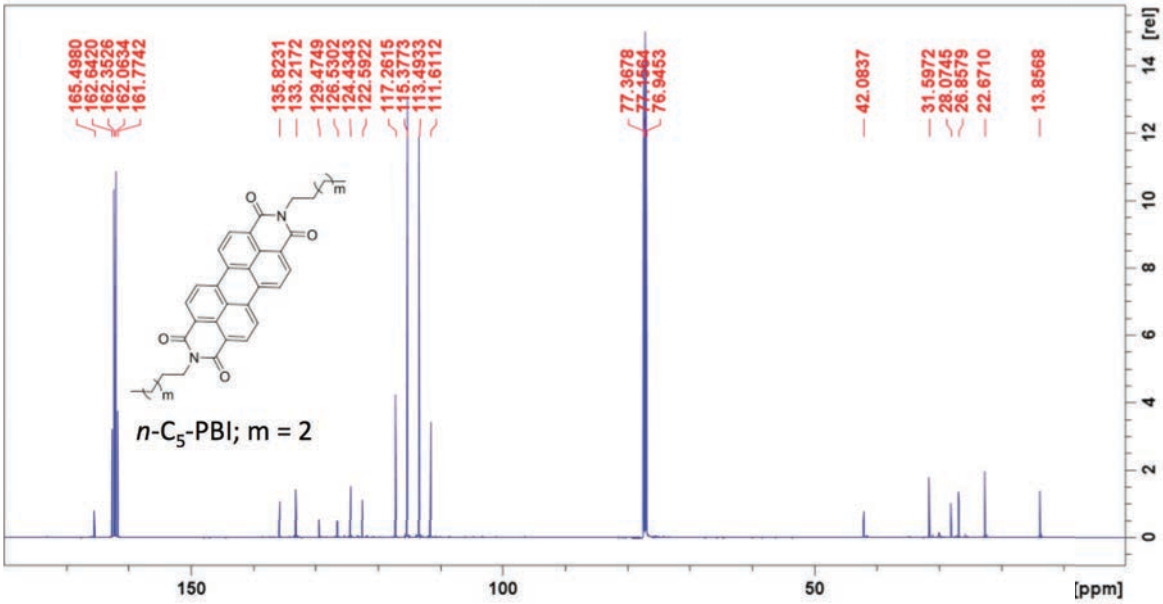


**FigureS15:** *[13]C NMR spectra of n-C$_5$-PBI, synthesized at 200 °C for 24 h.*

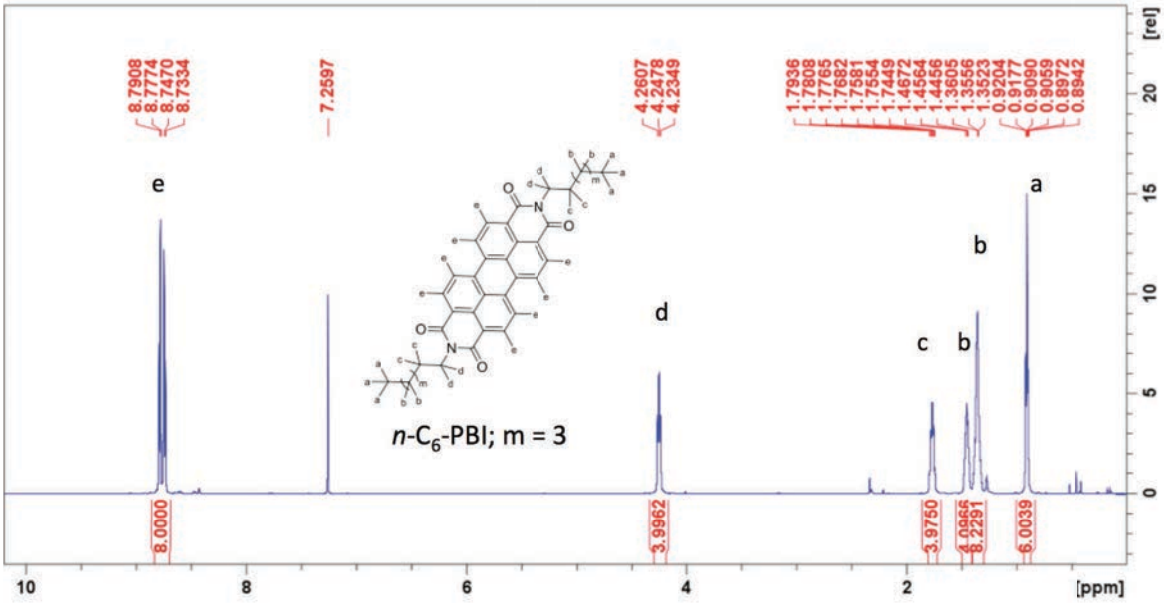


**FigureS16:** *[1]H NMR spectra of n-C$_6$-PBI, synthesized at 200 °C for 24 h.*

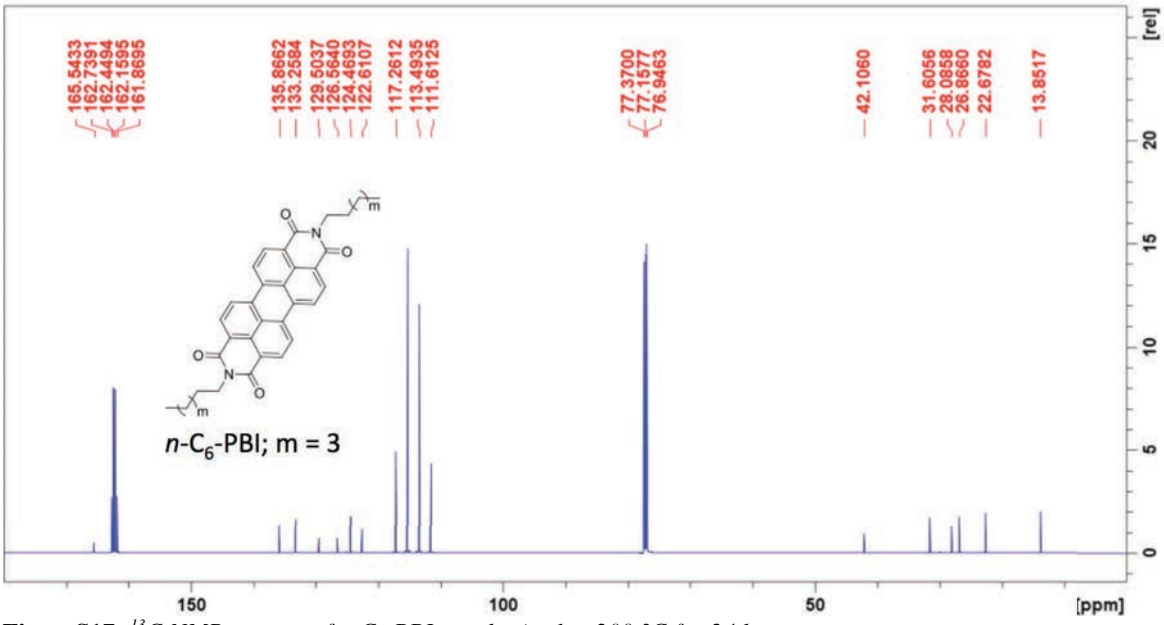


**FigureS17:** *[13]C NMR spectra of n-C$_6$-PBI, synthesized at 200 °C for 24 h.*

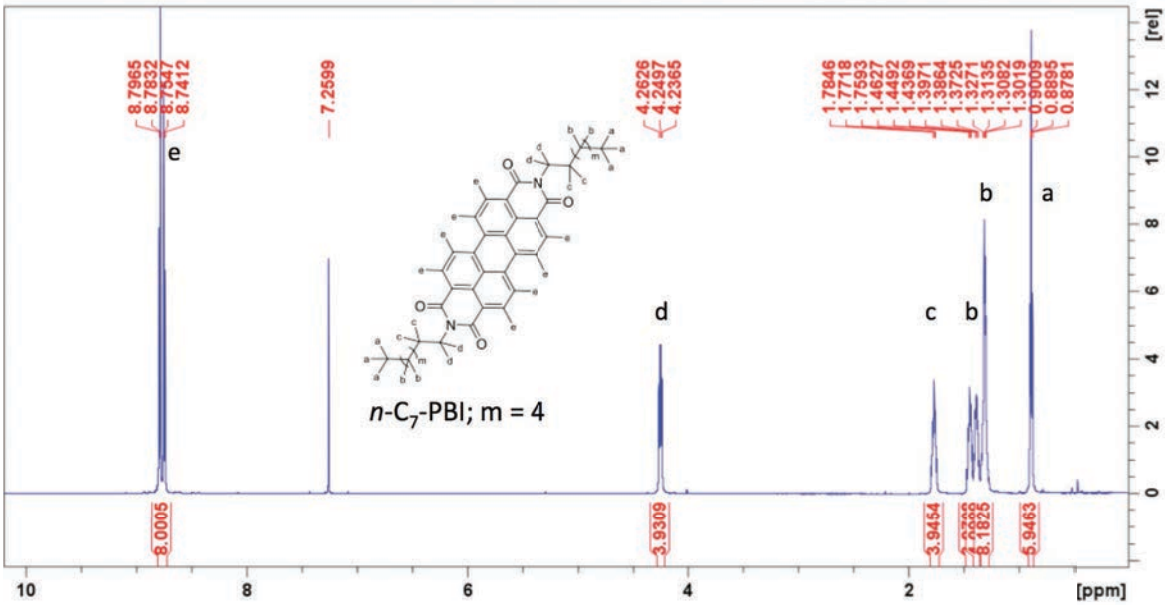


**FigureS18:** *[1]H NMR spectra of n-C7-PBI, synthesized at 200 °C for 24 h.*

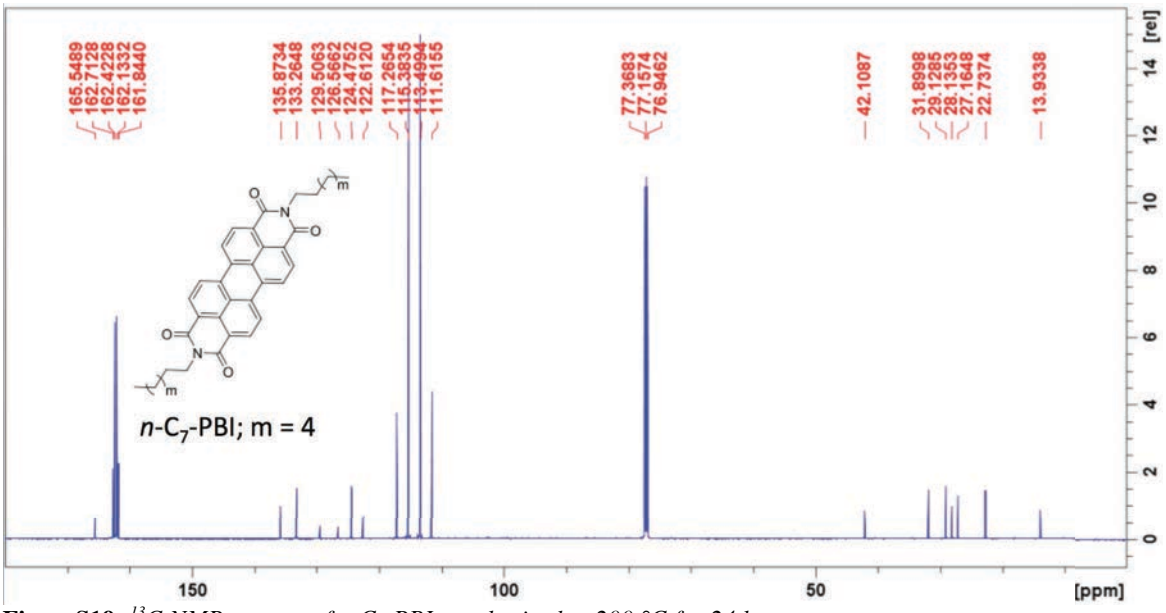


**FigureS19:** *[13]C NMR spectra of n-C7-PBI, synthesized at 200 °C for 24 h.*

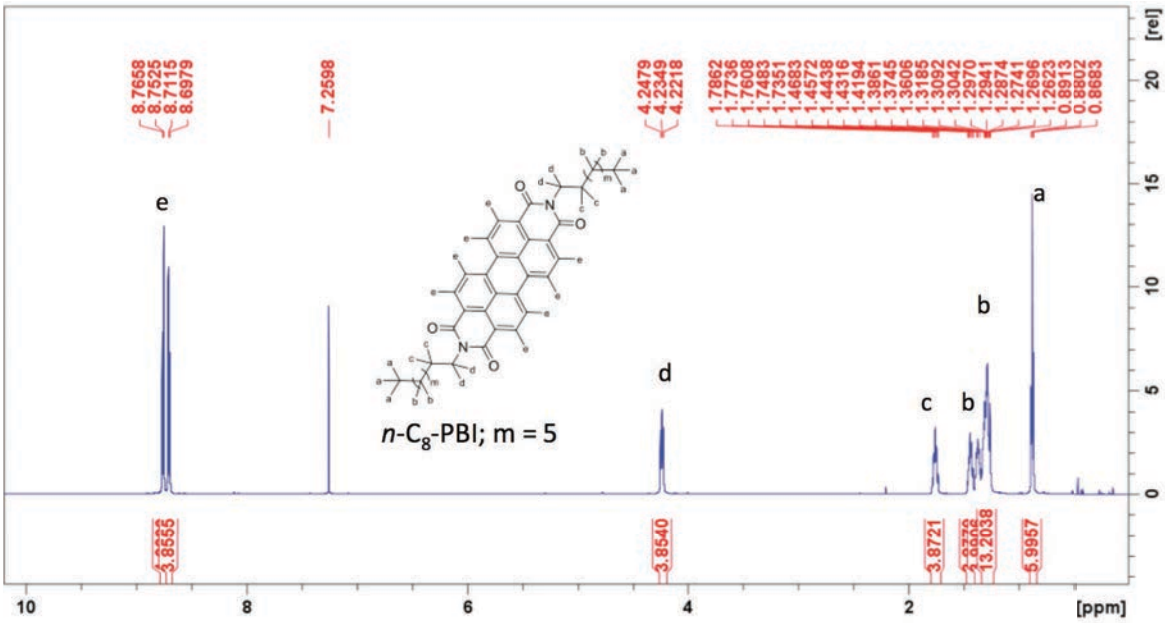


**FigureS20:** *[1]H NMR spectra of n-C8-PBI, synthesized at 200 °C for 24 h.*

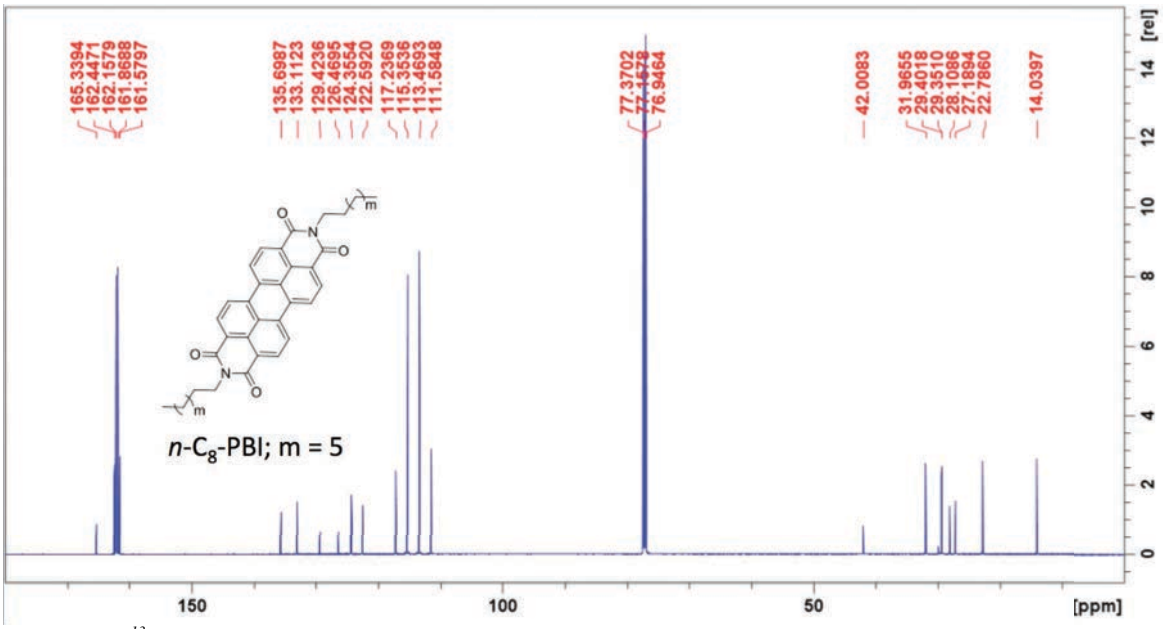


**FigureS21:** *[13]C NMR spectra of n-C8-PBI, synthesized at 200 °C for 24 h.*

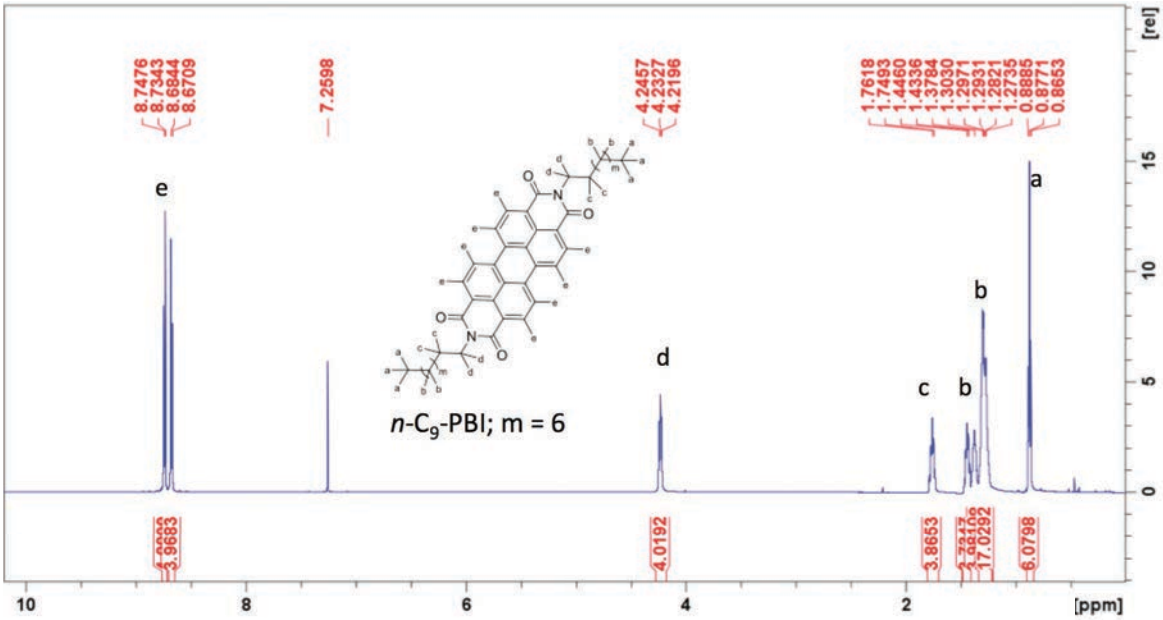


**FigureS22:** *$^{1}$H NMR spectra of n-$C_9$-PBI, synthesized at 200 °C for 24 h.*

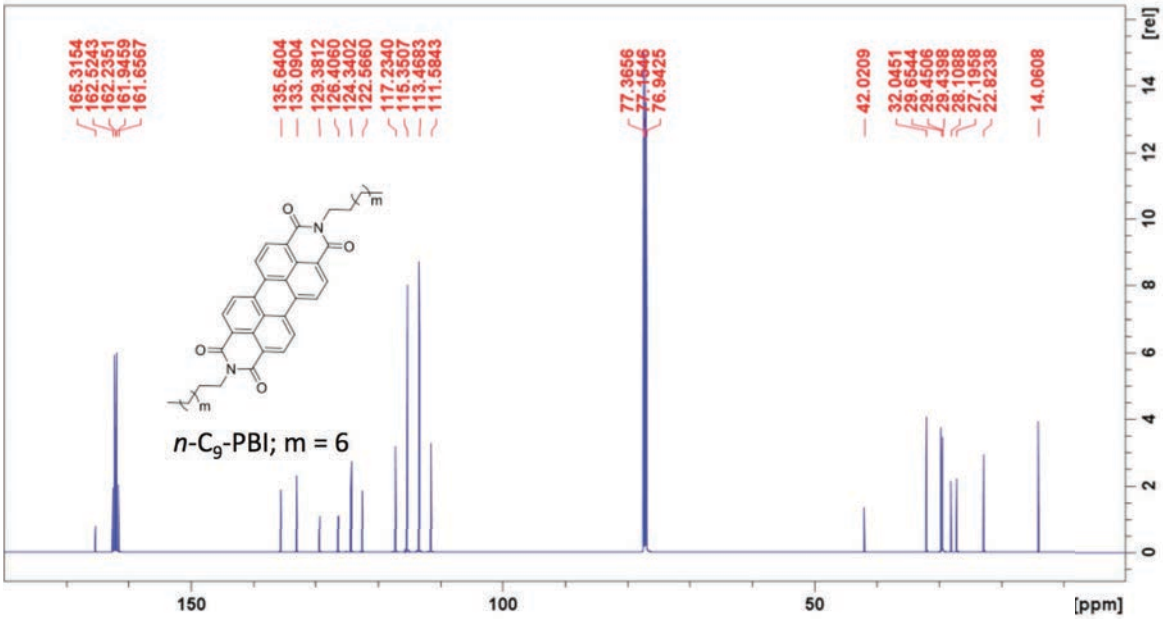


**FigureS23:** *$^{13}$C NMR spectra of n-$C_9$-PBI, synthesized at 200 °C for 24 h.*

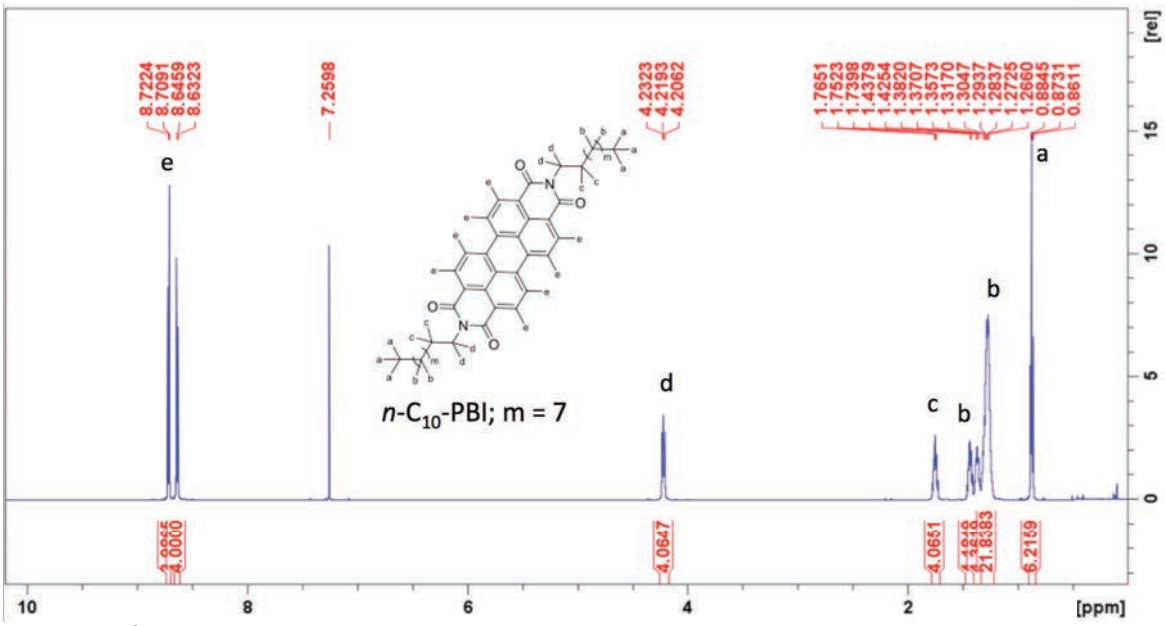


**FigureS24:** *$^{1}$H NMR spectra of n-$C_{10}$-PBI, synthesized at 200 °C for 24 h.*

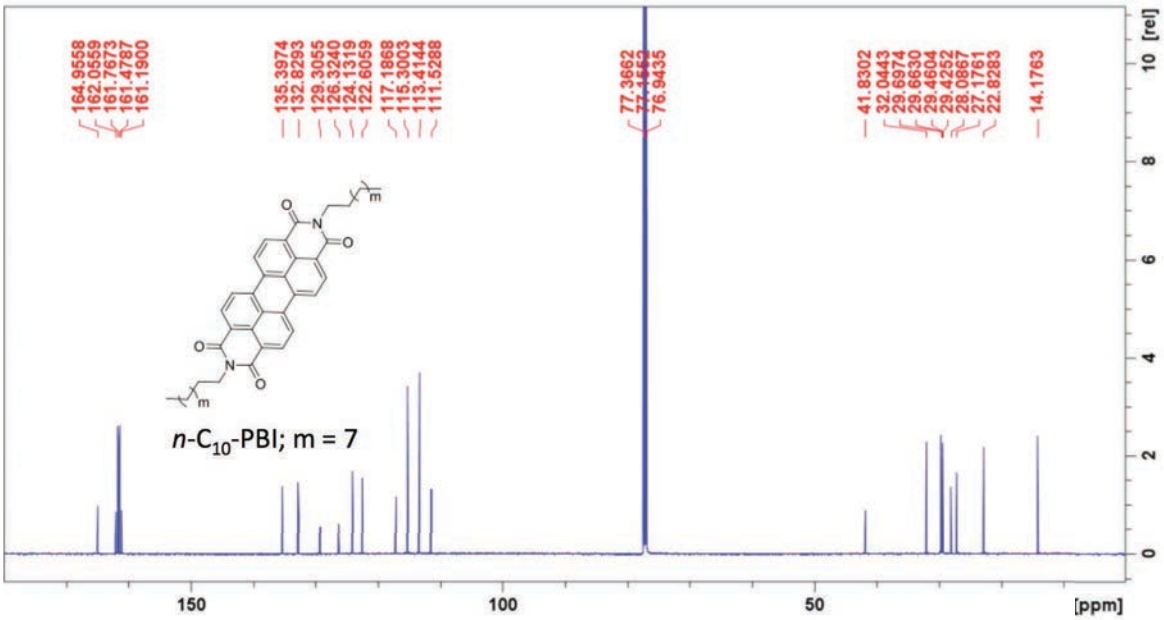


**FigureS25:** *$^{13}$C NMR spectra of n-$C_{10}$-PBI, synthesized at 200 °C for 24 h.*

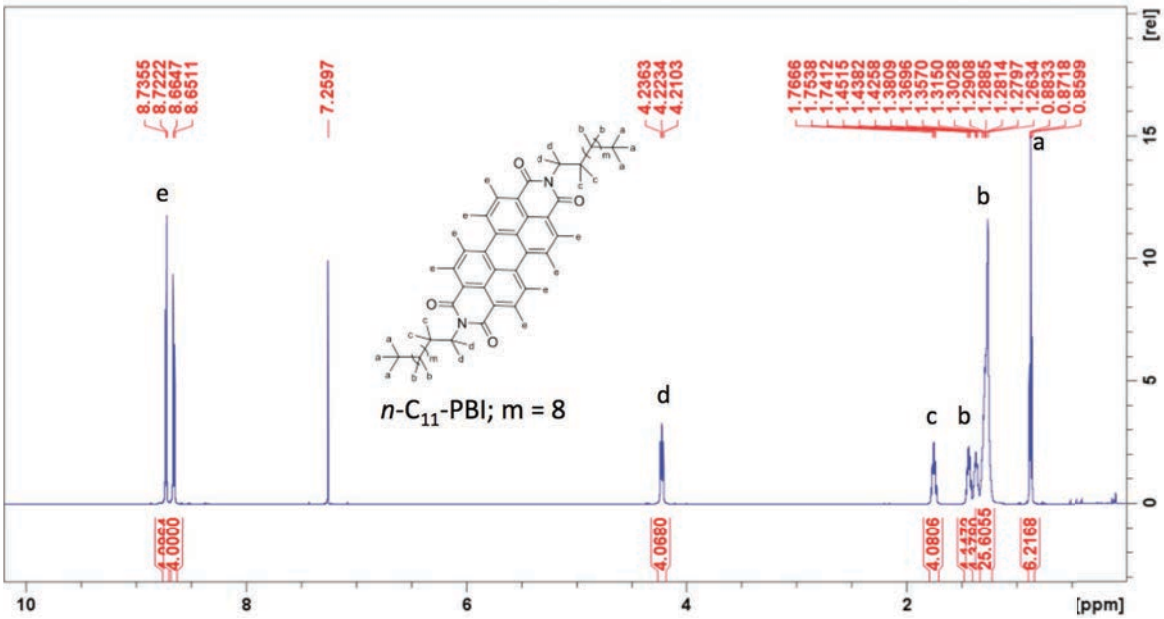


**FigureS26:** *[1]H NMR spectra of n-C11-PBI, synthesized at 200 °C for 24 h.*

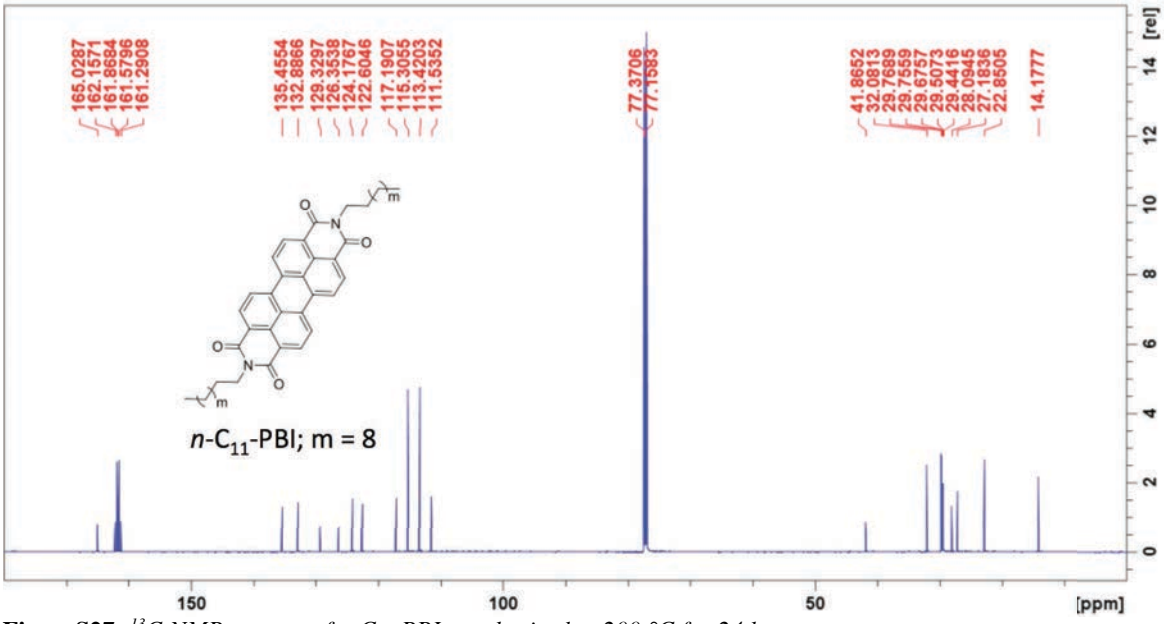


**FigureS27:** *[13]C NMR spectra of n-C11-PBI, synthesized at 200 °C for 24 h.*

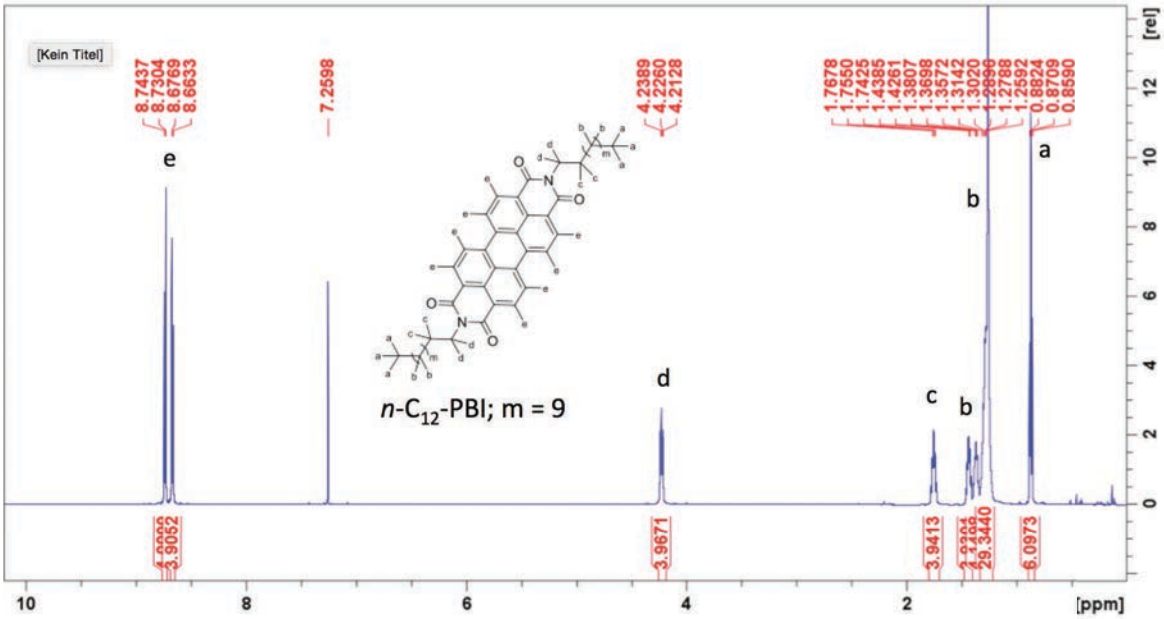


**FigureS28:** *[1]H NMR spectra of n-$C_{12}$-PBI, synthesized at 200 °C for 24 h.*

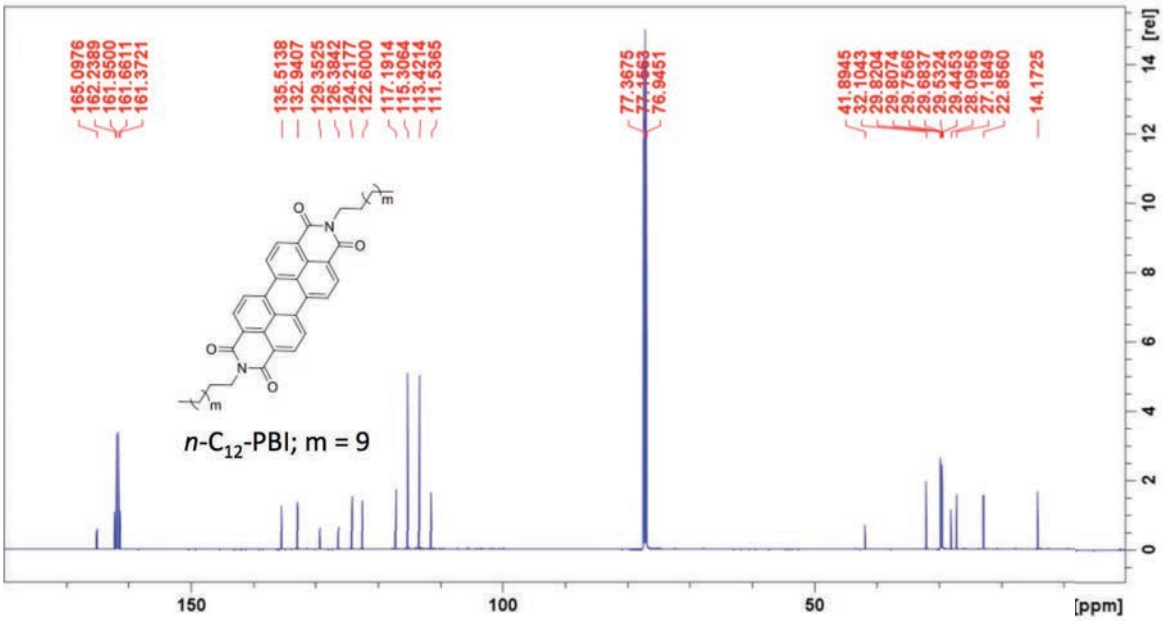


**FigureS29:** *[13]C NMR spectra of n-$C_{12}$-PBI, synthesized at 200 °C for 24 h.*

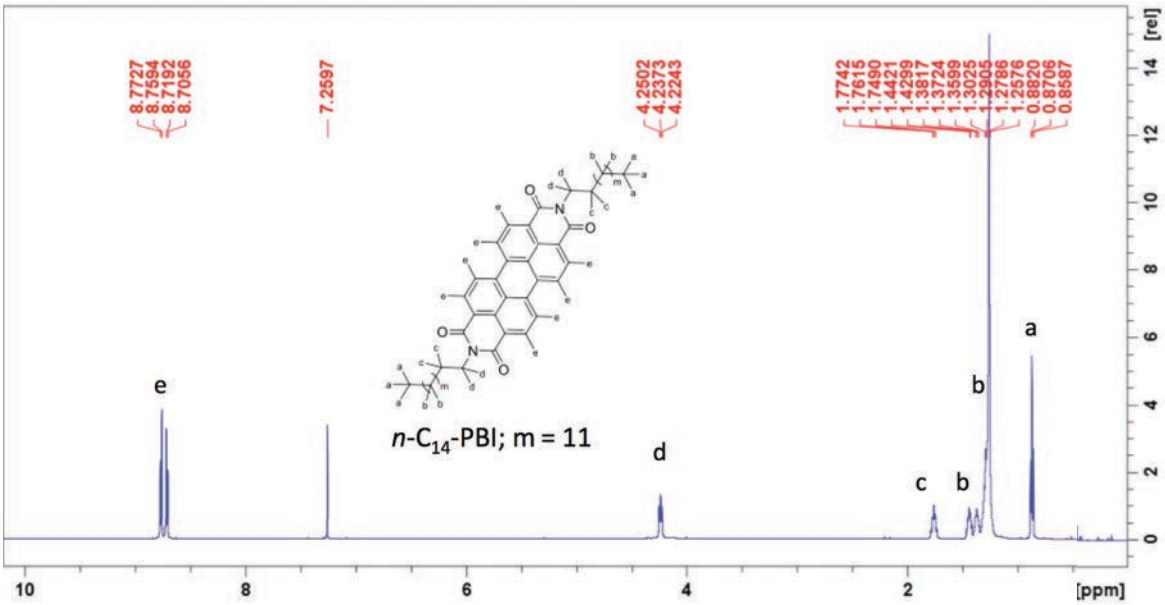


**FigureS30:** *[1]H NMR spectra of n-C$_{14}$-PBI, synthesized at 200 °C for 24 h.*

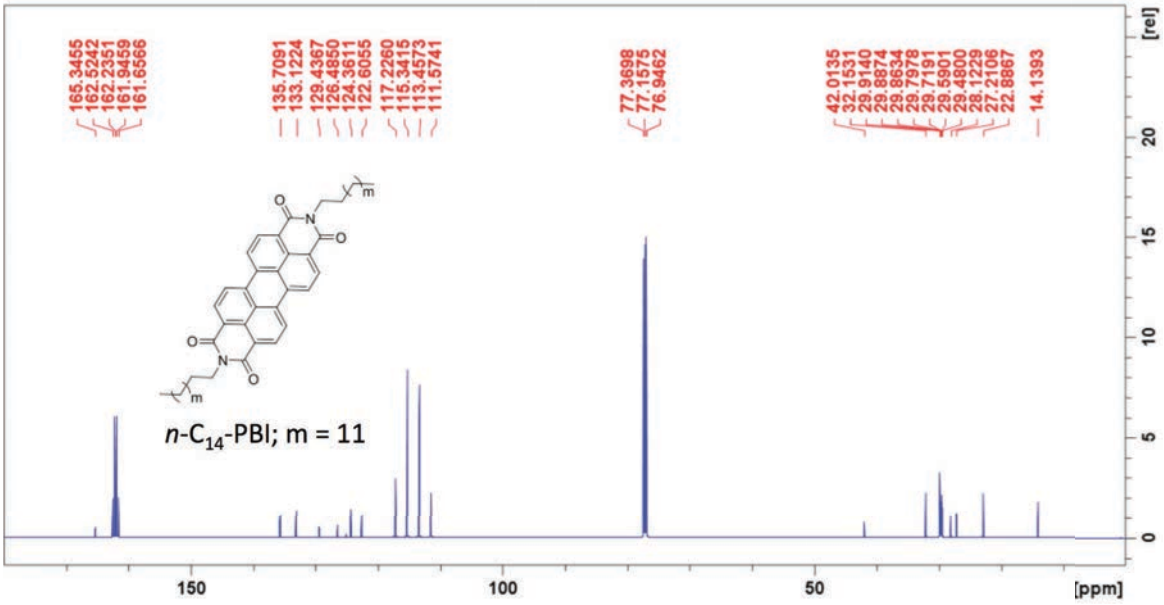


**FigureS31:** *[13]C NMR spectra of n-C$_{14}$-PBI, synthesized at 200 °C for 24 h.*

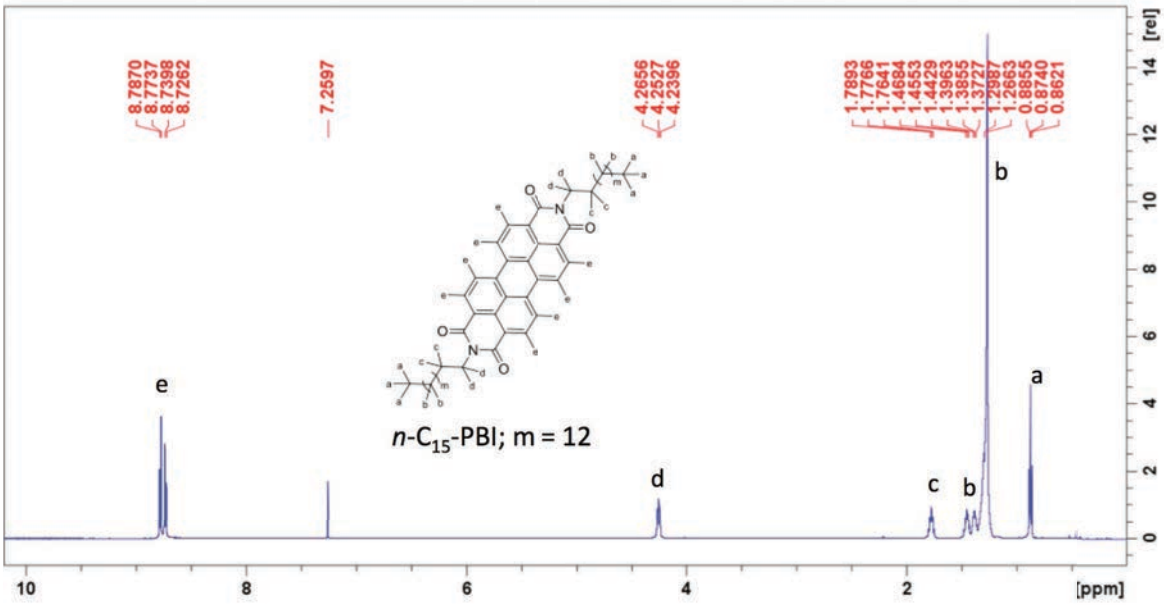


**FigureS32:** *$^{1}$H NMR spectra of n-$C_{15}$-PBI, synthesized at 200 °C for 24 h.*

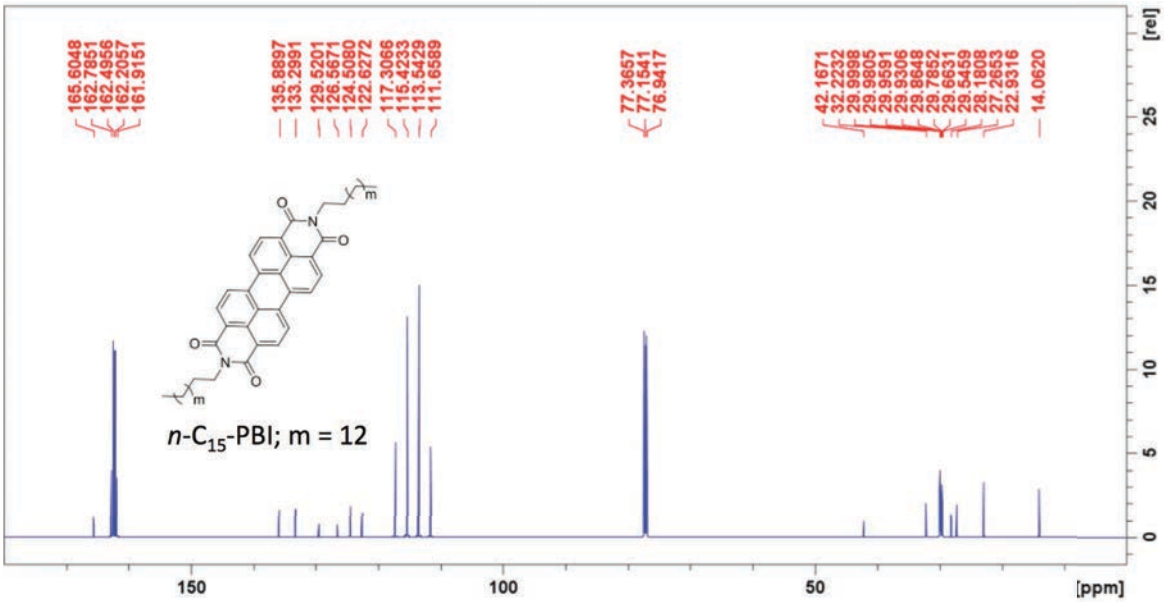


**FigureS33:** *$^{13}$C NMR spectra of n-$C_{15}$-PBI, synthesized at 200 °C for 24 h.*

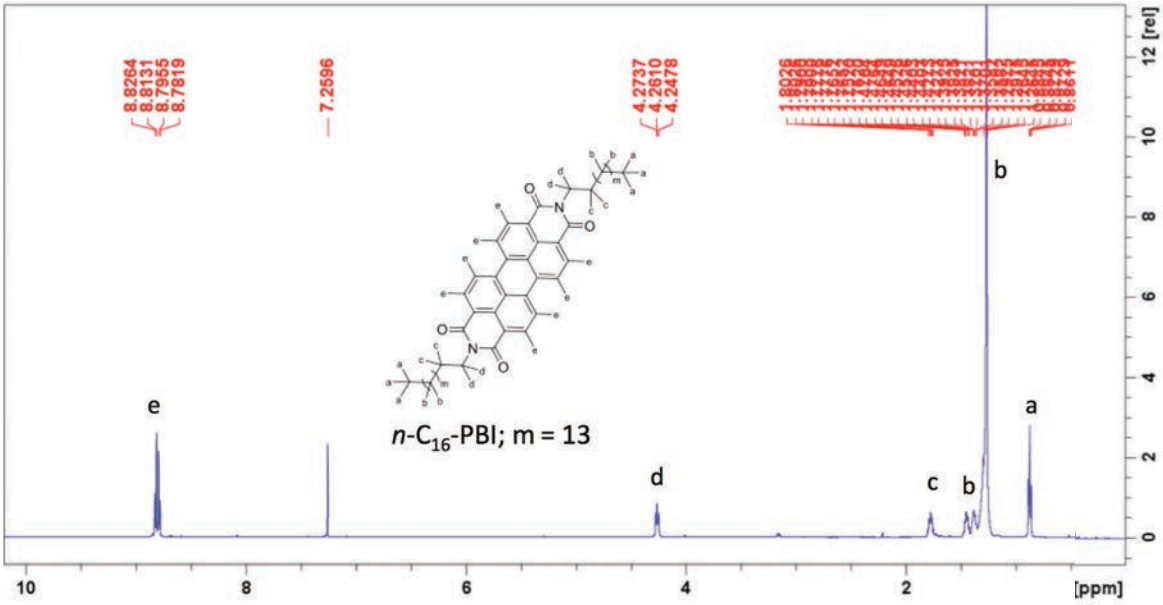


**FigureS34:** *[1]H NMR spectra of n-$C_{16}$-PBI, synthesized at 200 °C for 24 h.*

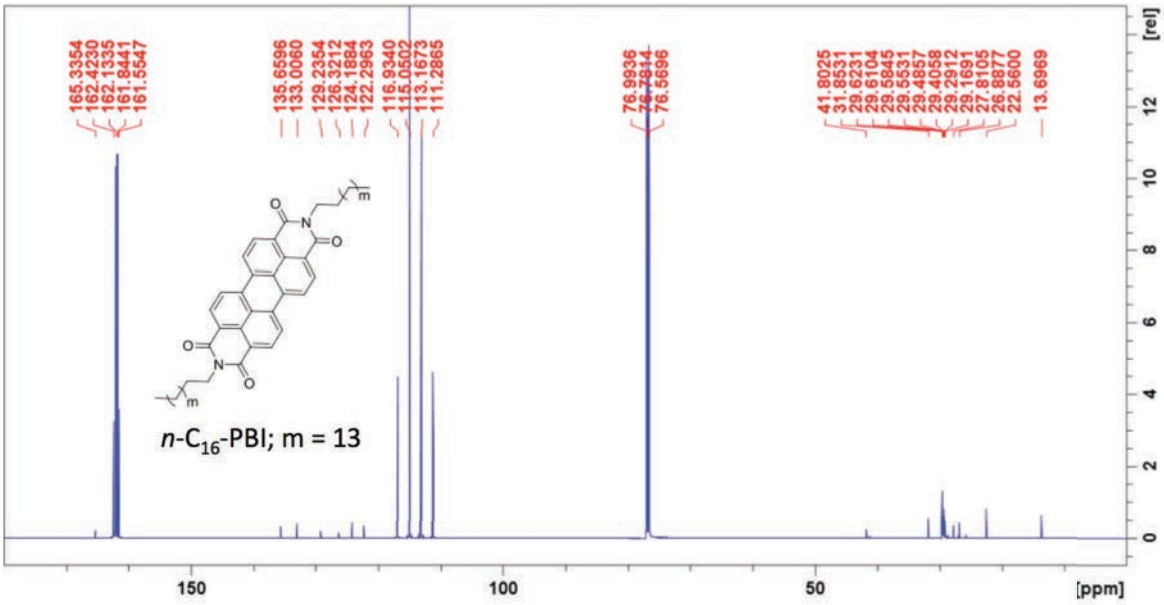


**FigureS35:** *[13]C NMR spectra of n-$C_{16}$-PBI, synthesized at 200 °C for 24 h.*

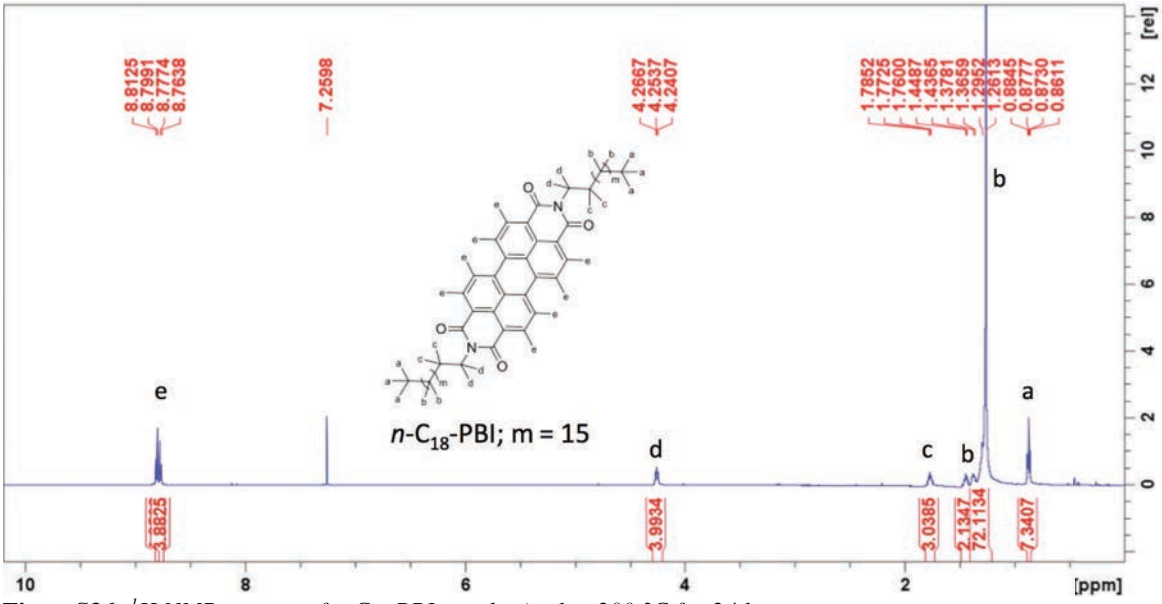


**FigureS36:** *$^{1}H$ NMR spectra of n-$C_{18}$-PBI, synthesized at 200 °C for 24 h.*

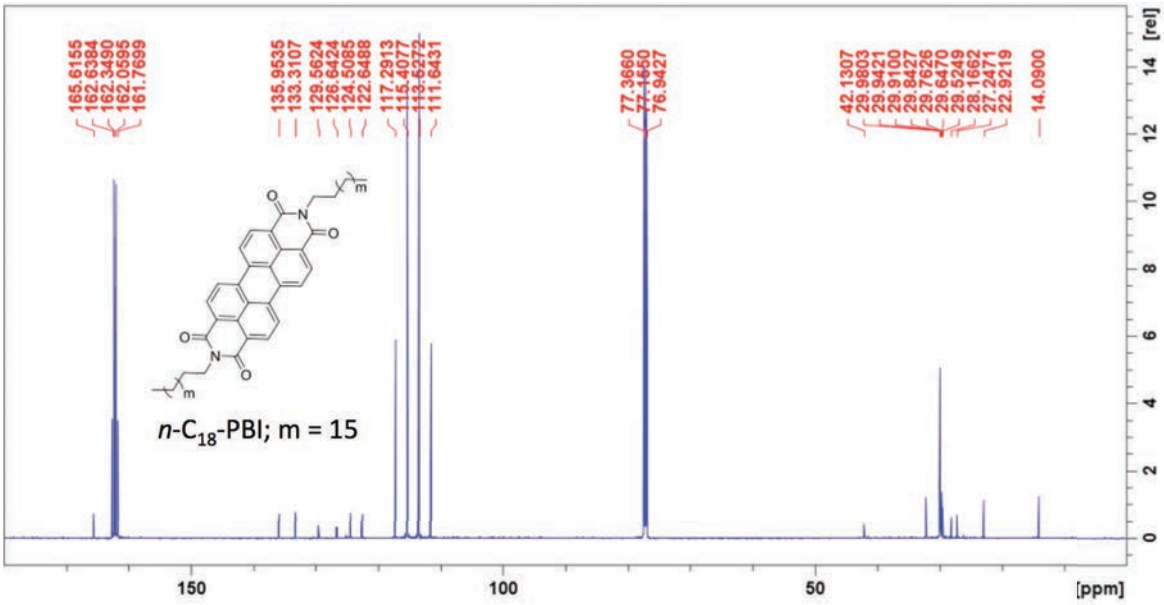


**FigureS37:** *$^{13}C$ NMR spectra of n-$C_{18}$-PBI, synthesized at 200 °C for 24 h.*

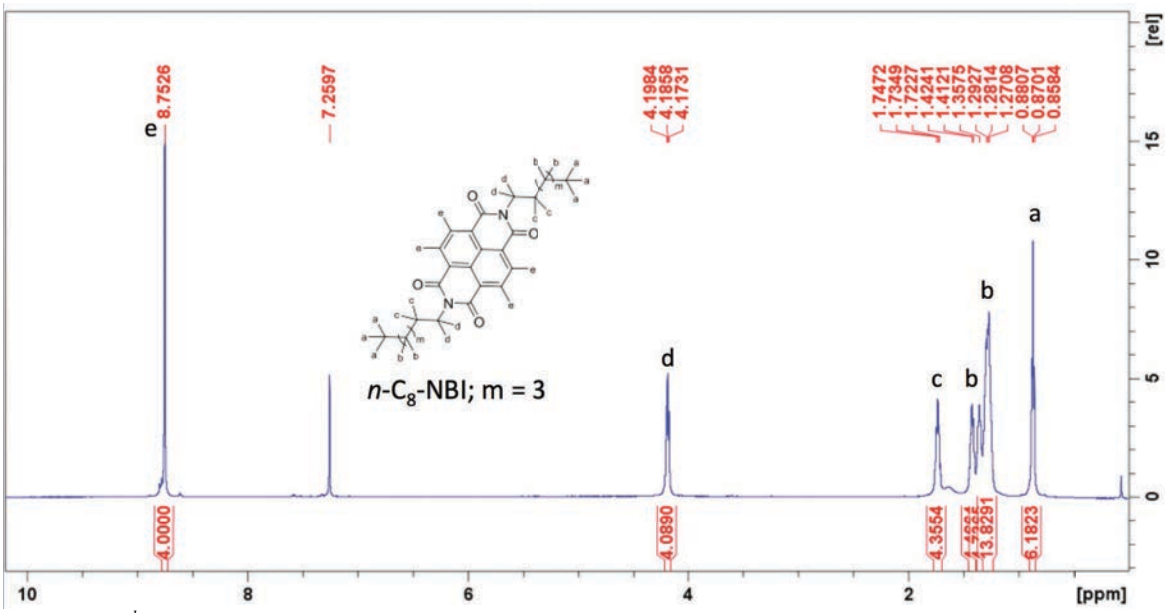


**FigureS38:** *[1]H NMR spectra of n-C8-NBI.*

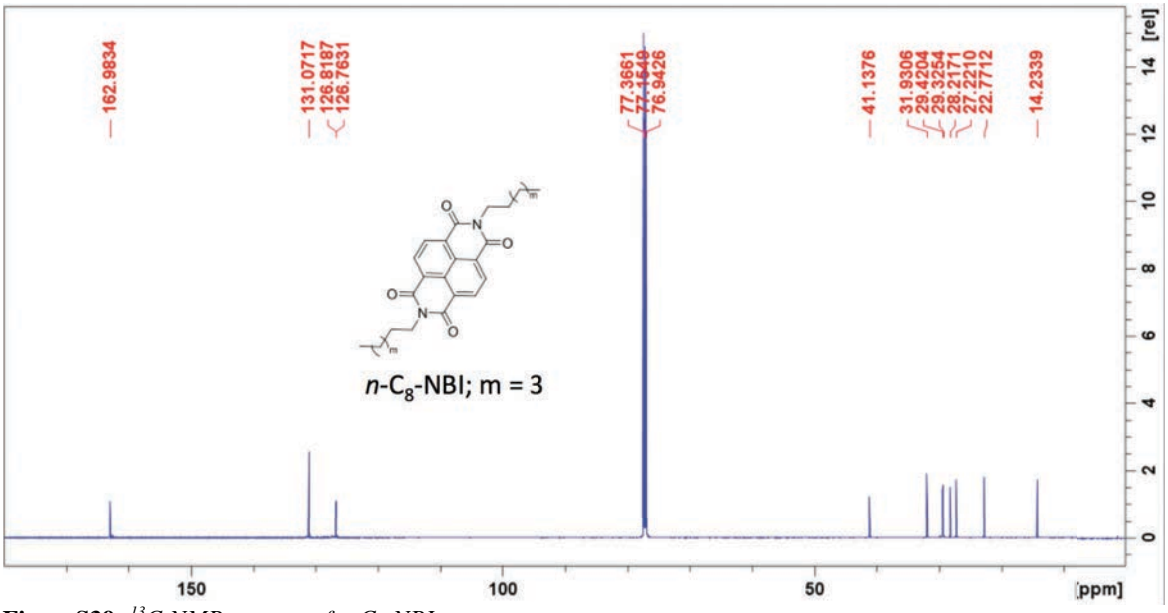


**FigureS39:** *[13]C NMR spectra of n-C8-NBI.*

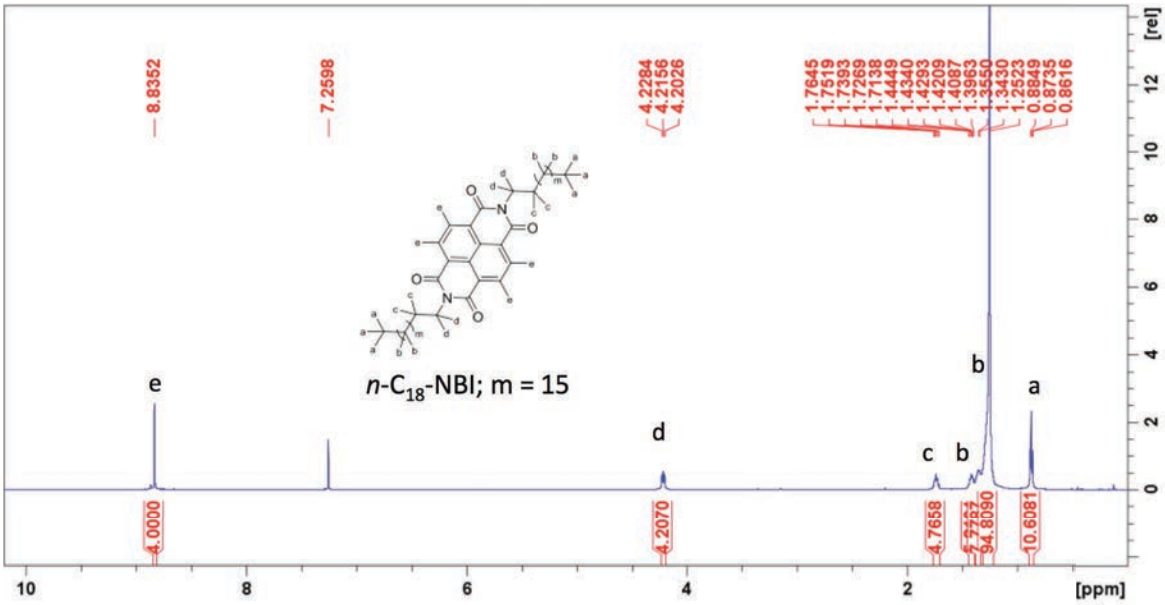


**FigureS40:** *[1]H NMR spectra of n-C$_{18}$-NBI.*

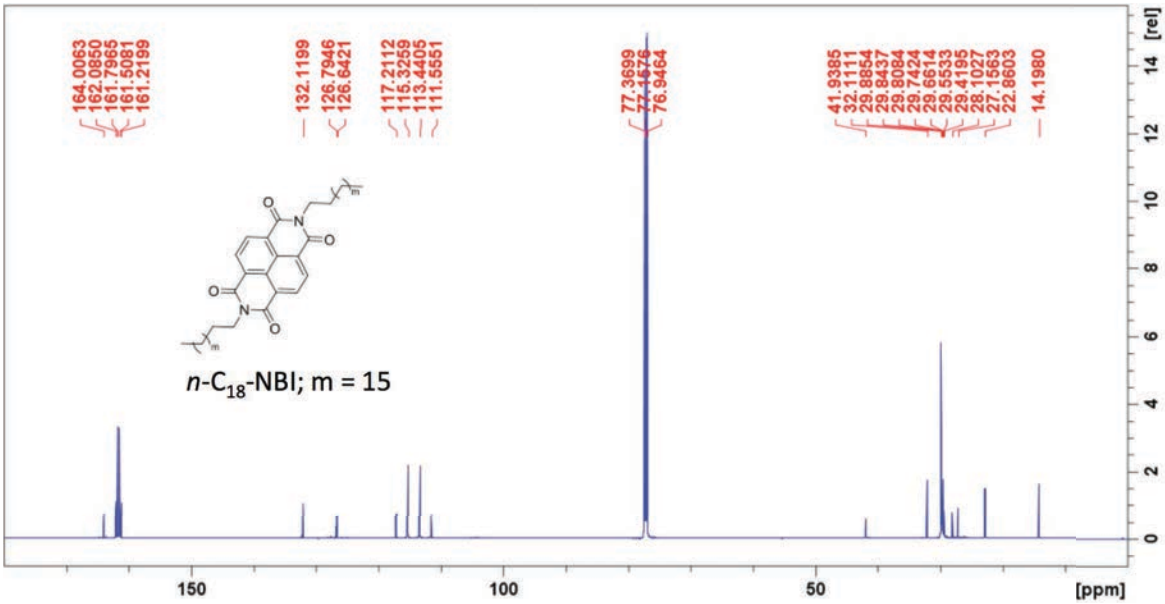


**FigureS41:** *[13]C NMR spectra of n-C$_{18}$-NBI.*

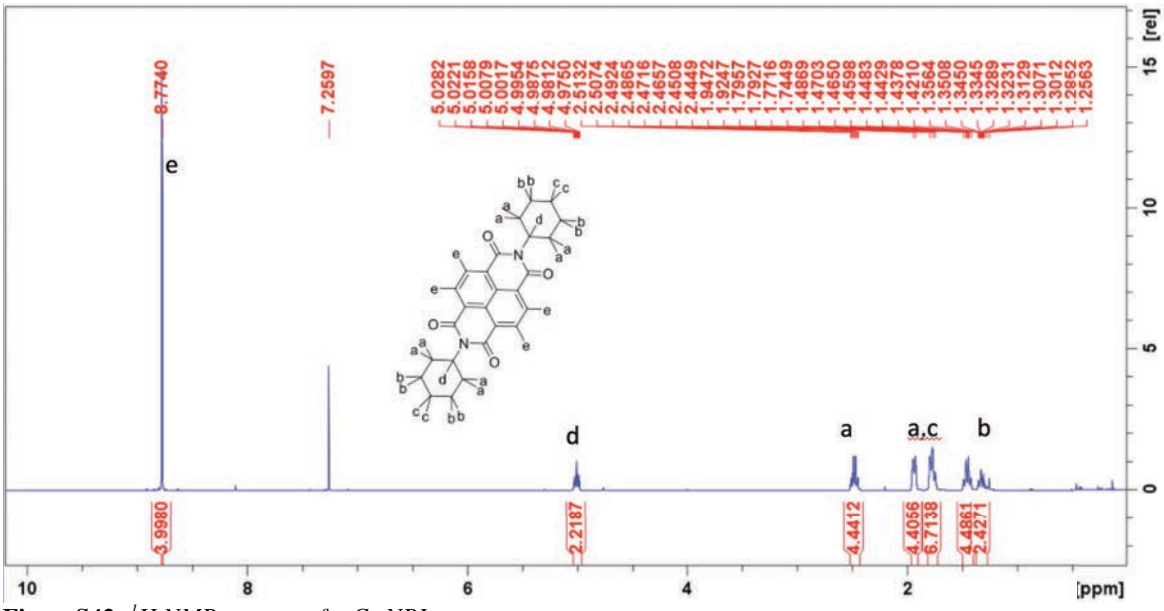


**FigureS42:** *[1]H NMR spectra of c-C$_6$-NBI.*

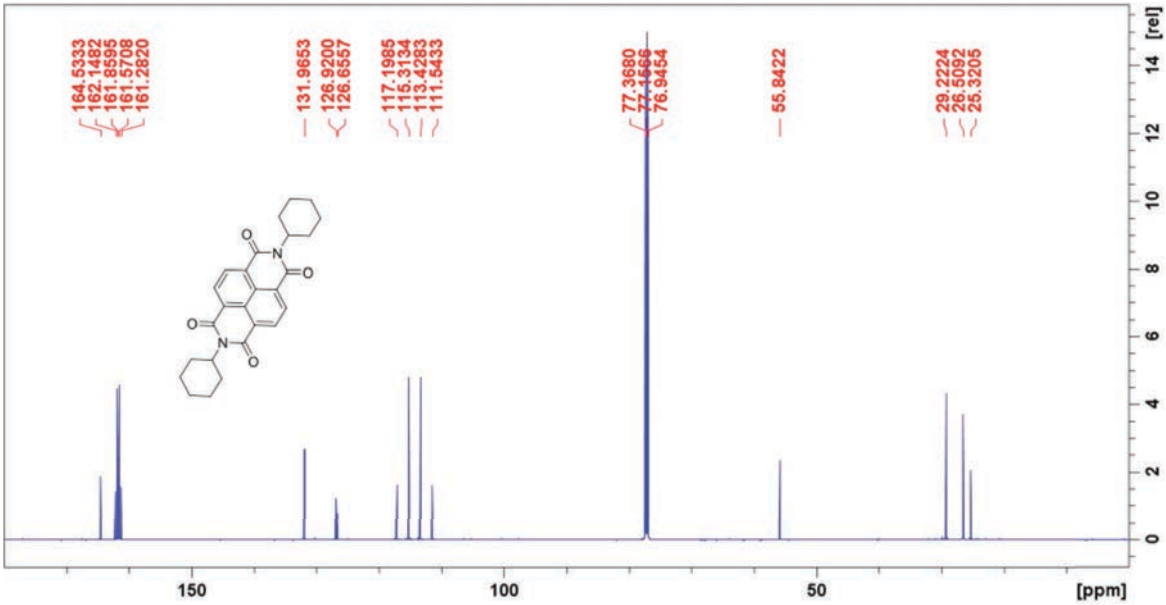


**FigureS43:** *[13]C NMR spectra of c-C$_6$-NBI.*

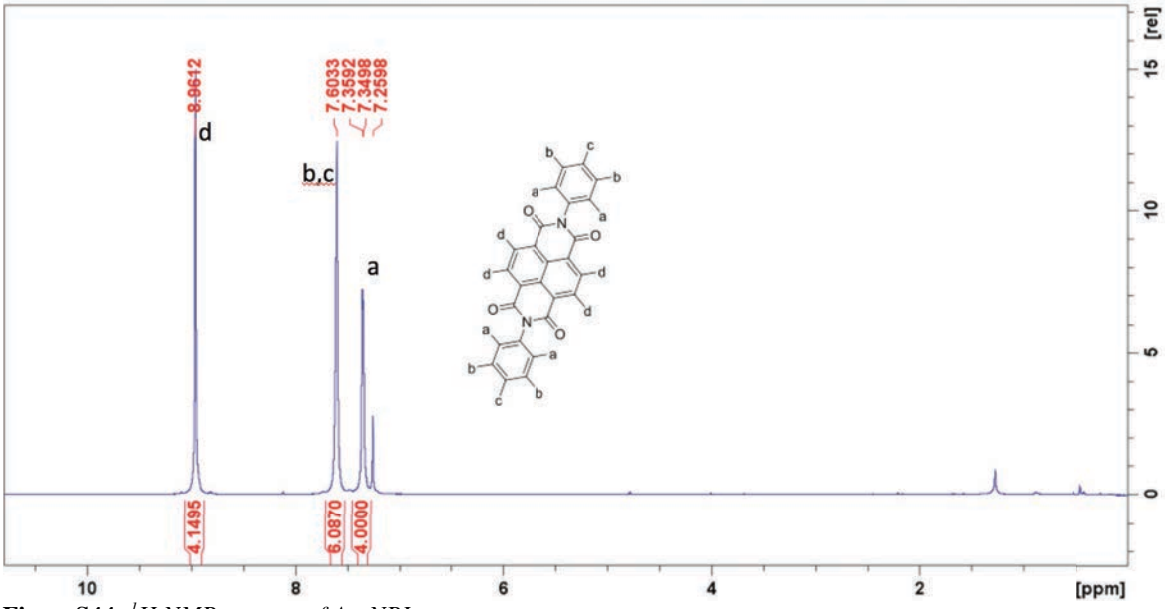


**FigureS44:** *$^{1}H$ NMR spectra of An-NBI.*

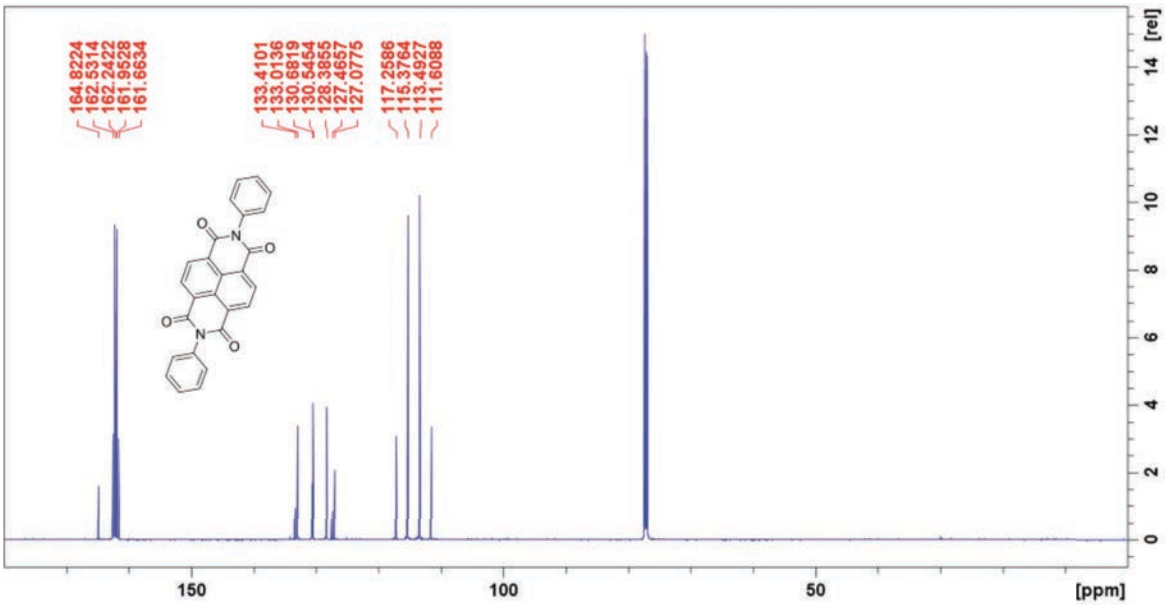


**FigureS45:** *$^{13}C$ NMR spectra of An-NBI.*

### 3.7. UV/VIS and Fluorescence Spectroscopy

FigureS46 and FigureS47 show absorption and emission spectra of crude PBIs synthesized at 200 °C for 24 h. Measurements were performed in either $CH_2Cl_2$ or $CHCl_3$ at concentrations of 0.1 – 1 nmol $L^{-1}$. Emission spectra were recorded at excitation wavelengths of 497 nm for samples in $CH_2Cl_2$ and 499 nm for $CHCl_3$ between 499 and 670 nm.

For all spectra we find peaks in absorbance (458 nm, 490 nm, 526 nm) and fluorescence (533 nm, 574 nm, 624 nm in $CH_2Cl_2$ or 530, 572, 620 nm in $CHCl_3$).

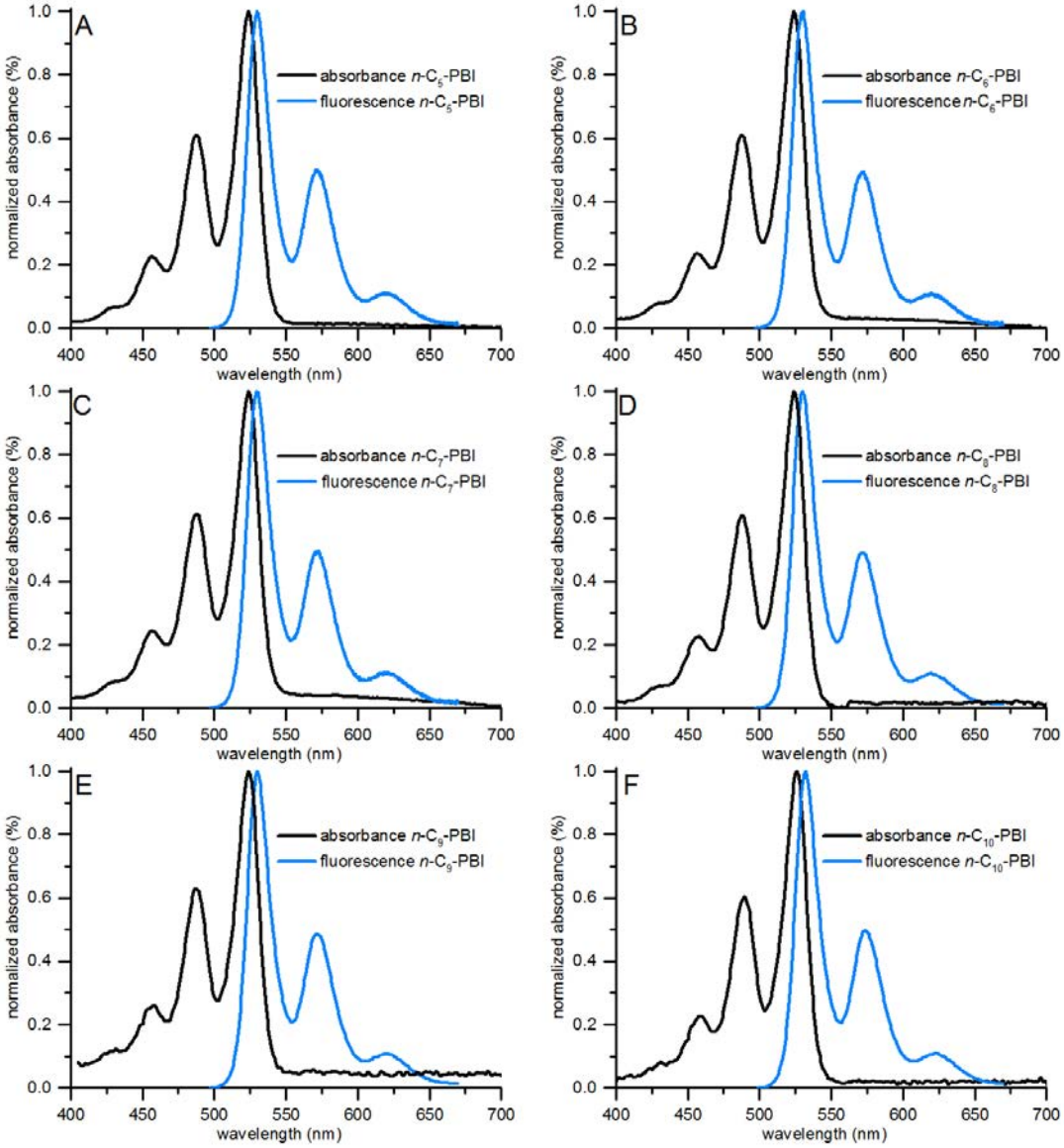


**FigureS46:** *UV/Vis and Fluorescence spectra of PBIs in $CH_2Cl_2$.*

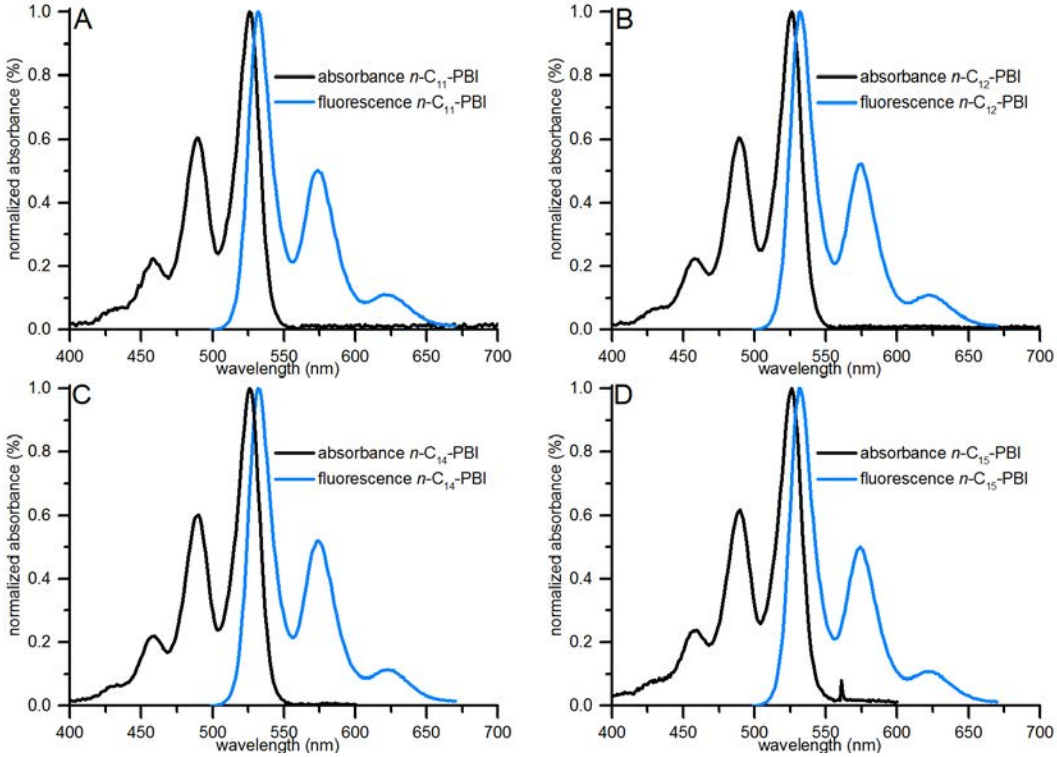


**FigureS47:** *UV/Vis and Fluorescence spectra of PBIs in $CHCl_3$.*

### 3.8. Quantum Yield

Quantum Yields were obtained by comparative method with Fluorescein ($\Phi_{Fluorescin}$ = 0.79 in 0.1 M NaOH) as standard.[S28,S29,S30] Therefore, three samples of Fluorescein and PBIs with different absorbance between 0.01 and 0.1 were prepared. Fluorescence spectra were recorded between 499 and 670 nm at excitation wavelength 489 nm. From these spectra, the integrated fluorescence intensity was calculated and plotted against the absorbance of the solution absorbance at the excitation wavelength. The magnitude of the resulting plot was inserted into equation (1).

$$\Phi F = \Phi_{St} \cdot \frac{m}{m_R} \cdot \left(\frac{n}{n_R}\right)^2 \qquad (1)$$

| | |
|---|---|
| $\Phi_F$ | Quantum Yield |
| $\Phi_{St}$ | Quantum Yield of Standard ($\Phi_{Fluorescein}$ = 0.79 in 0.1 M NaOH) |
| m | slope of of the line obtained from the plot of the integrated fluorescence intensity vs. absorbance |
| n | refractive index (n($CHCl_3$) = 1.445, n($CH_2Cl_2$) = 1.4242, n(0.1 M NaOH) = 1.33) |

**TableS4**: *Quantum yield of PBIs synthesized at 200 °C for 24 h.*

| | solvent | $\Phi_F$ |
|---|---|---|
| *n*-$C_5$-PBI | $CH_2Cl_2$ | 1.03 ± 0.05 |
| *n*-$C_6$-PBI | $CH_2Cl_2$ | 1.05 ± 0.06 |
| *n*-$C_7$-PBI | $CH_2Cl_2$ | 1.04 ± 0.06 |
| *n*-$C_8$-PBI | $CH_2Cl_2$ | 1.05 ± 0.08 |
| *n*-$C_9$-PBI | $CH_2Cl_2$ | 1.03 ± 0.16 |
| *n*-$C_{10}$-PBI | $CHCl_3$ | 1.01 ± 0.05 |
| *n*-$C_{11}$-PBI | $CHCl_3$ | 0.99 ± 0.09 |
| *n*-$C_{12}$-PBI | $CHCl_3$ | 1.01 ± 0.03 |
| *n*-$C_{14}$-PBI | $CHCl_3$ | 1.04 ± 0.02 |
| *n*-$C_{15}$-PBI | $CHCl_3$ | 0.98 ± 0.01 |
| | | |
| *c*-$C_6$-PBI | $CHCl_3$ | 0.97 ± 0.07 |

### 3.9. Powder X-ray Diffraction

Powder X-ray patterns of crude *n*-$C_x$-PBI (x = 5-12, 14, 15, 16, 18) synthesized at 200 °C for 24 h are depicted in **FigureS48**, **FigureS49** and **FigureS50**. Reflections that correspond to unreacted PBA are found in the pattern of *n*-$C_6$-PBI, *n*-$C_7$-PBI, *n*-$C_{11}$-PBI, *n*-$C_{12}$-PBI, *n*-$C_{16}$-PBI and *n*-$C_{18}$-PBI and are assigned with an asterisk.

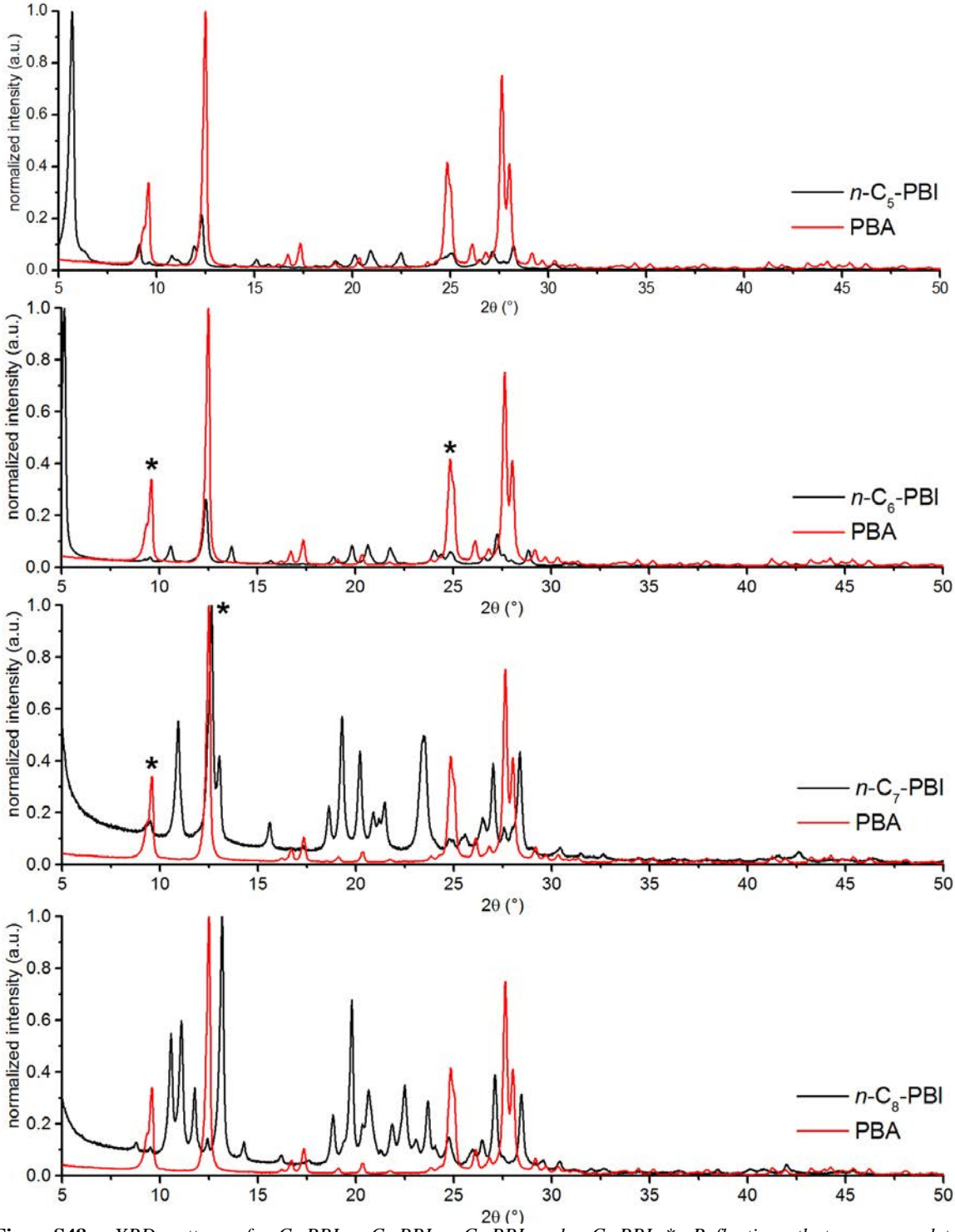


**FigureS48:** *pXRD pattern of n-$C_5$-PBI, n-$C_6$-PBI, n-$C_7$-PBI and n-$C_7$-PBI. *: Reflections that correspond to unreacted PBA.*

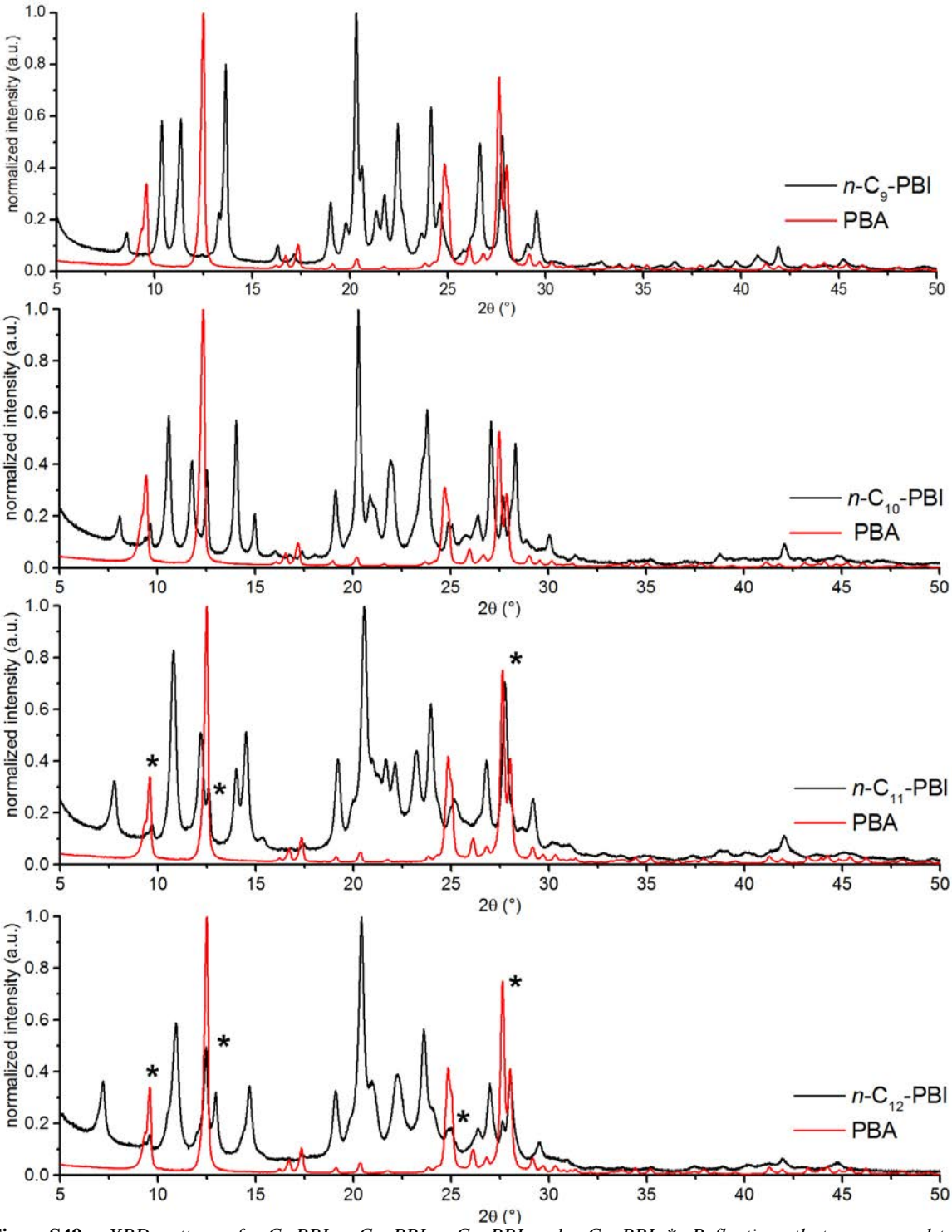


**FigureS49:** *pXRD pattern of n-$C_9$-PBI, n-$C_{10}$-PBI, n-$C_{11}$-PBI and n-$C_{12}$-PBI. *: Reflections that correspond to unreacted PBA.*

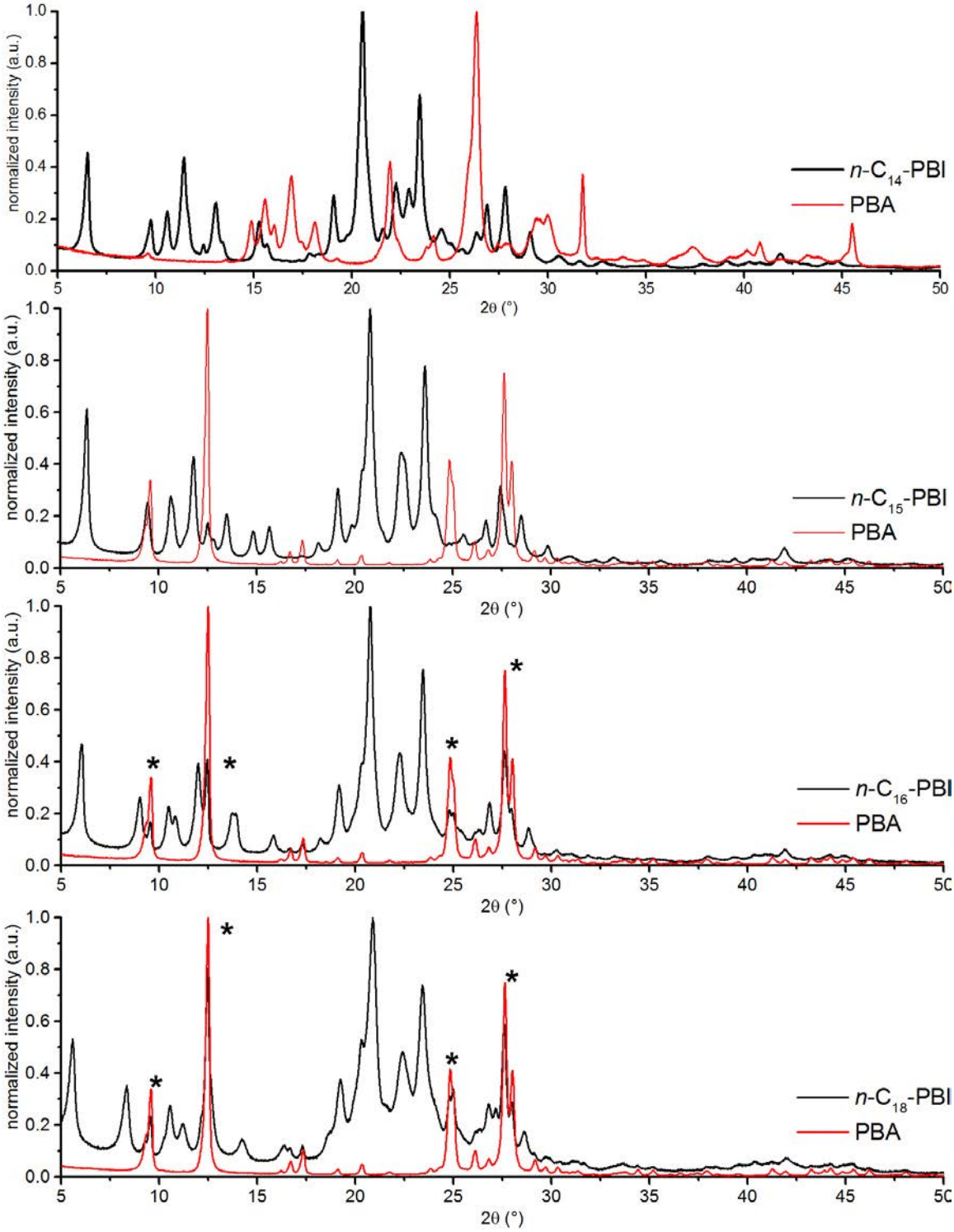


**FigureS50:** *pXRD pattern of n-$C_{14}$-PBI, n-$C_{15}$-PBI, n-$C_{16}$-PBI and n-$C_{18}$-PBI. *: Reflections that correspond to unreacted PBA.*

**FigureS51** shows pXRD patterns of *n-$C_8$-NBI, n-$C_{18}$-NBI, c-$C_6$-NBI and An-NBI*.

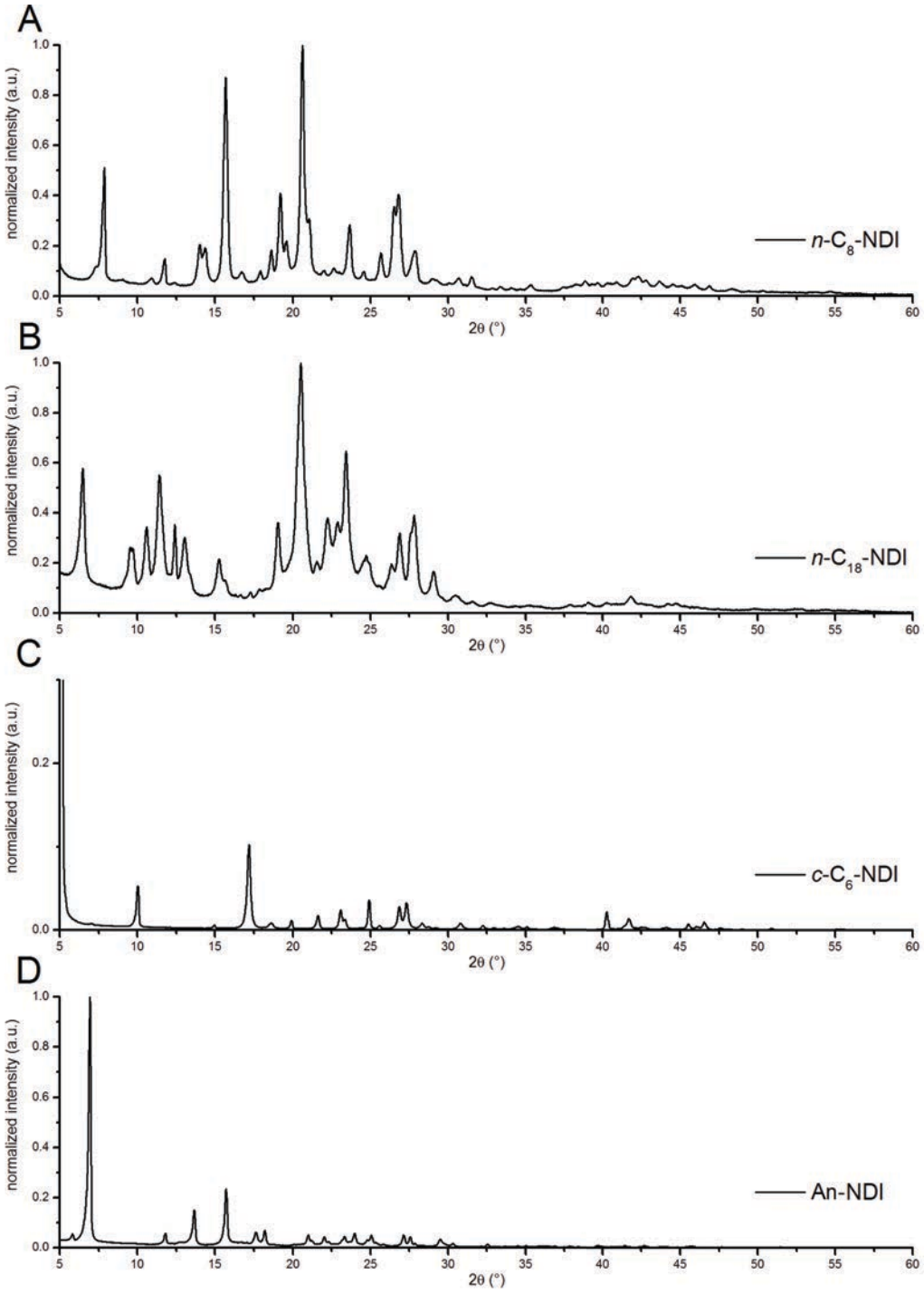


**FigureS51:** *pXRD pattern of NBIs*.

### 3.10. Mass Spectrometry Data

For selected PBIs (*n*-$C_5$-PBI, *n*-$C_6$-PBI, *n*-$C_8$-PBI, *n*-$C_9$-PBI, *n*-$C_{14}$-PBI, *n*-$C_{15}$-PBI, *n*-$C_{18}$-PBI and *c*-$C_6$-PBI) synthesized for 24 h at 200 °C and for shorter reaction times with *Hünig's* base catalyst and for all NBIs MALDI MS and LDI MS experiments were performed. The m/z values measured in positive and negative ion mode are listed in TableS5.

**TableS5:** *Results of MALD MS and LDI MS experiments. Color code: green = Δppm < 40, yellow = Δppm 40-80. HB = Hünig's Base.*

| sample | | theoretical molecular weight (MW) | | measured m/z (+) | | | | measured m/z (-) | | | |
|---|---|---|---|---|---|---|---|---|---|---|---|
| | catalyst | MW | substance | $[M+H]^+$ | error (ppm) | ΔDa | lock mass | $[M]^{\cdot-}$ | error (ppm) | ΔDa | lock mass |
| *n*-$C_5$-PBI | HB | 530.2206 | 531.2279 | 531.2318 | 7.34 | 0.0039 | 379.0930 | 530.2113 | -17.54 | -0.0093 | 576.5872 |
| *n*-$C_6$-PBI | HB | 558.2519 | 559.2592 | - | - | - | - | - | - | - | 576.5872 |
| *n*-$C_8$-PBI | HB | 614.3145 | 615.3218 | 615.3311 | 15.11 | 0.0093 | 379.0930 | 614.3052 | -15.14 | -0.0093 | 576.5872 |
| *n*-$C_8$-PBI | - | 614.3145 | 615.3218 | 615.3311 | 15.11 | 0.0093 | 379.0930 | 614.3129 | -2.60 | -0.0016 | 576.5872 |
| *n*-$C_9$-PBI | - | 642.3458 | 643.3531 | 643.3658 | 19.74 | 0.0127 | 379.0930 | 642.3379 | -12.30 | -0.0079 | 576.5872 |
| *n*-$C_{14}$-PBI | HB | 782.5023 | 783.5096 | 783.5079 | -2.17 | -0.0017 | 757.3992 | 782.5035 | 1.53 | 0.0012 | 726.4815 |
| *n*-$C_{14}$-PBI | - | 782.5023 | 783.5096 | 783.5101 | 0.64 | 0.0005 | 757.3992 | 782.4922 | -12.91 | -0.0101 | 726.4815 |
| *n*-$C_{15}$-PBI | - | 810.5336 | 811.5409 | 811.5757 | 42.88 | 0.0348 | 379.0930 | 810.5411 | 9.25 | 0.0075 | 726.4815 |
| *n*-$C_{18}$-PBI | - | 894.6275 | 895.6348 | - | - | | 379.0930 | 894.6451 | 19.67 | 0.0176 | 726.4815 |
| *n*-$C_{18}$-PBI | HB | 894.6275 | 895.6348 | - | - | | 379.0930 | 894.6521 | 27.50 | 0.0246 | 726.4815 |
| *c*-$C_6$-PBI | HB | 554.2206 | 555.2279 | 555.2297 | 3.24 | 0.0018 | 568.1356 | 554.2153 | -9.56 | -0.0053 | 576.5872 |
| | | | | | | | | | | | |
| *n*-$C_8$-NBI | - | 490.2832 | 491.2905 | 491.2935 | 6.11 | 0.003 | 379.0930 | 490.2574 | -52.62 | -0.0258 | 576.5872 |
| *n*-$C_{18}$-NBI | - | 770.5962 | 771.6035 | - | - | | 379.0930 | 770.6016 | 7.01 | 0.0054 | 726.4815 |
| *c*-$C_6$-NBI | - | 430.1893 | 431.1966 | 431.2 | 7.89 | 0.0034 | 379.0930 | 430.1886 | -1.63 | -0.0007 | 426.6930 |
| *An*-NBI | - | 418.0954 | 419.1027 | 419.1004 | -5.49 | -0.0023 | 379.0930 | 418.0851 | -24.64 | -0.0103 | 426.6930 |

All substances were measured in positive and negative ion mode. Most of the compounds showed $[M+H]^+$ and $[M]^{\cdot-}$ ions, however of differing intensities.

### 3.1. Scanning Electron Microscopy

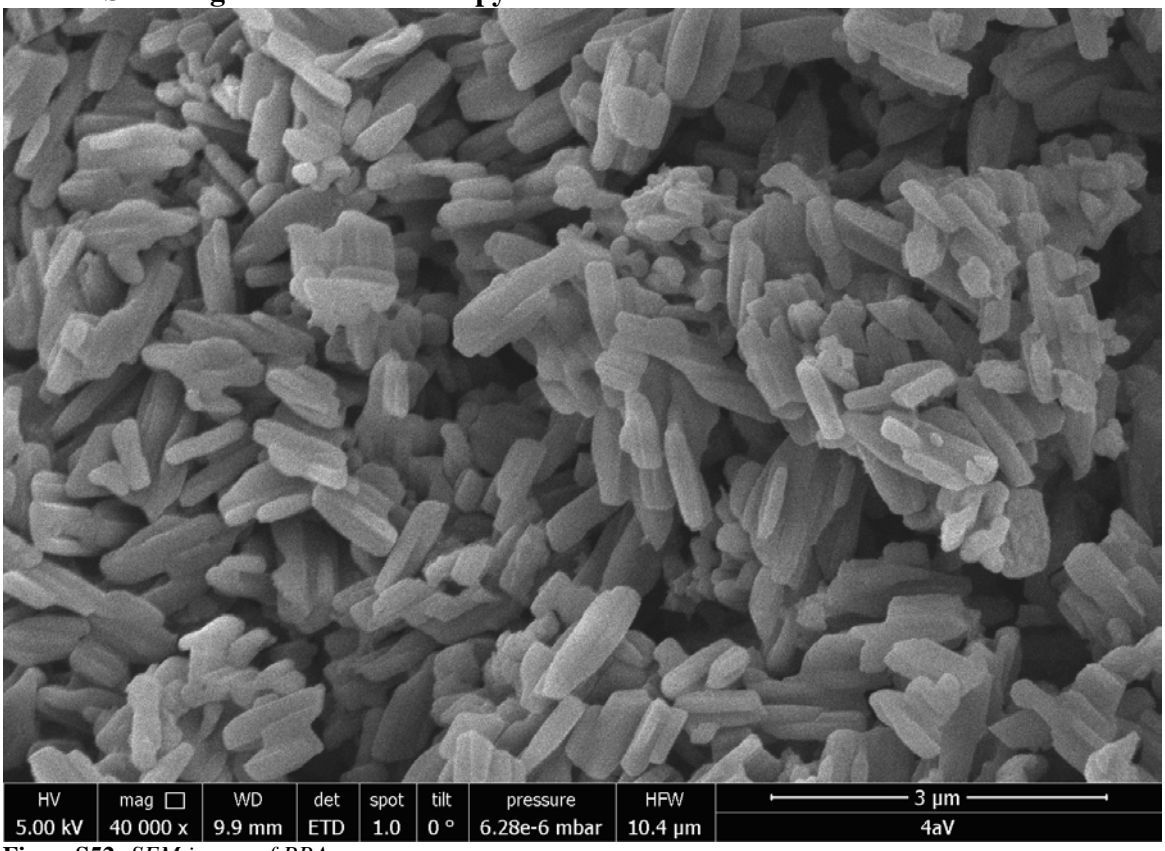


**FigureS52:** *SEM image of PBA.*

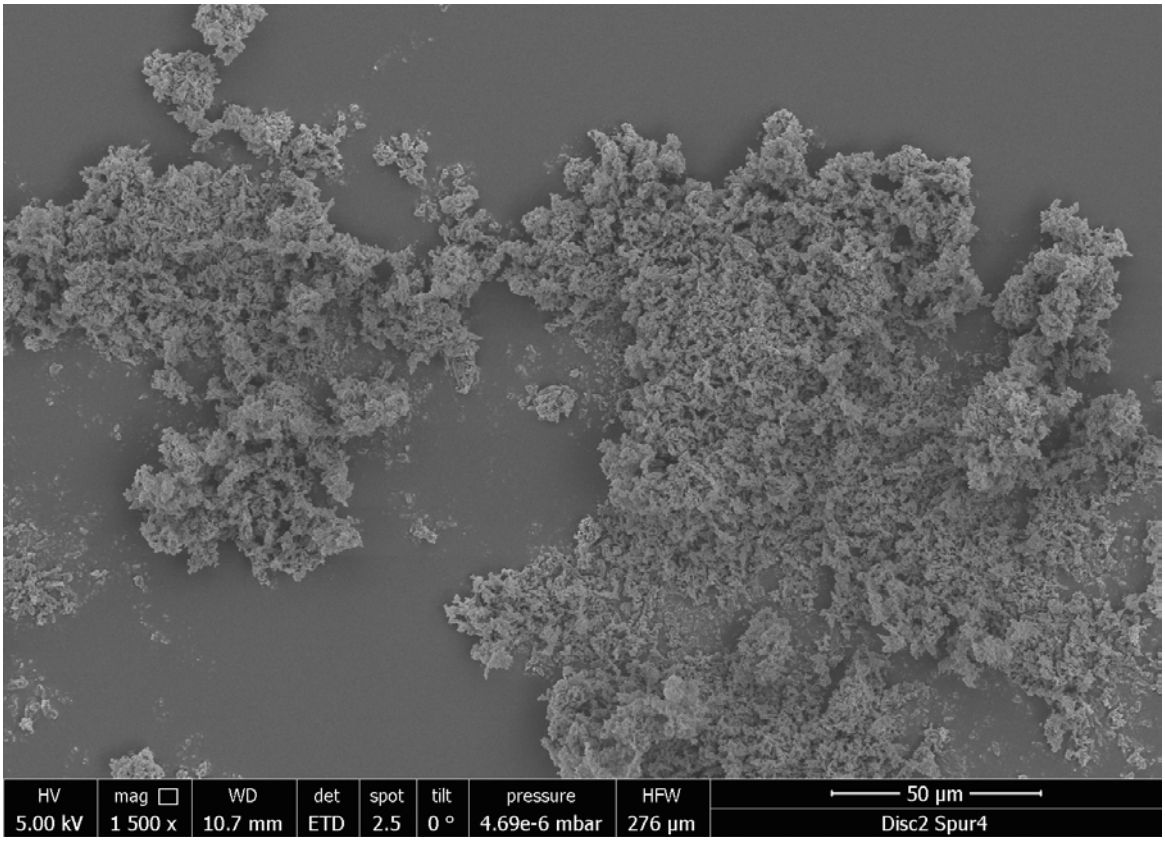


**FigureS53:** *SEM overview image of PBA.*

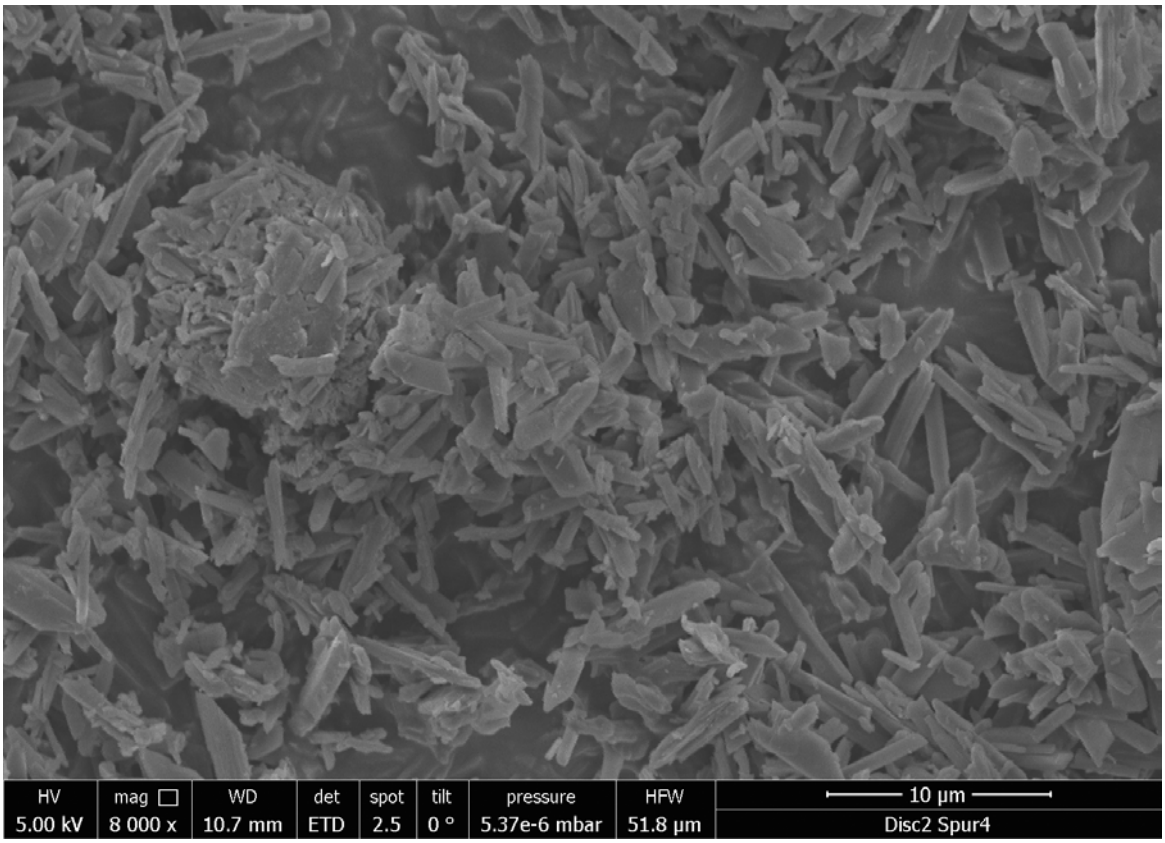


**FigureS54:** *SEM image of n-$C_5$-PBI synthesized at 200 °C for 24 h.*

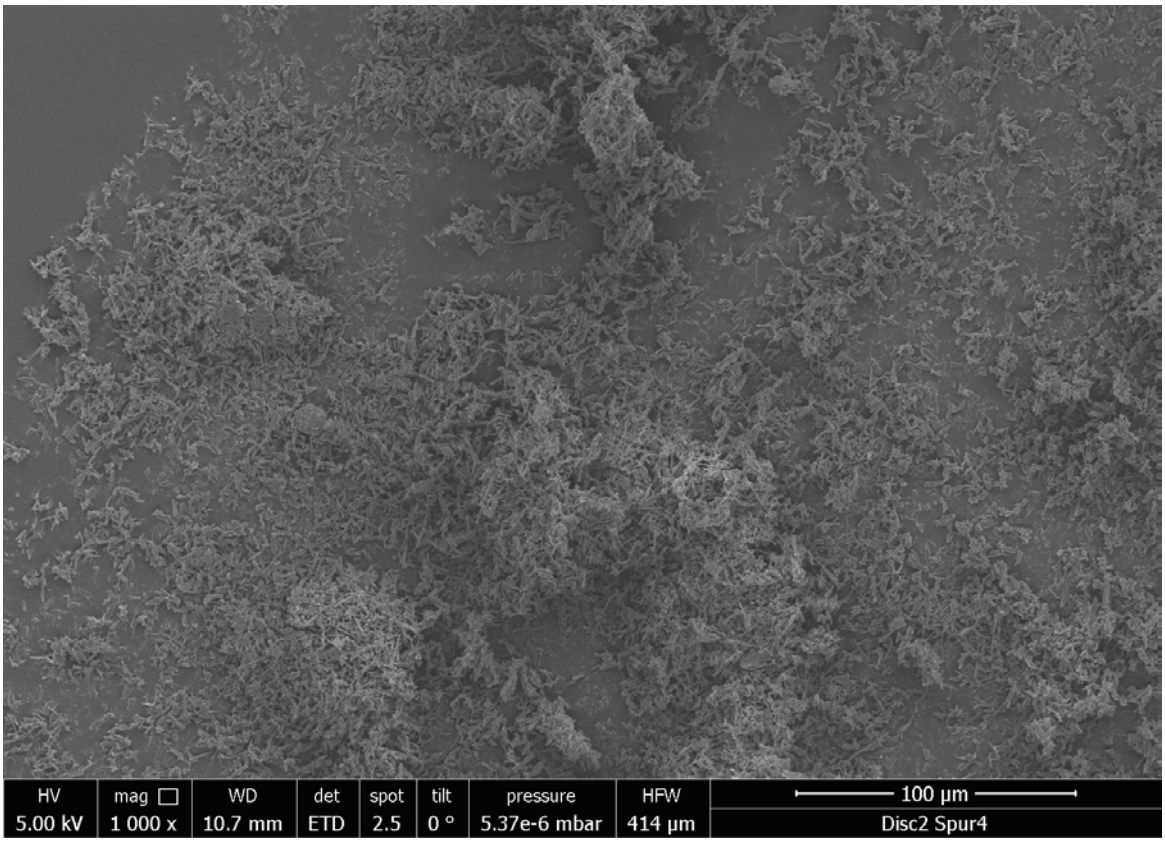


**FigureS55:** *SEM overview image of n-$C_5$-PBI synthesized at 200 °C for 24 h.*

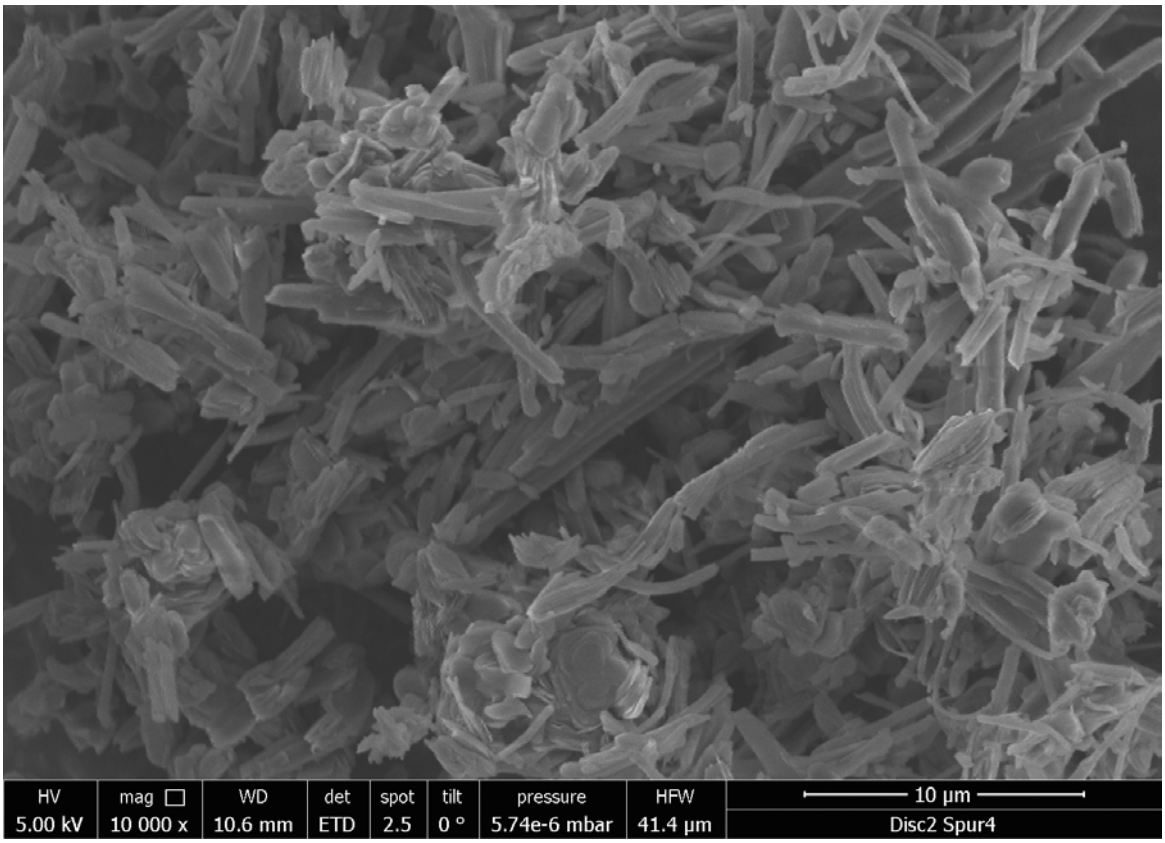


**FigureS56:** *SEM image of n-$C_6$-PBI synthesized at 200 °C for 24 h.*

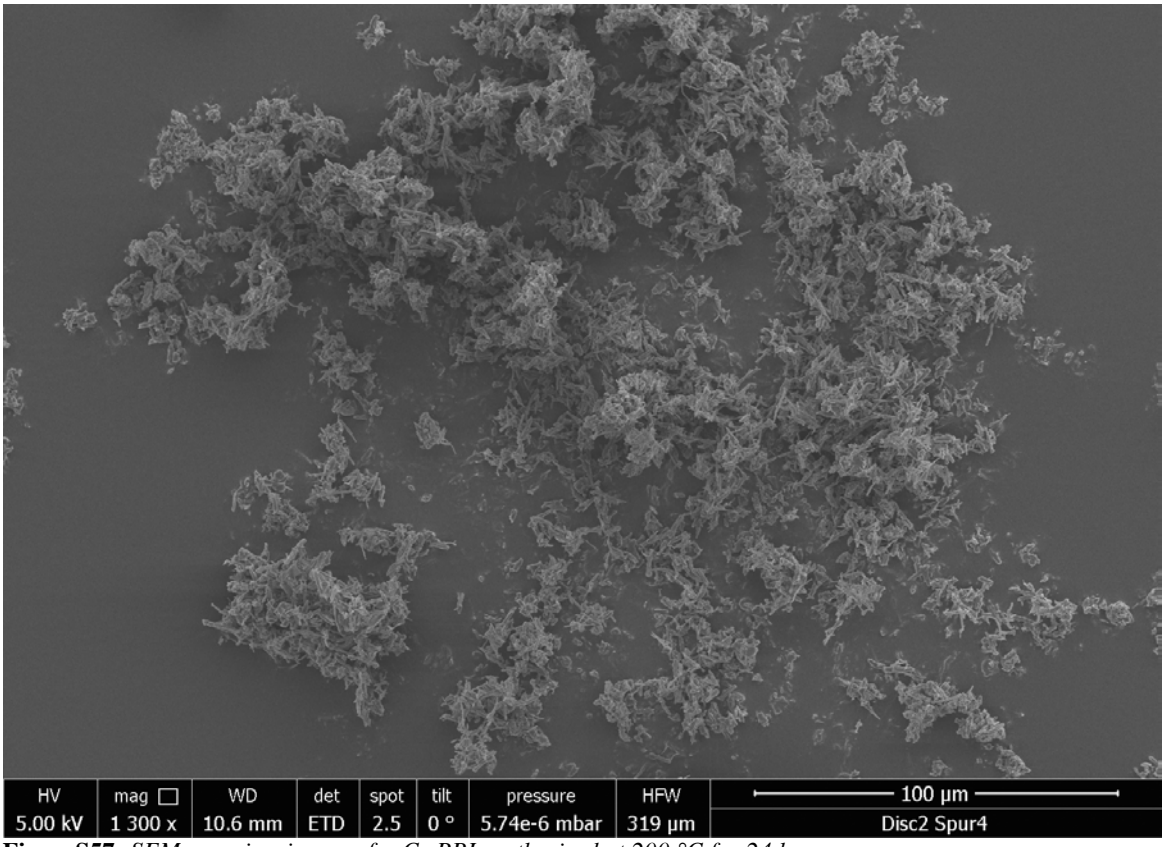


**FigureS57:** *SEM overview image of n-$C_6$-PBI synthesized at 200 °C for 24 h.*

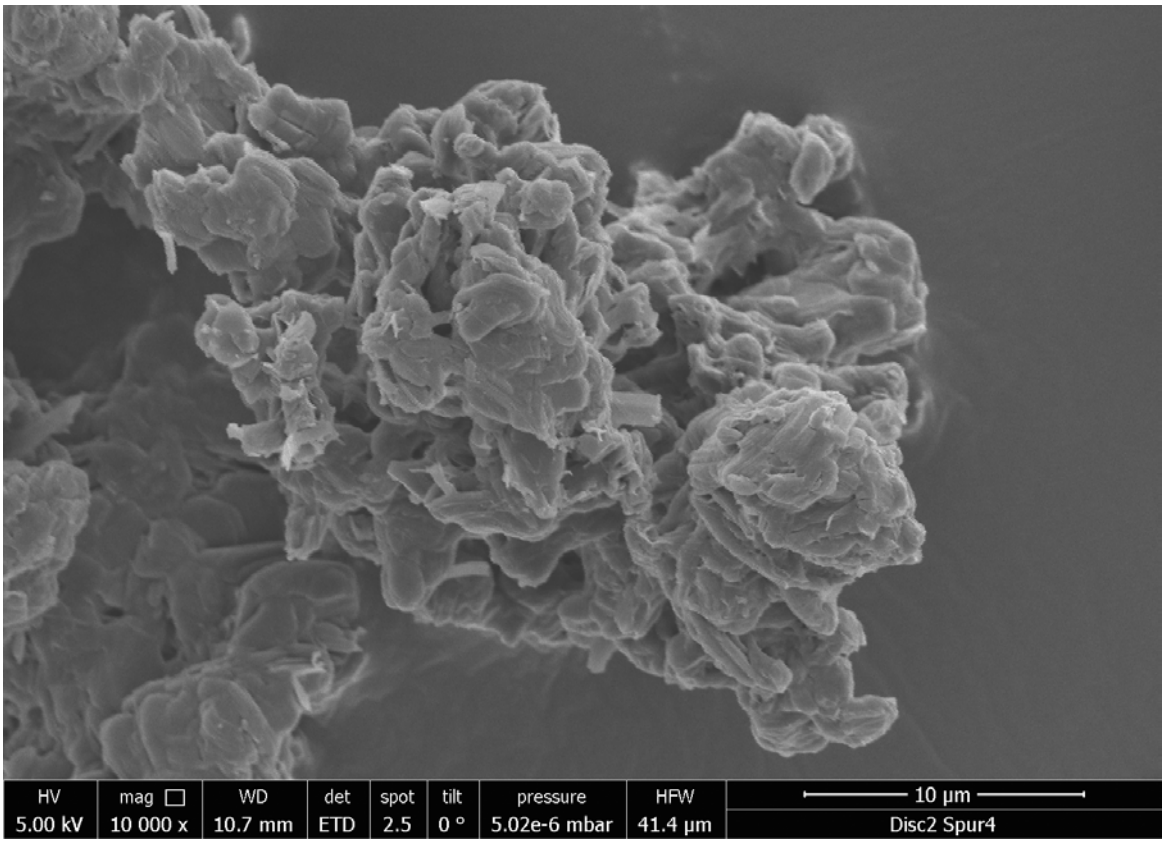


**FigureS58:** *SEM image of n-$C_7$-PBI synthesized at 200 °C for 24 h.*

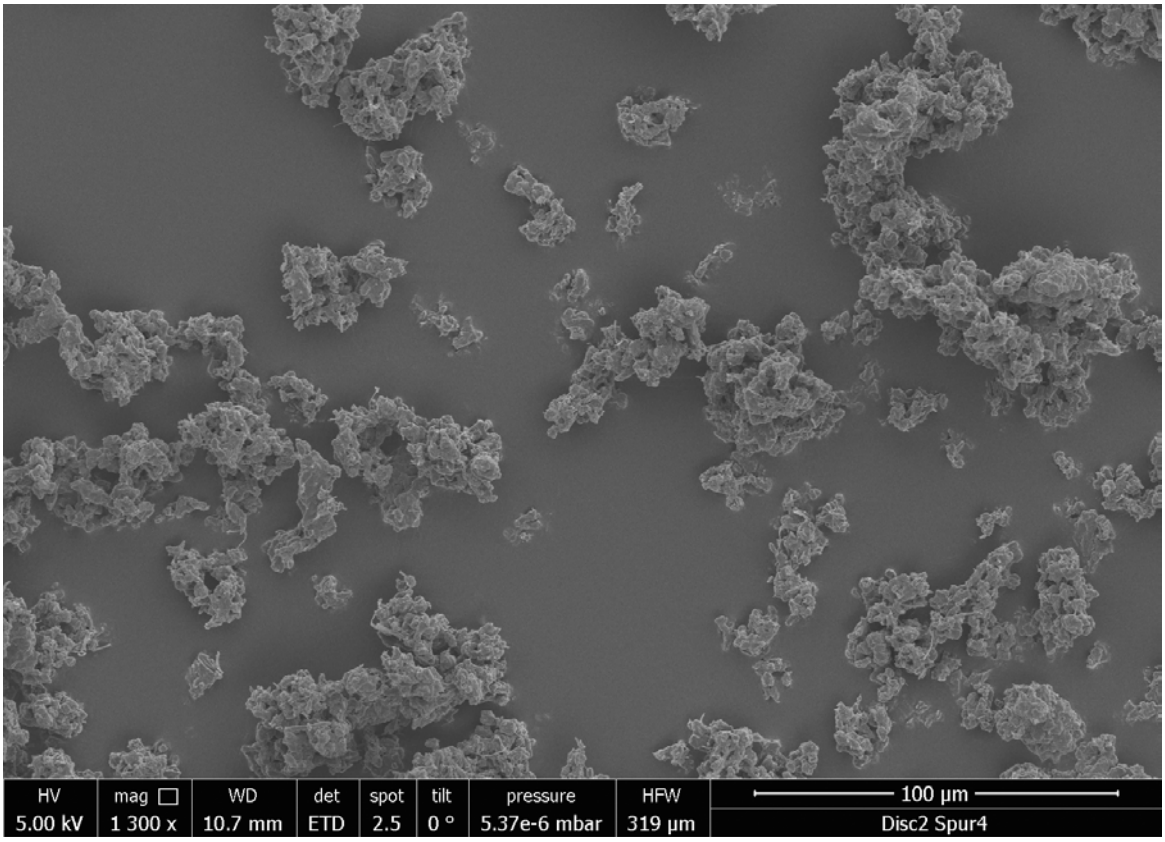


**FigureS59:** *SEM overview image of n-$C_7$-PBI synthesized at 200 °C for 24 h.*

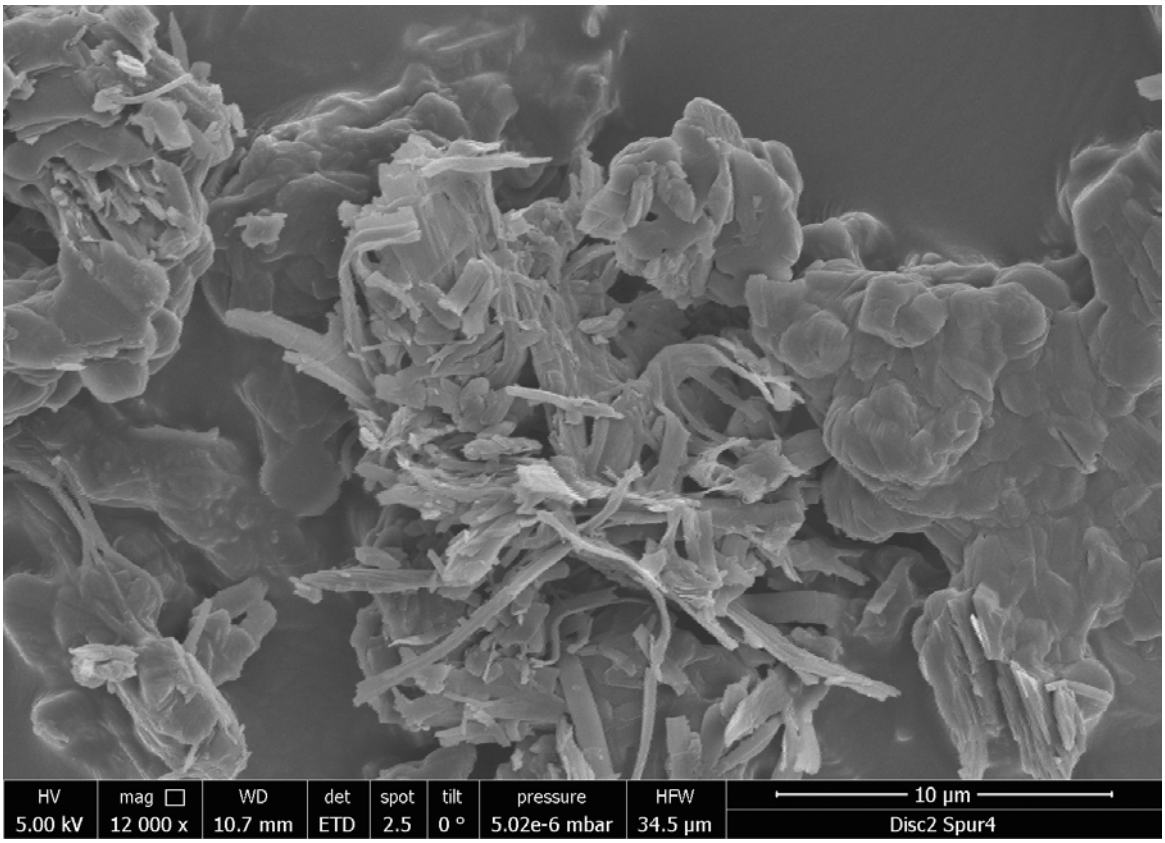


**FigureS60:** *SEM image of n-$C_8$-PBI synthesized at 200 °C for 24 h.*

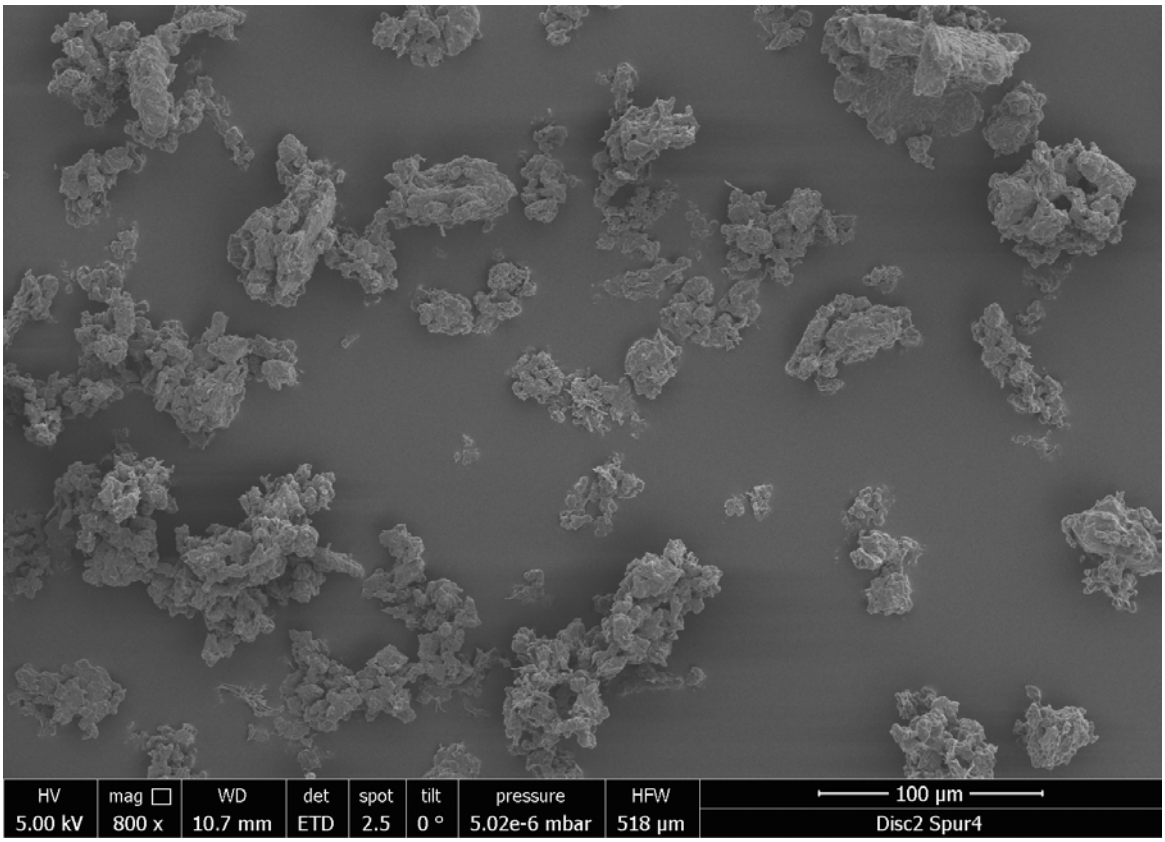


**FigureS61:** *SEM overview image of n-$C_8$-PBI synthesized at 200 °C for 24 h.*

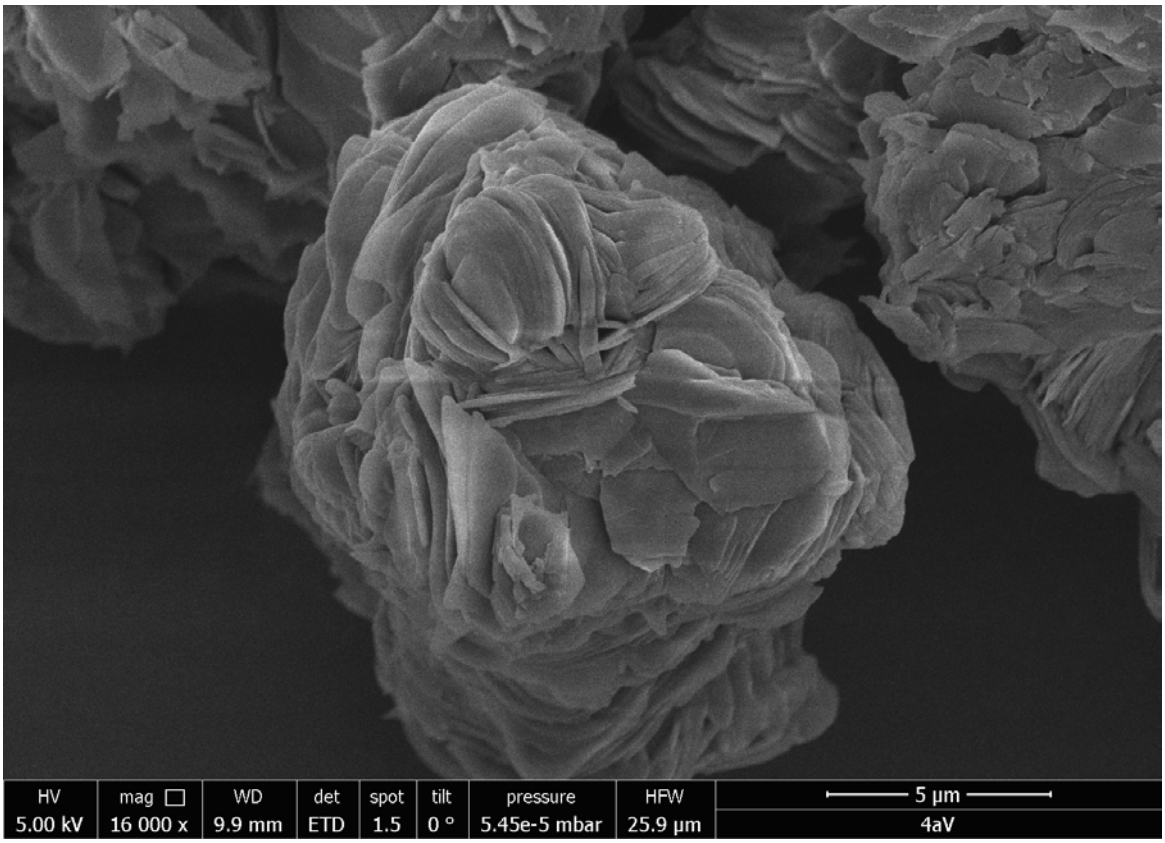


**FigureS62:** *SEM image of n-$C_9$-PBI synthesized at 200 °C for 24 h.*

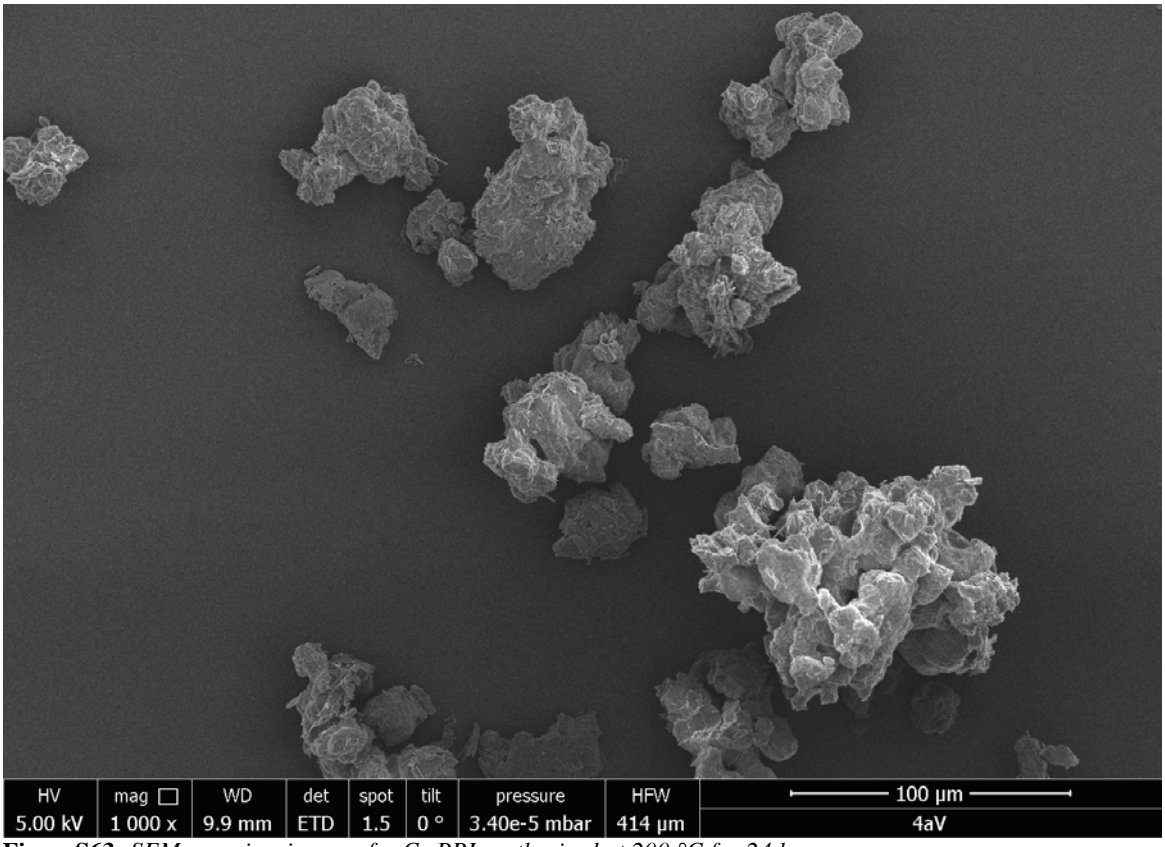


**FigureS63:** *SEM overview image of n-$C_9$-PBI synthesized at 200 °C for 24 h.*

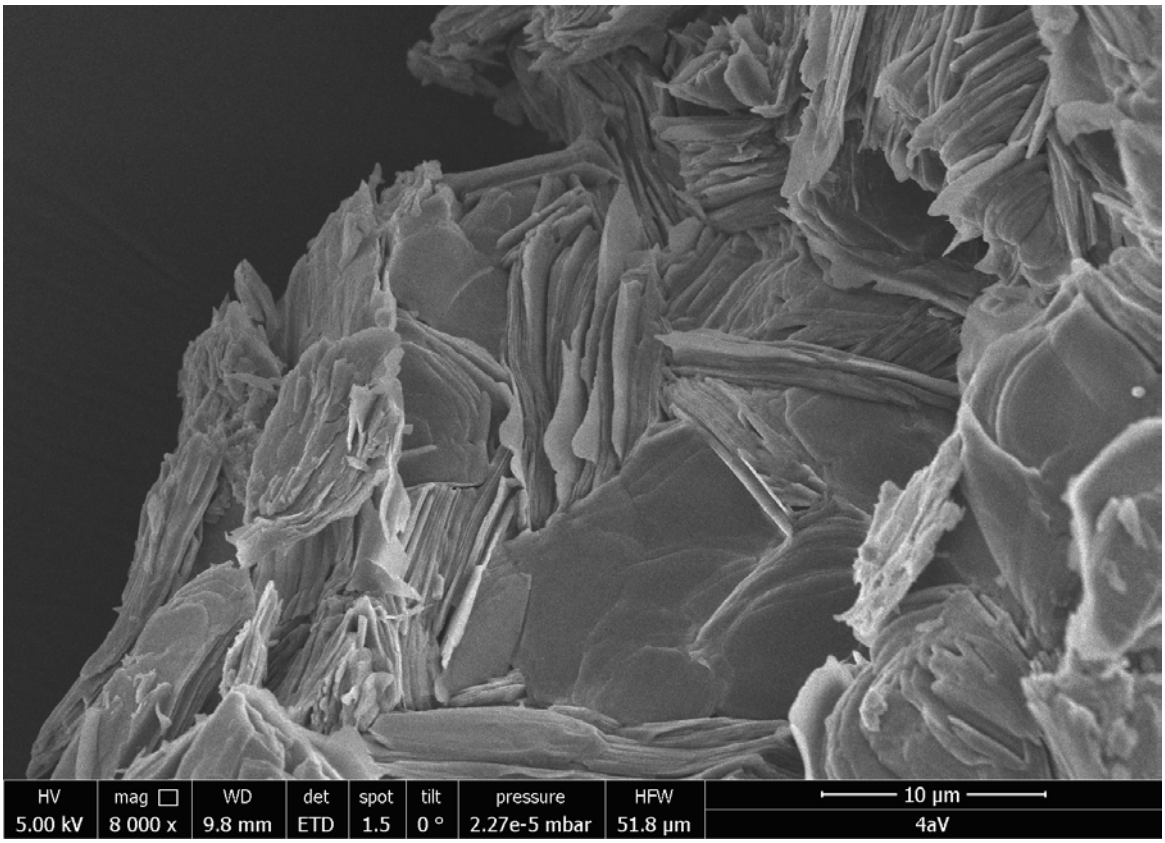


**FigureS64:** *SEM image of n-$C_{10}$-PBI synthesized at 200 °C for 24 h.*

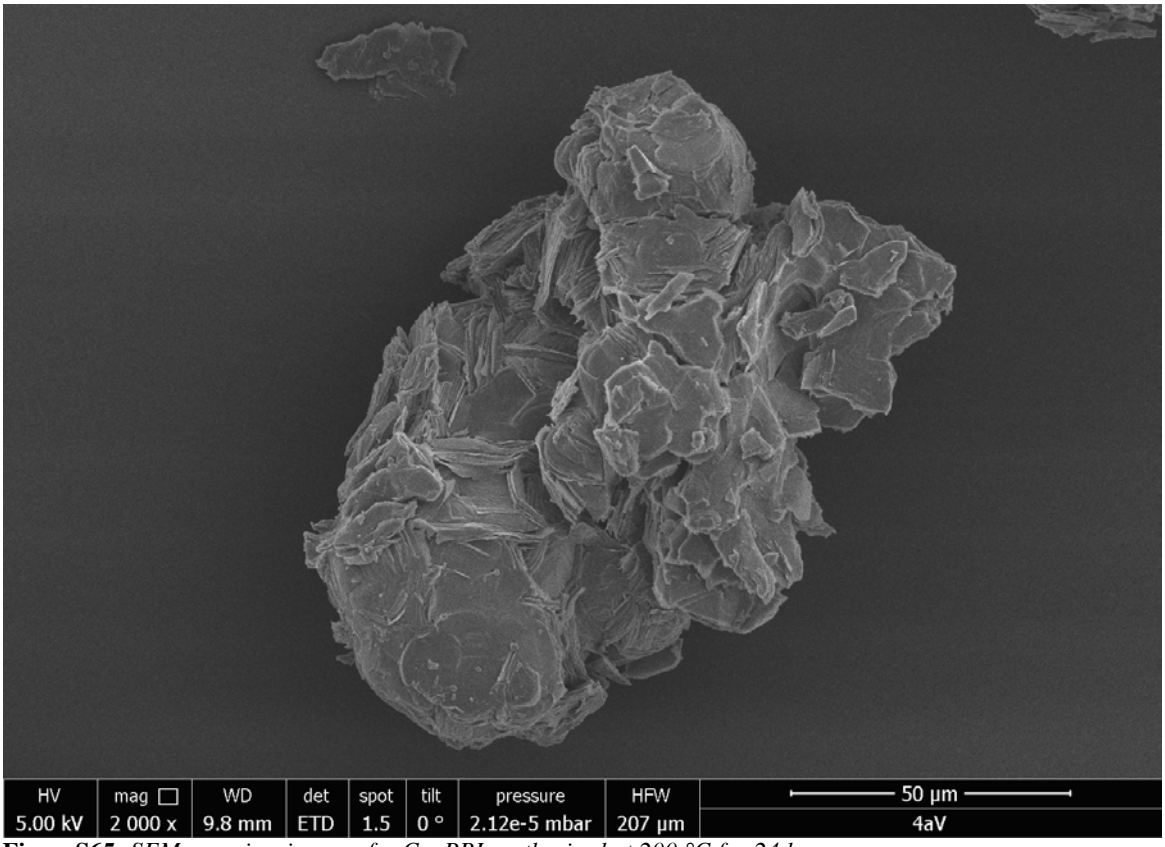


**FigureS65:** *SEM overview image of n-$C_{10}$-PBI synthesized at 200 °C for 24 h.*

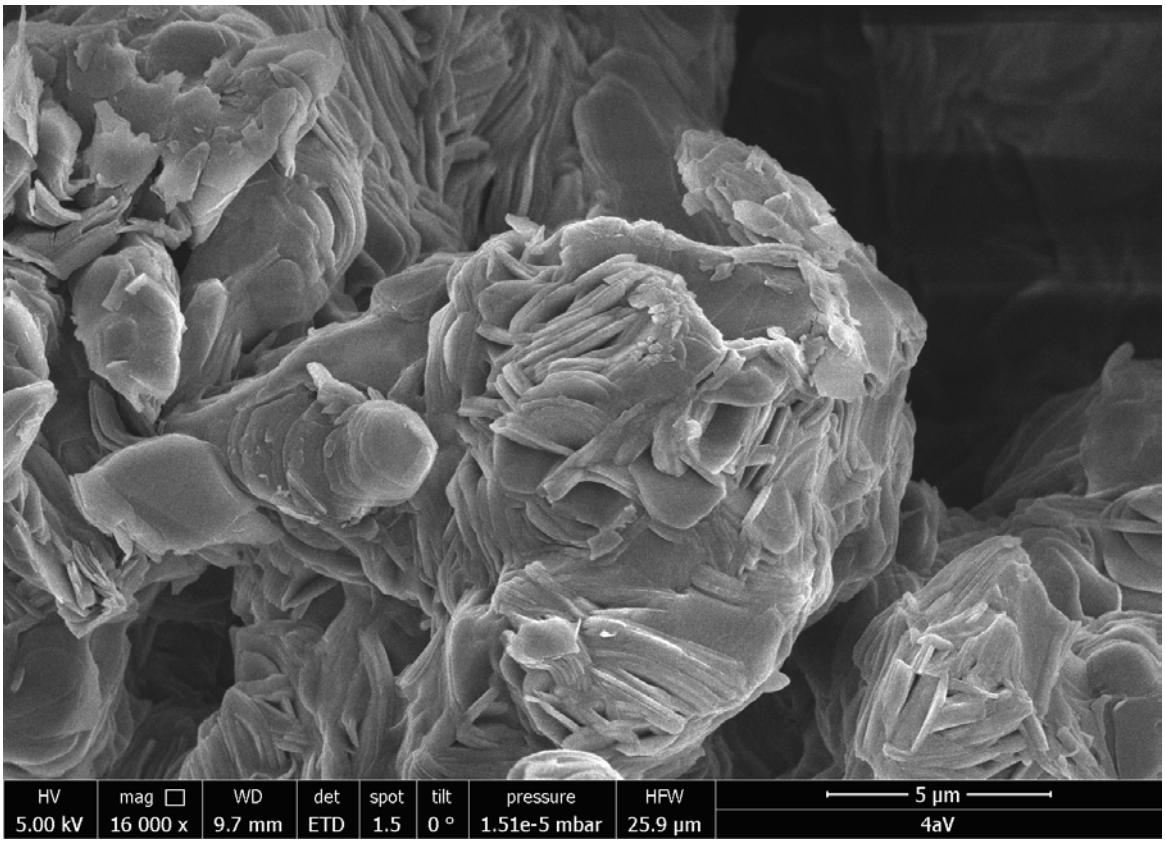


**FigureS66:** *SEM image of n-$C_{11}$-PBI synthesized at 200 °C for 24 h.*

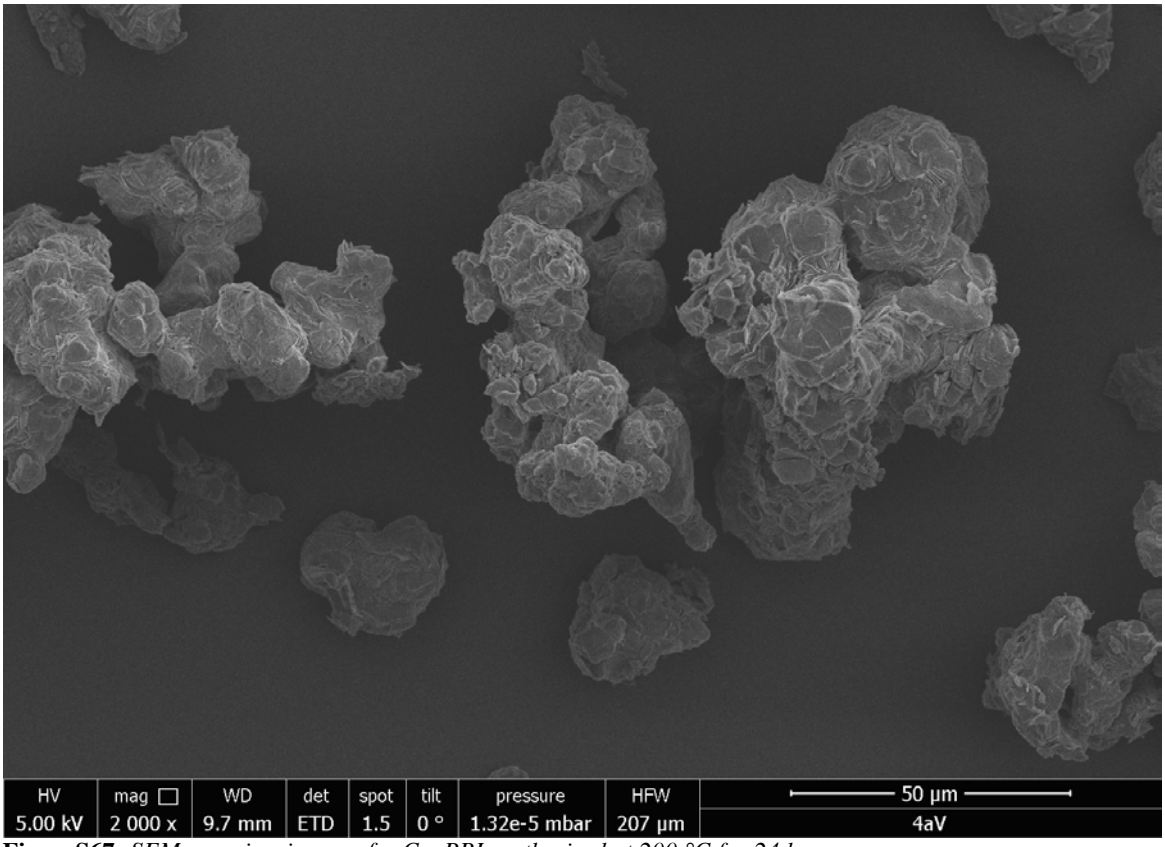


**FigureS67:** *SEM overview image of n-$C_{11}$-PBI synthesized at 200 °C for 24 h.*

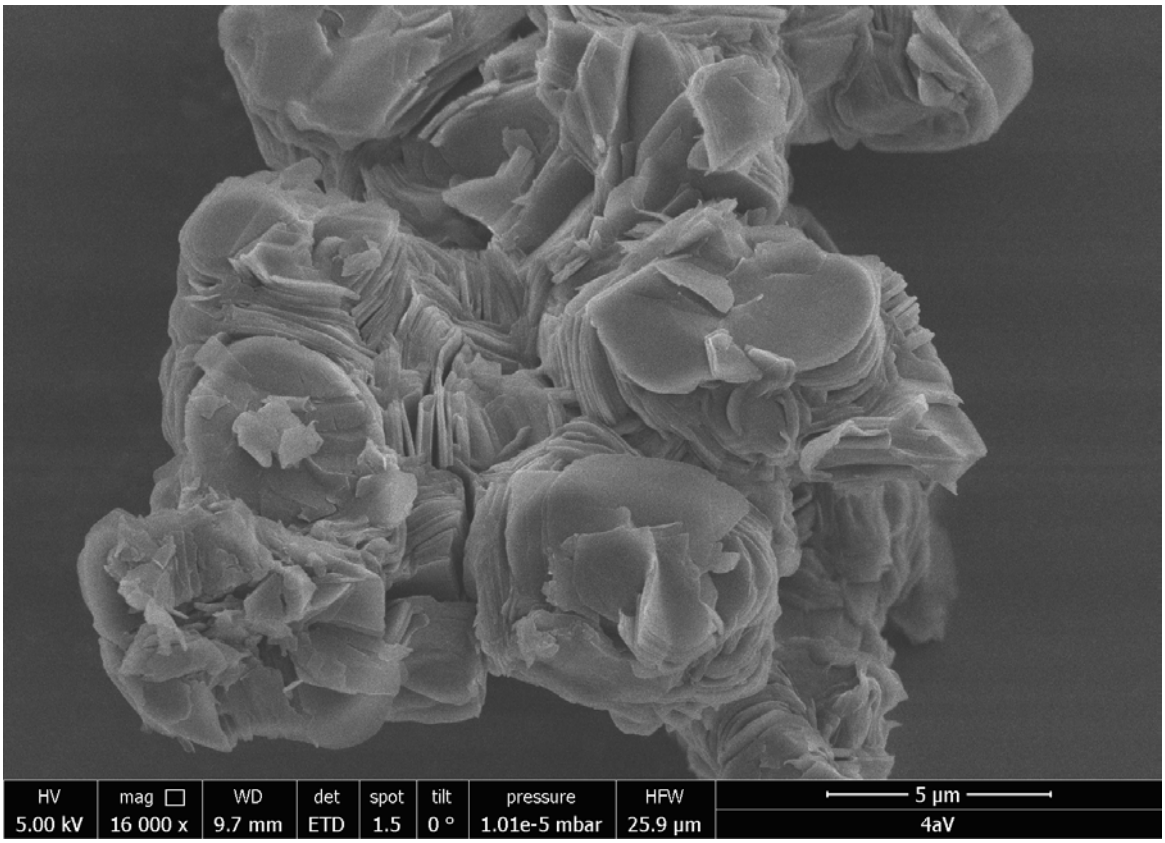


**FigureS68:** *SEM image of n-$C_{12}$-PBI synthesized at 200 °C for 24 h.*

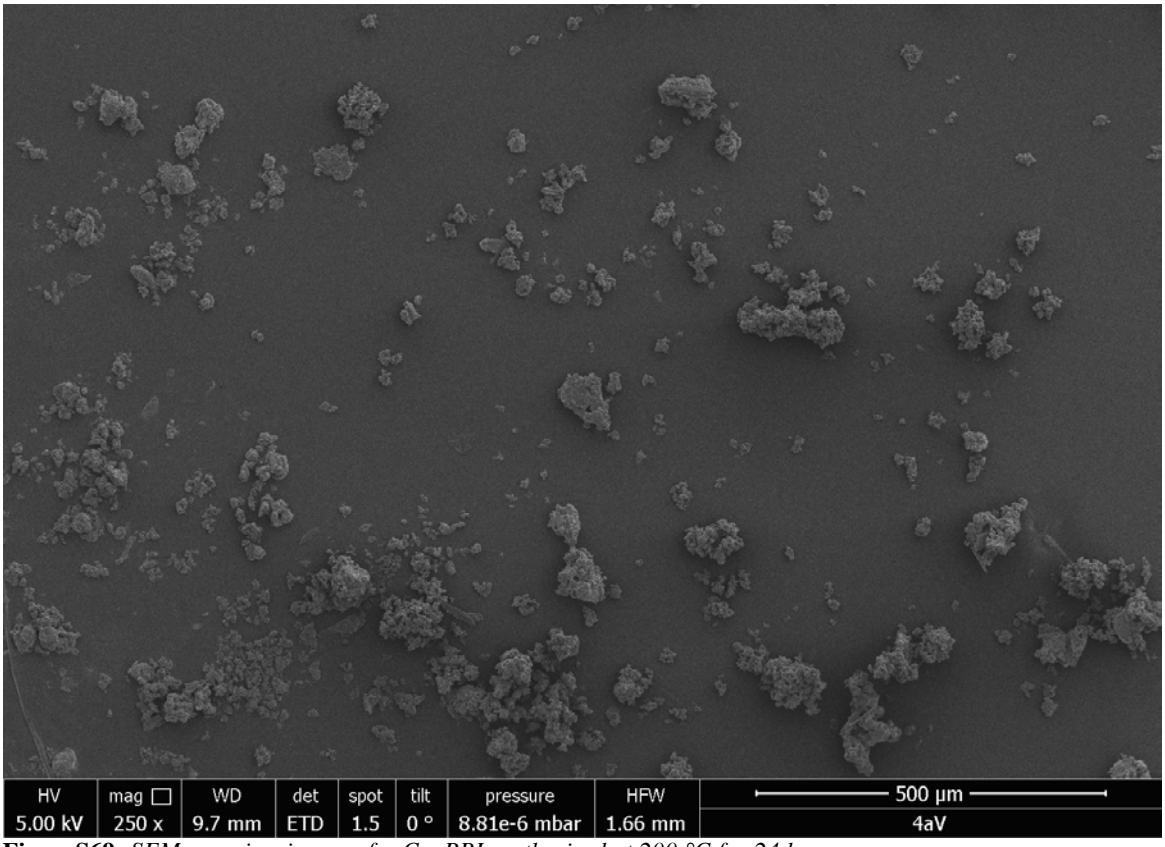


**FigureS69:** *SEM overview image of n-$C_{12}$-PBI synthesized at 200 °C for 24 h.*

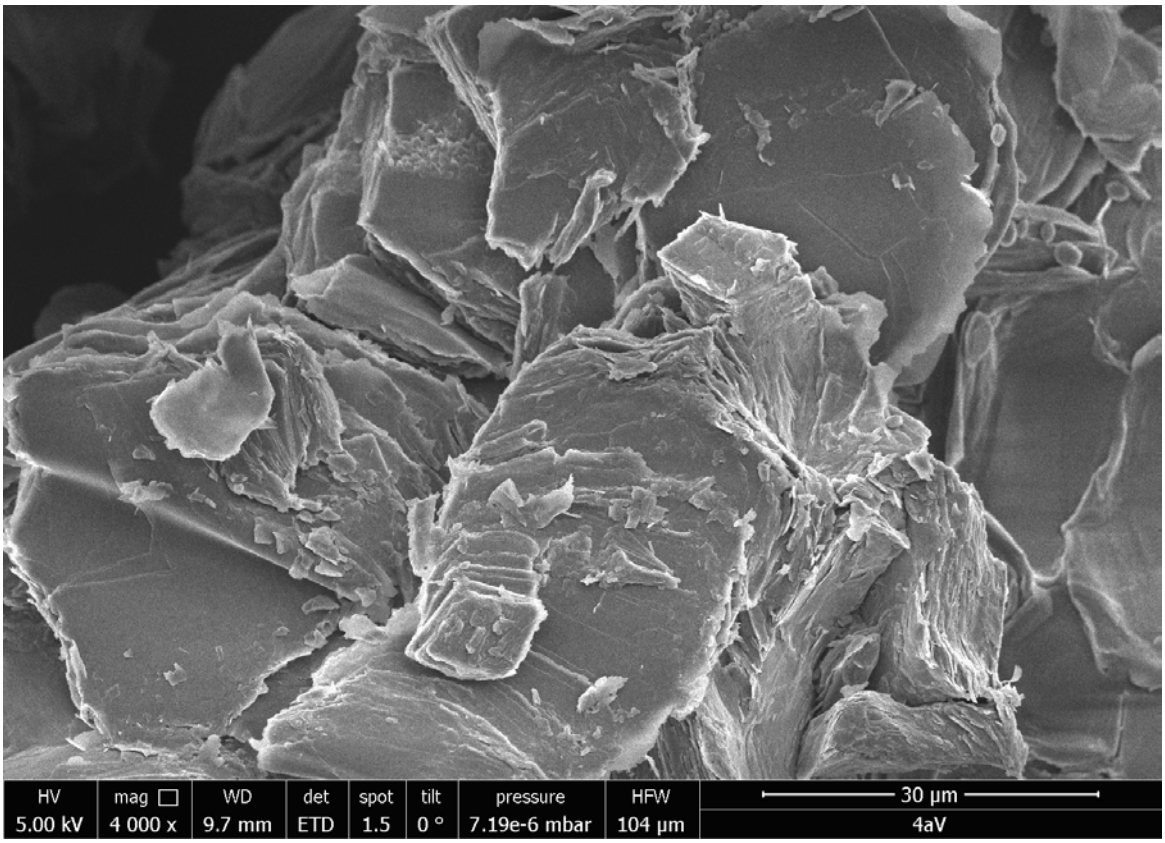


**FigureS70:** *SEM image of n-$C_{14}$-PBI synthesized at 200 °C for 24 h.*

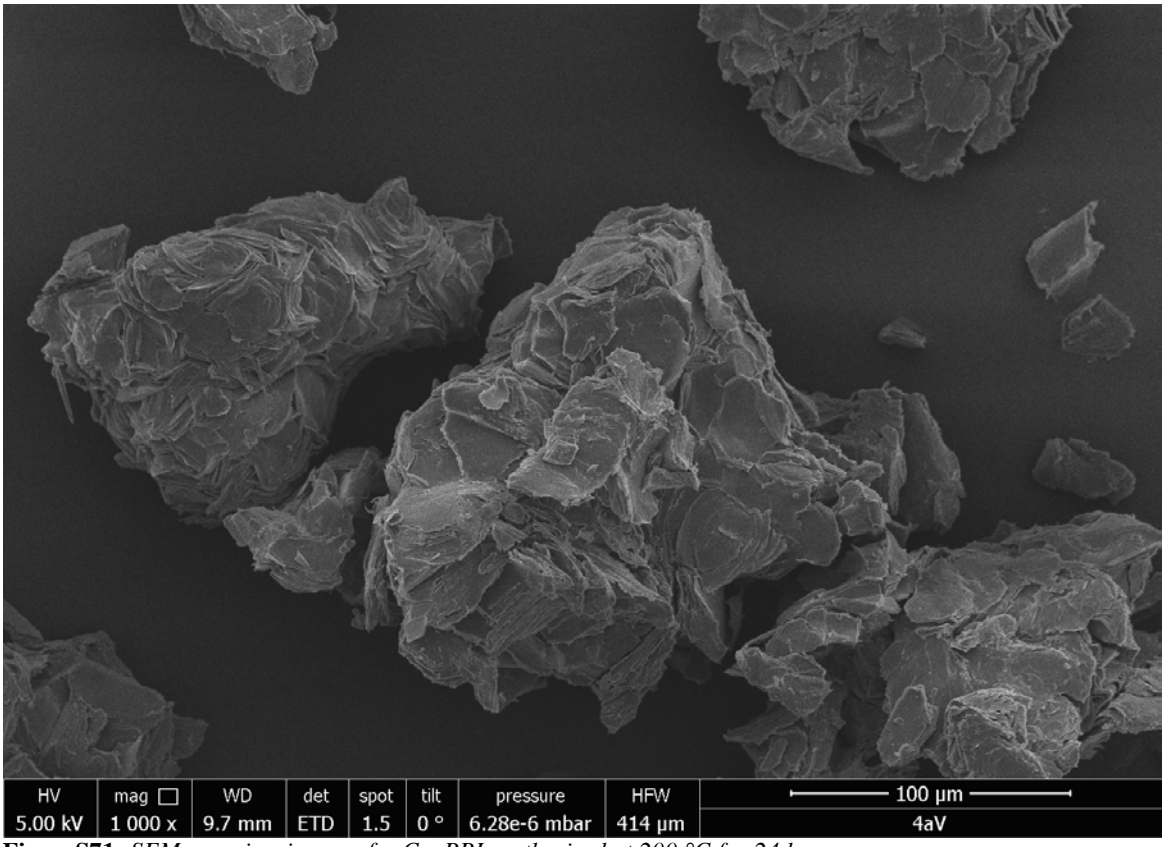


**FigureS71:** *SEM overview image of n-$C_{14}$-PBI synthesized at 200 °C for 24 h.*

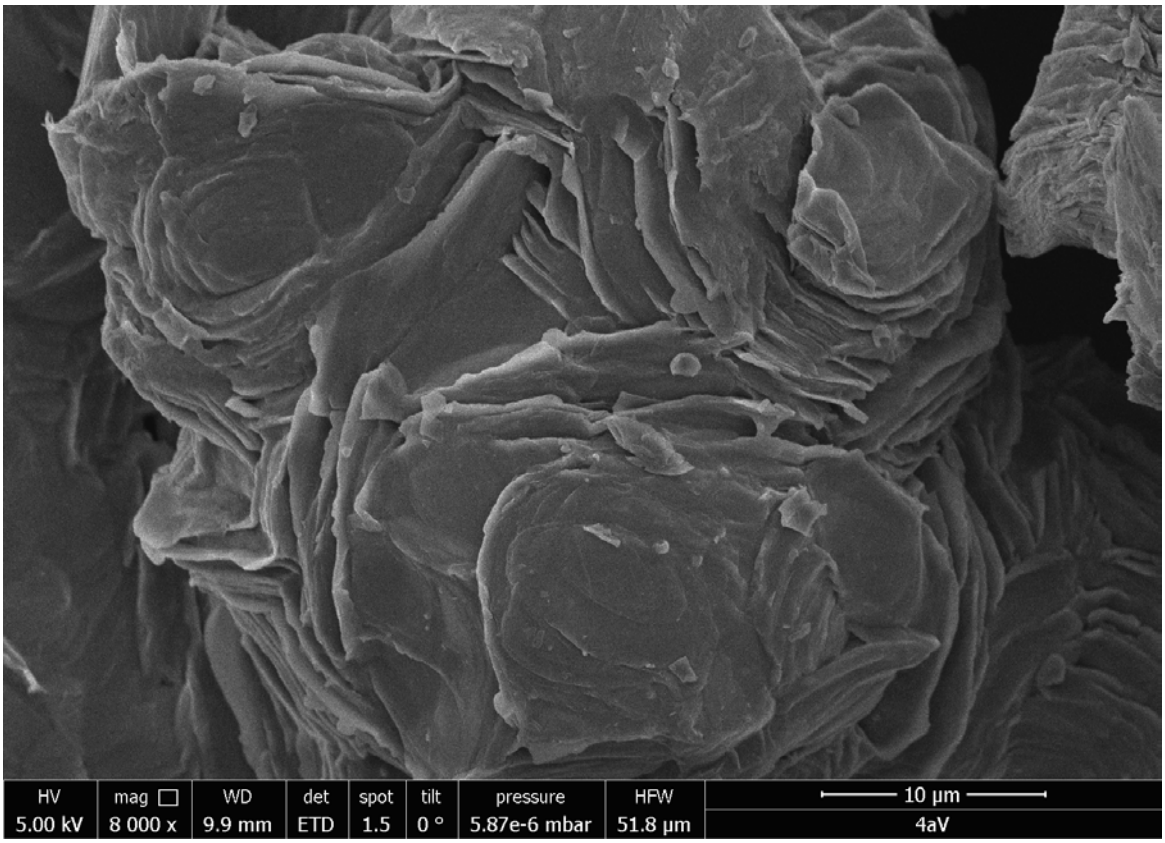


**FigureS72:** *SEM image of n-$C_{15}$-PBI synthesized at 200 °C for 24 h.*

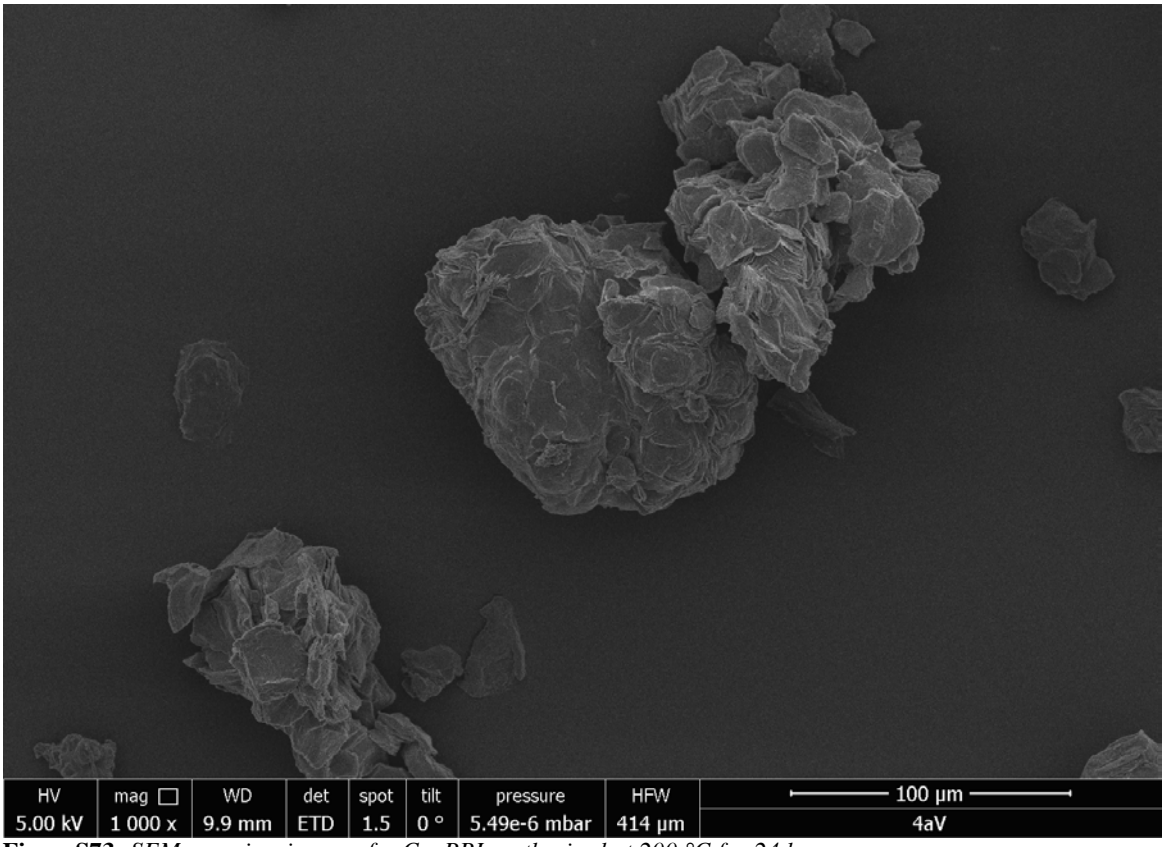


**FigureS73:** *SEM overview image of n-$C_{15}$-PBI synthesized at 200 °C for 24 h.*

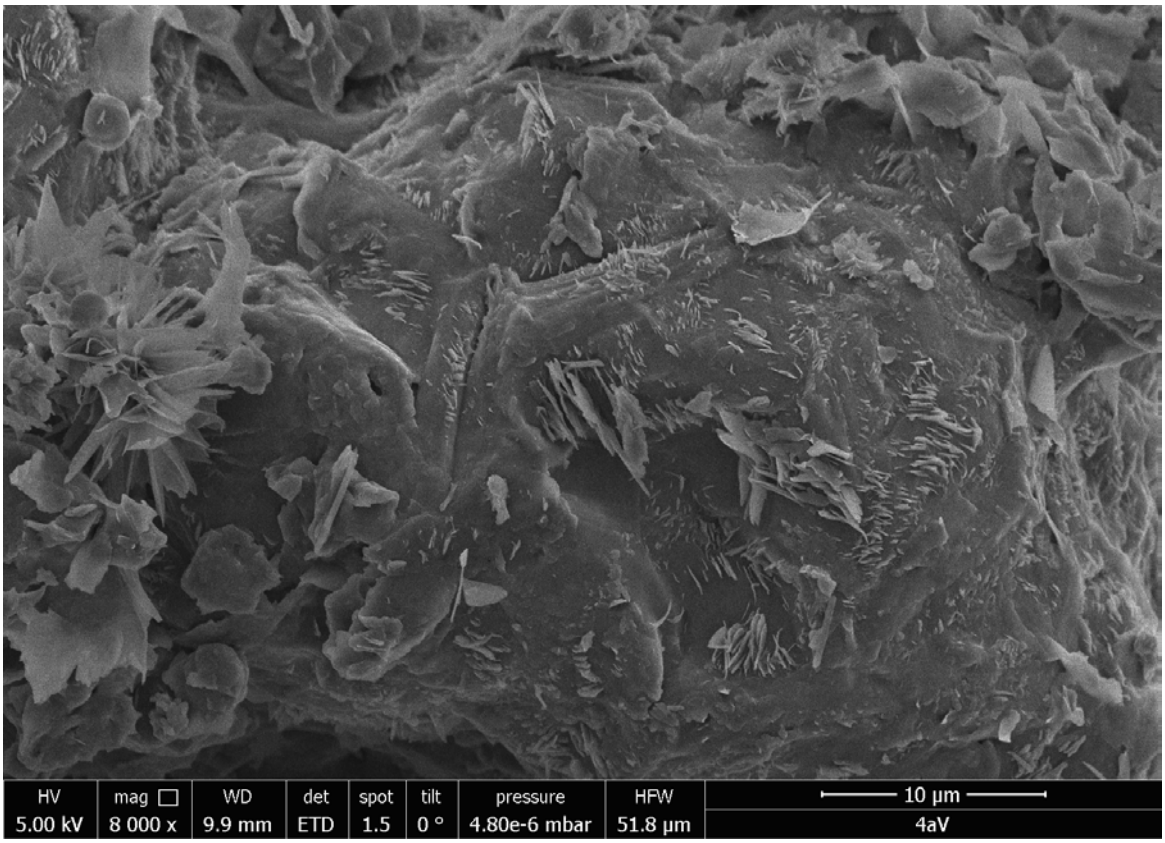


**FigureS74:** *SEM image of n-$C_{16}$-PBI synthesized at 200 °C for 24 h.*

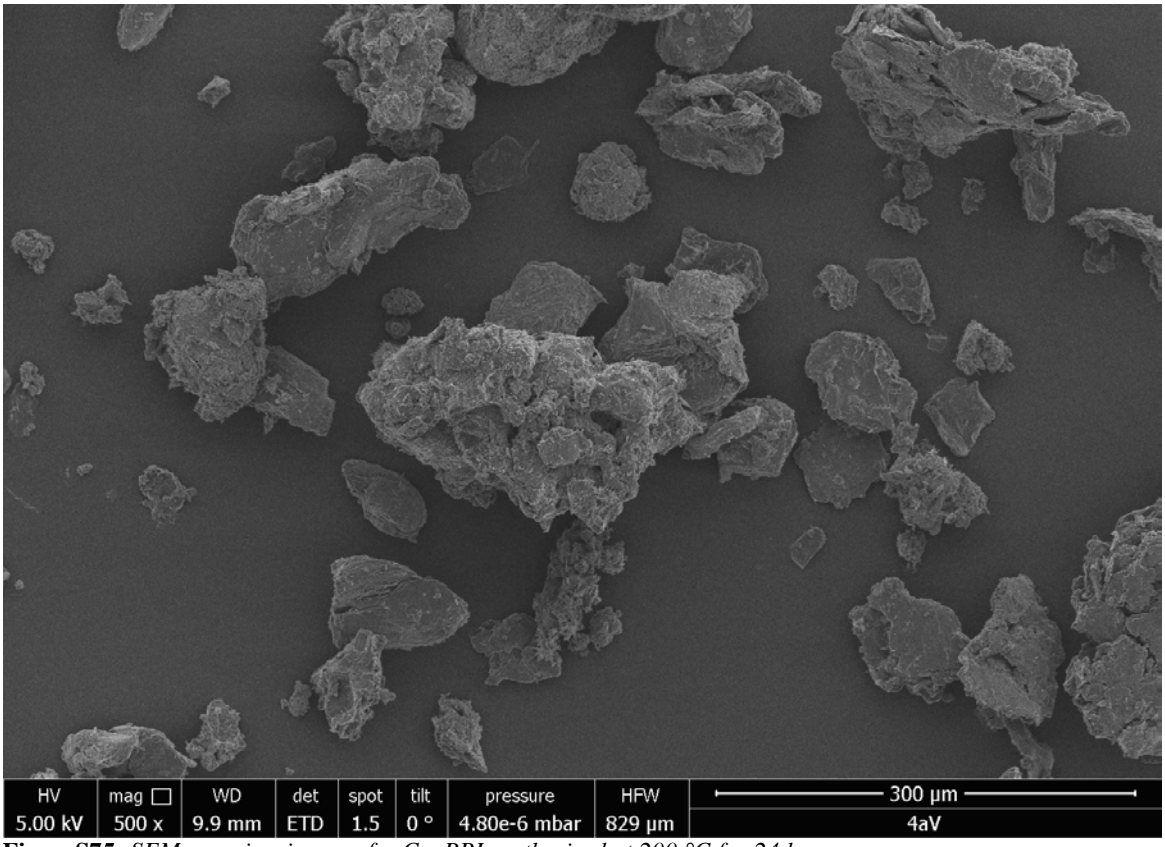


**FigureS75:** *SEM overview image of n-$C_{16}$-PBI synthesized at 200 °C for 24 h.*

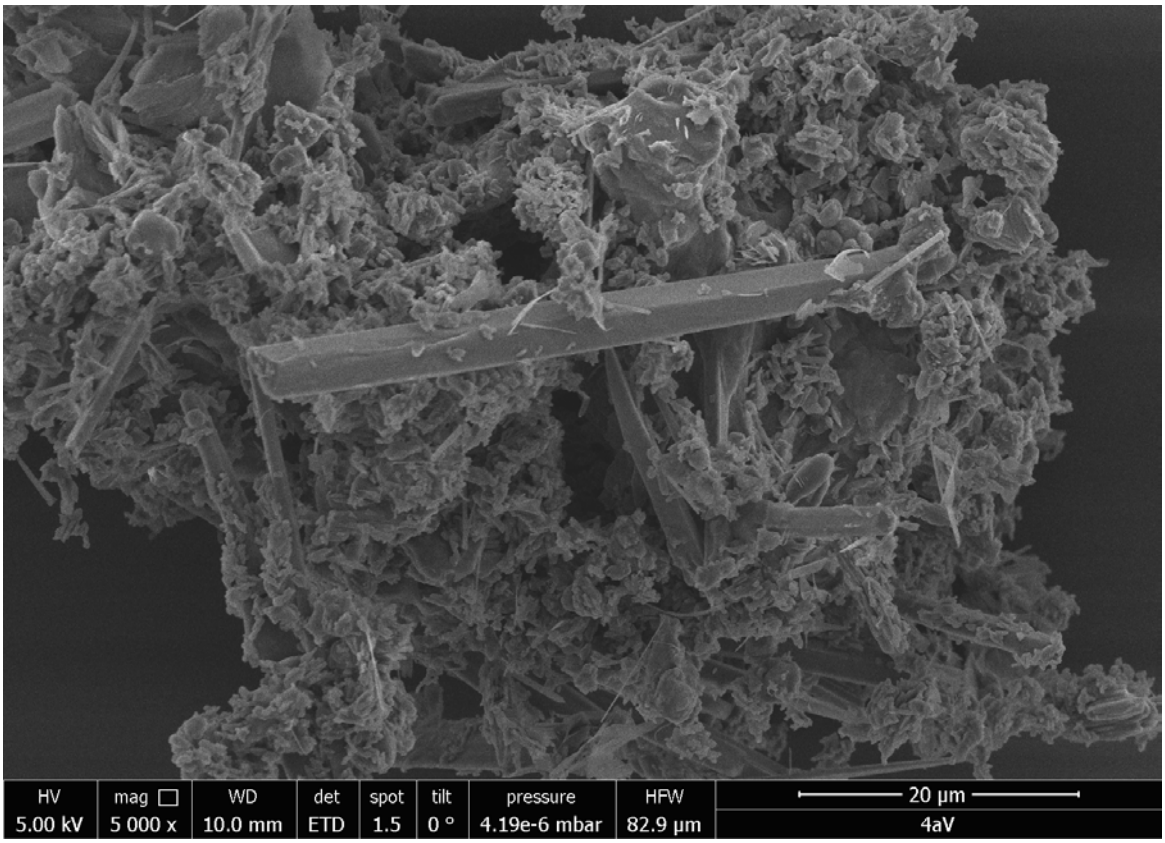


**FigureS76:** *SEM image of n-$C_{18}$-PBI synthesized at 200 °C for 24 h.*

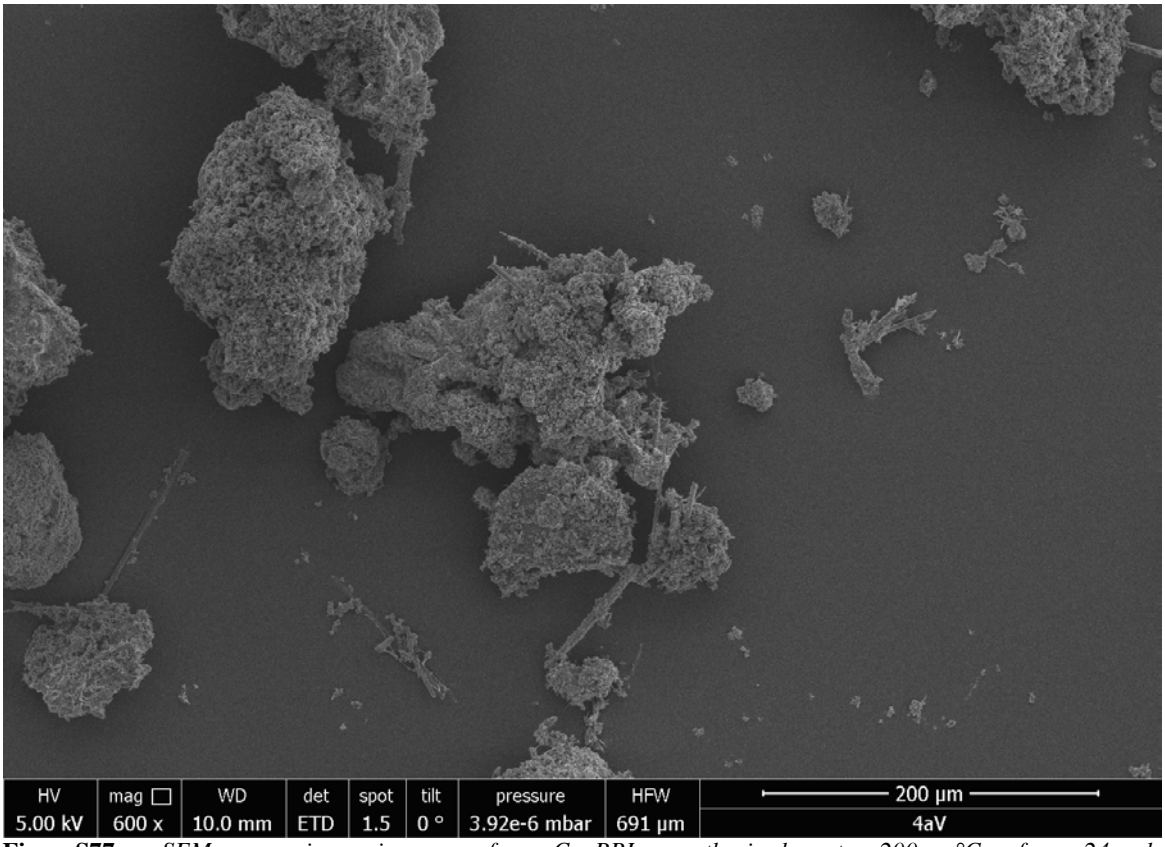


**FigureS77:** *SEM overview image of n-$C_{18}$-PBI synthesized at 200 °C for 24 h.*

## 4. PBI Data Table

The information listed in the following Table (**Table Sx**) is based on several CAS SciFinder searches carried out from July 15th to Aug 7th 2016. Data that has been supplied by this contribution and that was previously not reported is highlighted by blue background color. Dark grey background that these data have not been reported yet. References are listed as [Sn] at the end of this document. Abbreviations: $T_m$ = melting point; $T_d$ = decomposition temperature; $T_{LCn}$ = liquid crystal transition temperature (wit n = number of the transition); $T_I$ = temperature of transition of liquid crystal to isotropic liquid; EA = elemental analysis; MS = mass spectrometry; * = no measurement details given in the reference;

| Name | CAS no. | EA data | MS data | IR data | $^1$H-NMR | $^{13}$C-NMR | Solubility data | Fluorescence data | UV-Vis data | Fluorescence quantum yield | Thermal data | PXRD data | Crystal structure | Other data |
|---|---|---|---|---|---|---|---|---|---|---|---|---|---|---|
| ***n*-C$_5$-PBI** | 76372-75-3 | [S1], [S3] | [S1], [S2], [S3] | [S1], [S2], [S3] | [S2] | *Cf.* Figure S15 | 47mg/100mL $CHCl_3$. [S1] | [S1] | $\lambda_{max}$ ($CHCl_3$)= 534nm [S1]; $\lambda_{max}$ ($CH_2Cl_2$) = 526nm [S2]; $\lambda_{max}$ ($H_2SO_4$) = 598nm [S3]; | *Cf.* **Table S4** | $T_m$ >350°C [S1]; $T_d$ = 432 °C [S2]; | *Cf.* **Figure S48** | [S4]. [S5]. [S6] | $R_f$ [S1]; Cyclic voltamograms [S2]; reduction potential [S2]; determination of HOMO and LUMO energy [S2]; charge carrier mobility [S20]; |
| ***n*-C$_6$-PBI** | 25811-56-7 | [S7], [S3] | [S3] | [S7], [S3] | *Cf.* FigureS16 | *Cf.* Figure S17 | $CHCl_3$, 20°C: 23 mg/100 mL [S7,S1] | [S7] | $\lambda_{max}$ ($CHCl_3$)= 458nm, 489nm, 526nm [S7]; $\lambda_{max}$ ($H_2SO_4$) = 598nm [S3]; | *Cf.* **Table S4** | $T_m$>360°C [S1] | *Cf.* **Figure S48** | | $R_f$ [S1,S7]; charge carrier mobility [S20]; |
| ***n*-C$_7$-PBI** | 95689-91-1 | | | *Cf.* FigureS5 | [S8] | *Cf.* Figure S19 | | *Cf.* FigureS46 | spectrum [S9]*<br>Spectrum in $CH_2Cl_2$ and maxima, *cf.* FigureS46 | *Cf.* **Table S4** | $T_d$ > 410°C, $T_{d,20\%}$ = 455°C [S8]; LC behavior (DSC): $T_{LC1}$ = 214°C, $T_{LC2}$ = 387°C, $T_I$ = 403°C [S8] | 2-10 °(2θ, Cu-Kα)<br>5-50 °(2θ, Cu-Kα), *Cf.* **Figure S48** | | determination of HOMO and LUMO energy [S9]; charge carrier mobility [S20]; |
| ***n*-C$_8$-PBI** | 78151-58-3 | [S3] | [S3] | [S3],[S14] | [S13] | *Cf.* Figure S21 | 0.13 mg/mL (4′-pentyl-4-cyanobiphenyl) [S15]; | [S15] | $\lambda_{max}$ ($H_2SO_4$) = 598nm [S3]; $\lambda_{max}$ ($CHCl_3$)= 526nm [S15]; | $\Phi_F$ ($CHCl_3$, 25°C) = 0.95 [S15]; | | *Cf.* **Figure S48** | [S10] | determination of HOMO and LUMO energy [S11], [S13]; cyclic voltamograms [S13]; non-linear optical susceptibility [S12]; solid-state absorption spectrum [S16]; charge carrier mobility [S20]; |
| ***n*-C$_9$-PBI** | 139260-28-9 | [S1] | [S1] | [S1] | *Cf.* FigureS22 | *Cf.* Figure S23 | 11mg/100mL $CHCl_3$, [S1] | [S1] | $\lambda_{max}$ ($CHCl_3$)= 532nm [S1]; | *Cf.* **Table S4** | $T_m$ =343°C [S1]; | *Cf.* **Figure S49** | | $R_f$ [S1] |

| Name | CAS no. | EA data | MS data | IR data | $^{1}$H-NMR | $^{13}$C-NMR | Solubility data | Fluorescence data | UV-Vis data | Fluorescence quantum yield | Thermal data | PXRD data | Crystal structure | Other data |
|---|---|---|---|---|---|---|---|---|---|---|---|---|---|---|
| ***n*-C$_{10}$-PBI** | 82531-04-2 | [S19] | | [S18] | *Cf.* FigureS24 | *Cf.* Figure S25 | | [S17] | $\lambda_{max}$ ($CHCl_3$)= 537nm [S17] | $\Phi_F$ ($CHCl_3$) = 0.98 [S17] | $T_m$ > 250°C [S17]; | *Cf.* **Figure S48** | | solid-state UV-Vis [S17]; charge carrier mobility [S20]; |
| ***n*-C$_{11}$-PBI** | 1357350-43-6 | [S21] | | [S21] | [S21] | *Cf.* Figure S27 | | *Cf.* FigureS47 | Simulated [S22]; | *Cf.* **Table S4** | | *Cf.* **Figure S49** | | determination of HOMO and LUMO energy [S22]; solid-state UV-Vis [23]; cycovoltametry & LUMO energy [S23] |
| ***n*-C$_{12}$-PBI** | 106822-31-5 | [S7] | | [S7] | *Cf.* FigureS28 | *Cf.* Figure S29 | 8.5 mg/100mL; 20°C $CHCl_3$, [S7] | In $CHCl_3$ [S7]; in DMF [S23] | $\lambda_{max}$ ($CHCl_3$)= 458nm, 489nm, 525.5nm [S7]; $\lambda_{max}$ (DMF)= 454nm, 487nm, 523nm [S23]; | $\Phi_F$ (DMF) = 0.83 [S23] | $T_m$ > 360°C [S7]; $T_d$ =412°C, $T_{LC1}$ = 110°C,$T_{LC2}$ = 138°C, $T_I$ = 178°C [S23]; DSC curve [S24] | *Cf.* **Figure S49** | | charge carrier mobility [S20]; $R_f$ [S7]; solid-state UV-Vis [23] |
| ***n*-C$_{14}$-PBI** | 139260-29-0 | [S1] | [S1] | [S1] | *Cf.* FigureS30 | *Cf.* Figure S31 | 5.4 mg/100mL; $CHCl_3$, [S1] | [S1] | $\lambda_{max}$ ($CHCl_3$)= 458nm, 488.5nm, 525nm [S1] | *Cf.* **Table S4** | DSC curve [S24]; $T_m$ = 327-338°C [S1] | *Cf.* **Figure S50** | | $R_f$ [S1] |
| ***n*-C$_{15}$-PBI** | 131336-80-6 | | *Cf.* **Table S5** | [S25] | *Cf.* FigureS32 | *Cf.* Figure S33 | | *Cf.* FigureS47 | [S25]* *Cf.* FigureS47 | *Cf.* **Table S4** | | *Cf.* **Figure S50** | | SERS data [S25]; solid-state UV-Vis [S26] |
| ***n*-C$_{16}$-PBI** | 139260-30-3 | [S1] | [S1],[S27] | [S1]; [S27] | [S27] | *Cf.* Figure S35 | 6 mg/100mL; $CHCl_3$, [S1] | [S1]; in DMSO [S27] | $\lambda_{max}$ ($CHCl_3$)= 457.5nm, 488nm, 524.5nm[S1]; in DMSO [S27] | | $T_m$ = 312-313°C [S1] | *Cf.* **Figure S50** | | $R_f$ [S1] |
| ***n*-C$_{18}$-PBI** | 25834-02-0 | [S7] | [S2] | [S7] | [S2] | *Cf.* Figure S37 | 1.8 mg/100mL; 20°C $CHCl_3$, [S7] | [S7]; [S23] | $\lambda_{max}$ ($CHCl_3$)= 458.5nm, 489nm, 525nm [S7]; $\lambda_{max}$ (DMF)= 454nm, 489nm, 525nm, 582nm [S23]; $\lambda_{max}$ ($CH_2Cl_2$)= | $\Phi_F$ (DMF) = 0.80 [S23] | $T_m$ >360°C [S1]; $T_d$ =314°C [S23]; DSC curve [S23]: $T_{LC1}$ = 83.2 °C, $T_{LC2}$ = 147.8 °C, | *Cf.* **Figure S50** | | $R_f$ [S7]; solid-state UV-Vis [23]; cycovoltametry & LUMO energy [S23] |

| | | | | | | | | | | | | | | |
|---|---|---|---|---|---|---|---|---|---|---|---|---|---|---|
| | | | | | | | | | 526nm [S2] | | $T_I$ = 175.8 °C; $T_d$ = 216 °C [S2] | | | |

# 5. References


[S1] H. Langhals, S. Demmig, and T. H. Potrawa. "**The relation between packing effects and solid state fluorescence of dyes**" *Journal für Praktische Chemie* **1991**, *333(5)*, 733-748.

[S2] L. Perrin, and P. Hudhomme. "**Synthesis, Electrochemical and Optical Absorption Properties of New Perylene - 3, 4: 9, 10 - bis (dicarboximide) and Perylene - 3, 4: 9, 10 - bis (benzimidazole) Derivatives**" *European Journal of Organic Chemistry* **2011**, *28*, 5427-5440.

[S3] Y. Nagao, and T. Misono. "**Synthesis and reactions of perylenecarboxylic acid derivatives. VIII. Synthesis of N-alkyl-3, 4: 9, 10-perylenetetracarboxylic monoanhydride monoimide**" *Bulletin of the Chemical Society of Japan* **1981**, *54(4)*, 1191-1194.

[S4] F. Graser, and E. Hädicke. "**Kristallstruktur und Farbe bei Perylen-3,4:9,10-bis(dicarboximid)-Pigmenten,2**" *Liebigs Ann. Chem.* **1984**, *3*, 483-494.

[S5] F. Graser, and E. Hädicke. "**Kristallstruktur und Farbe bei Perylen-3,4:9,10-bis(dicarboximid)-Pigmenten**" *Liebigs Ann. Chem.* **1980**, *3*, 1994-2011.

[S6] E. Hädicke, and F. Graser. "**Structures of Eleven Perylene-3,4:9,10-bis(dicarboximide) Pigments**" *Acta Cryst.* **1986**, *C42*, 189-195.

[S7] S. Demmig, and H. Langhals. "**Leichtlösliche, lichtechte Perylen - Fluoreszenzfarbstoffe**" *Chem. Ber.* **1988**, *121(2)*, 225-230.

[S8] J. Y. Kim, and A. J. Bard. "**Organic donor/acceptor heterojunction photovoltaic devices based on zinc phthalocyanine and a liquid crystalline perylene diimide**" *Chem. Phys. Lett.* **2004**, *383(1)*, 11-15.

[S9] Y. Berredjem, *et al.* "**The open circuit voltage of encapsulated plastic photovoltaic cells**" *Dyes and Pigments* **2008**, *78(2)*, 148-156.

[S10] A. Briseno, *et al.* "**Perylenediimide nanowires and their use in fabricating field-effect transistors and complementary inverters**" *Nano Lett.* **2007**, *7(9)*, 2847-2853.

[S11] M. C. Ruiz Delgado, *et al.* "**Tuning the charge-transport parameters of perylene diimide single crystals via end and/or core functionalization: a density functional theory investigation**" *J. Am. Chem. Soc.* **2010**, *132(10)*, 3375-3387.

[S12] D. B. O'Brien, and A. M. Massari "**Experimental evidence for an optical interference model for vibrational sum frequency generation on multilayer organic thin film systems. II. Consideration for higher order terms**" *J. Chem. Phys.* **2015**, *142(2)*, 024704:1-19.

[S13] A. Kalita, *et al.* "**Vapor phase sensing of ammonia at the sub-ppm level using a perylene diimide thin film device**" *J. Mater. Chem. C* **2015**, *3(41)*, 10767-10774.

[S14] L. G. Kaake, *et al.* "**Vibrational spectroscopy reveals electrostatic and electrochemical doping in organic thin film transistors gated with a polymer electrolyte dielectric**" *J. Am. Chem. Soc.* **2007**, *129(25)*, 7824-7830.

[S15] B. E. Willie, *et al.* "**Sterically engineered perylene dyes for high efficiency oriented fluorophore luminescent solar concentrators**" *Chem. Mater.* **2014**, *26(3)*, 1291-1293

[S16] S.-H. Wu, *et al.* "**High performance small molecule photodetector with broad spectral response range from 200 to 900 nm**" *Appl. Phys. Lett.* **2011**, *99(2)*, 023305:1-3.

[S17] T. Hassheider, *et al.* "**Electroluminescence and photovoltaic effects using columnar mesogenic compounds**" *Proc. SPIE* **2003**, Liquid Crystal Materials, Devices, and Applications IX, 10.1117/12.473864.

[S18] P. A. Antunes, *et al.* "**Reflection absorption infrared spectra of thin solid films. Molecular orientation and film structure**" *Appl. Spectros.* **2001**, *55(10)*, 1341-1346.

[S19] P. A. Antunes, *et al.* "**Langmuir and Langmuir-Blodgett films of perylene tetracarboxylic derivatives with varying alkyl chain length: film packing and surface-enhanced fluorescence studies**" *Langmuir* **2001**, *17(10)*, 2958-2964.

[S20] A. V. Mumyatov, *et al.* "**Organic field-effect transistors based on disubstituted perylene diimides: effect of alkyl chains on the device performance**" *Mendeleev Communications* **2014**, *24(5)*, 306-307.

[S21] A. Godoy, L. Cattin, J. C. Bernède, F. Díaz, and M. A. del Valle "**Effect of Perylene as Electron Acceptor and poly(tetrabromo-p-phenylene Diselenide) as "Buffer Layer" on Heterojunction Solar Cells Performances**" *Macromolecular Symposia* **2011**, 304(1), 109-114.

[S22] C. R. Medrano, M. B. Oviedo, and C. G. Sánchez "**Photoinduced charge-transfer dynamics simulations in noncovalently bonded molecular aggregates**" *Phys. Chem. Chem. Phys.* **2016**, *18(22)*, 14840-14849.

[S23] N. Pasaogullari, I. Huriye Icil, and M. Demuth "**Symmetrical and unsymmetrical perylene diimides: Their synthesis, photophysical and electrochemical properties**" *Dyes and pigments* **2006**, *69(3)*, 118-127.

[S24] H.-G. Jeon, *et al.* "**Thermal treatment effects on N-alkyl perylene diimide thin-film transistors with different alkyl chain**" *J. Appl. Phys.* **2010**, *108(12)*, 124512: 1-6.

[S25] D. Volpati, *et al.* "**Langmuir and Langmuir-Blodgett films of perylene tetracarboxylic derivatives: Molecular arrangement and surface enhanced spectroscopy**" *Trends in Applied Spectroscopy* **2009**, *7*, 69-81.

[S26] J. M. Duff, A. M. Hor, A. R. Melnyk, and D. Teney, "**Spectral response and xerographic electrical characteristics of some perylene bisimide pigments**" *Proc. SPIE* **1990**, Vol. 1253, pp. 183-191, doi: 10.1117/12.19813.
[S27] G. Schnurpfeil, J. Stark, and D. Wöhrle "**Syntheses of uncharged, positively and negatively charged 3, 4, 9, 10-perylene-bis (dicarboximides)**" *Dyes and pigments* **1995**, *27(4)*, 339-350.
[S28]R. Lakowicz, *Principles of Fluorescence Spectroscopy*, 2nd Ed., Kluwer Academic, New York, 1999
[S29] A.T.R. Williams, S.A. Winfield and J.N. Miller. *Analyst*. 1983**, 108,** 1067.
[S30] Adolfas K. Gaigalas, Lili Wang, *Journal of Research of NIST*, 2008, **113.1**, 17